CRREL REPORT 93-4

A Mathematical Model for River Ice Processes

A.M. Wasantha Lal and Hung Tao Shen

May 1993

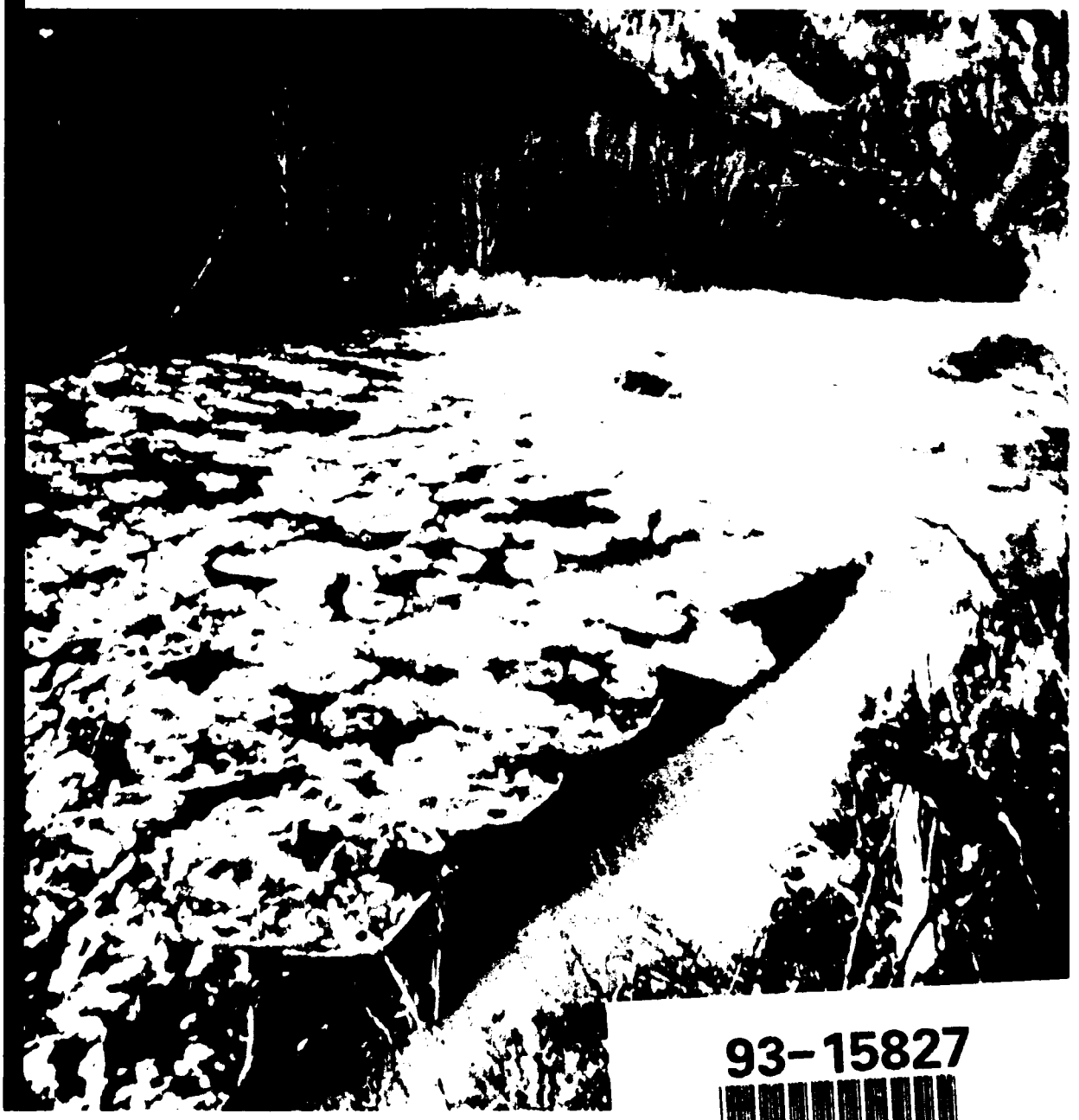

DISCLAIMER NOTICE

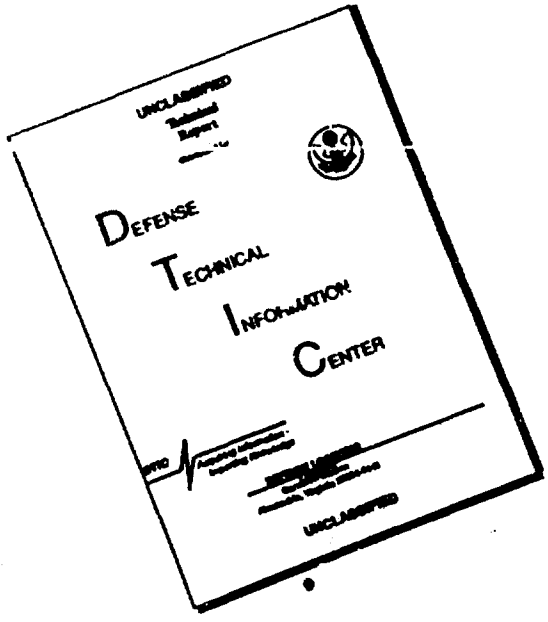

THIS DOCUMENT IS BEST QUALITY AVAILABLE. THE COPY FURNISHED TO DTIC CONTAINED A SIGNIFICANT NUMBER OF PAGES WHICH DO NOT REPRODUCE LEGIBLY.

Abstract

River ice processes are complex phenomena that are affected by many factors, including meteorological conditions, thermal inputs, hydraulic conditions and channel geometry. In this study a one-dimensional model called RICE is developed for simulating ice processes in rivers. In the river hydraulics component, the flow condition is determined by an implicit finite-difference solution of one-dimensional unsteady flow equations. In the thermal component, distributions of water temperature and ice concentration are determined by a Lagrangian–Eulerian solution scheme for equations of transport of thermal energy and ice. A two-layer formulation is introduced to model the ice transport. In this formulation the total ice discharge is considered to consist of the surface ice discharge of suspended ice distributed over the depth of the flow. The effect of surface ice on ice production, as well as the formation of skim ice and border ice, is included. The dynamic formation and stability of the ice cover is formulated according to existing equilibrium ice jam theories with due consideration to the interaction between the ice cover and the flow. The undercover ice accumulation is formulated according to the critical velocity criterion. The growth and decay of the ice cover is simulated using a finite-difference formulation applicable to composite ice covers consisting of snow, ice and frazil layers. The model has been applied to the St. Lawrence River and the Ohio River system, with simulated results comparing favorably with field observations. Future improvements on the mathematical model as well as theoretical formulations on various ice processes are discussed.

Cover: Ice floes on the Salmon River, Idaho.

For conversion of SI metric units to U.S./British customary units of measurement consult *Standard Practice for Use of the International System of Units (SI)*, ASTM Standard E380-89a, published by the American Society for Testing and Materials, 1916 Race St., Philadelphia, Pa. 19103.

CRREL Report 93-4

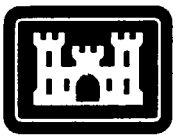

US Army Corps of Engineers
Cold Regions Research & Engineering Laboratory

A Mathematical Model for River Ice Processes

A.M. Wasantha Lal and Hung Tao Shen

May 1993

PREFACE

This report was prepared by A.M. Wasantha Lal, Research Engineer, Department of Civil and Environmental Engineering, and Hung Tao Shen, Professor of Civil and Environmental Engineering, Clarkson University. The study was supported by the U.S. Army Corps of Engineers under Contract No. DACA 89-84-K-0008, under the Clarkson–CRREL Joint Graduate Program in Ice Engineering. The report was technically reviewed by Dr. George Ashton and Steven Daly, both of CRREL.

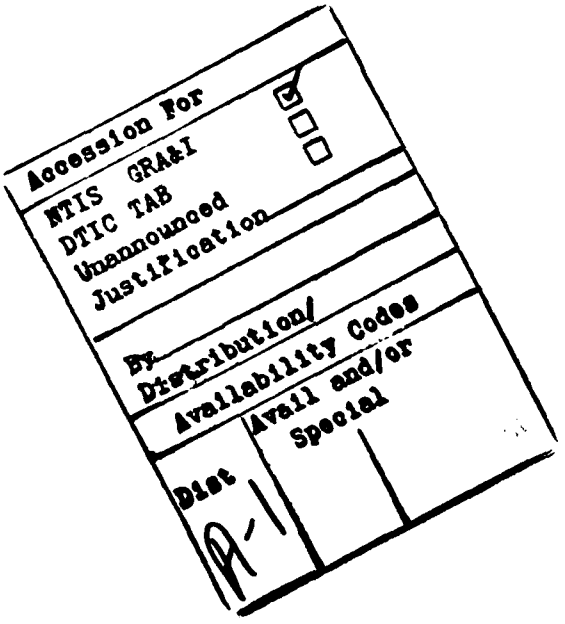

CONTENTS

ILLUSTRATIONS

Figure

TABLES

A Mathematical Model for River Ice Processes

A. M. WASANTHA LAL AND HUNG TAO SHEN

INTRODUCTION

Mathematical modeling techniques are increasingly being used to analyze river hydraulics. The numerical simulation of river hydraulics under open water conditions using one- or two-dimensional models is at an advanced stage due to the developments in the last few decades (Mahmood and Yevjevich 1975, Cunge et al. 1980, Fread 1985). When a river is subjected to ice conditions, the modeling of ice processes becomes important, not only because of the need to understand river ice phenomena, but also because of their effect on the hydraulic condition.

The river ice phenomena include the formation, evolution, transport, dissipation and deterioration of various forms of ice. These processes are not only affected by the ambient atmospheric conditions and the river geometry, they also interact in a complex manner with the flow condition in the river. Many river ice processes are not completely understood. However, by using existing theories, a comprehensive mathematical model can be developed. Such a model can be used to provide a continuous description of the river ice phenomena based on a limited amount of field data. From the engineering point of view, the model will assist engineers in evaluating the possible beneficial and detrimental consequences of the design and operation of river control works. A mathematical model can also be used by researchers to identify crucial gaps and weaknesses in the current knowledge of river ice. In addition, by interpreting the field data in a comprehensive manner, mathematical models can also be used to test new hypothetical formulations to advance our understanding of river ice processes. Since field data are often incomplete and the quantitative extrapolation from laboratory physical models to field conditions is still uncertain, this last aspect is particularly useful in river ice research.

Because of the complexity of river ice phenomena and the limited current understanding (Shen 1985), the development of a river ice model requires the maximum use of existing theories and mathematical techniques. In recent years a number of river ice models have been developed. Most of these models use backwater analysis in the hydraulic computation. These models include ones developed by Simonsen and Carson (1977), Petryk and Boisvert (1978), Michel and Drouin (1981), Petryk et al. (1981a) and Calkins (1984). Ice concentrations and water temperature distributions along the river are not considered in these models. Shen and Yapa (1984) developed a model that uses unsteady flow analysis in the hydraulic computation. The model also simulates water temperature and ice concentration distributions along the river by considering the longitudinal transport of thermal energy and frazil ice. A simulation model has been developed recently by Houkuna (1988) based on the model of Shen and Yapa and the unsteady flow model developed by Fread (1985). This model, however, does not consider mechanical thickening of the ice cover. Almost all of these models simulate river ice processes with various degrees of simplifications in the analytical formulation of physical phenomena.

River ice processes

At the beginning of winter, heat loss from the water surface due to the low ambient air temperature will exceed heat gain due mainly to the short-wave radiation. As a result the water temperature can drop to the freezing point. Further cooling will lead to supercooling of the river water and frazil ice formation. In slow flow areas,

where the turbulence intensity is not strong enough to mix the water or the frazil crystals over the depth, skim ice can form in the river even before the cross-sectional averaged water temperature drops to the freezing point. Frazil ice crystals, when mixed over the flow depth due to turbulence, can grow in size, multiply in number and agglomerate to form porous flocs. As the frazil particles and flocs grow in size, the increase in buoyancy can lead to the formation of a moving surface ice layer with a much higher concentration than the ice remaining in suspension.

The continuous increase in the surface ice concentration may lead to the formation of ice pans. Ice pans grow in size and strength when they travel along the river due to the freezing of interstitial water and the further accumulation of frazil ice, both around the circumference and on the bottom of pans. Ice pans may either sinter into still larger ice floes if they travel over a long distance, or they may break into fragments when passing through rapid sections. Partial coverage of the water surface by the moving surface ice layer results in a reduction of the net ice production due to the insulating effect. The downstream transport of the surface ice will cease when it reaches an artificial obstacle or a river section where an ice bridge across the river is formed by the congestion of the surface ice run. Once an obstacle is reached, the incoming surface ice will accumulate at its upstream side and extend the ice cover upstream. Frazil ice remaining in the suspension underneath the surface layer will be transported downstream and deposited on the underside of the ice cover to form frazil ice accumulations or hanging dams.

The phenomenon of ice bridging is not well understood, even though ice bridges usually form at the same location each winter. The formation of an ice bridge at a river section is related to the ice transport capacity of the section and the rate of ice discharge coming from upstream. The maximum rate of ice discharge that can pass through a river without forming an ice bridge depends on the flow velocity, the channel top width between banks or border ice boundaries, the surface slope, and the size, concentration and material properties of the ice in the surface layer (Ackermann and Shen 1983, Matousek 1984b, Shen et al. 1988).

Once an ice cover is initiated, it may progress upstream through the accumulation of incoming surface ice floes and slush. The rate of progression of the leading edge of an ice cover depends on the rate of surface ice supply and the thickness of the new ice cover, which is governed by the flow conditions at the leading edge. When the flow velocity is relatively low, incoming ice floes will form a smooth ice cover accumulated by a single layer of ice floes. This process is often called juxtaposition. During the freeze-up period, when the surface ice consists mainly of highly deformable frazil slush or loose frazil pans, the juxtaposition mode may not be clearly identifiable due to the compression of the surface ice elements. At a higher velocity range, surface ice elements can underturn or submerge at the leading edge to form a thicker ice cover. This mode of ice cover formation is often termed narrow jam or hydraulic thickening (Pariset and Hausser 1961). In this mode the ice cover thickness is limited by a critical under-cover entrainment velocity. When this velocity is exceeded, the ice particles that are swept under at the leading edge will be washed downstream, leading to the cessation of the leading edge progression, until flow velocity at the leading edge is reduced. Such a reduction in velocity can be caused either by the change in river discharge or the backwater effect induced by the increase in the size of the under-cover accumulation of ice.

The cover formed under any hydraulic condition has to be thick enough so that it is capable of withstanding the net force acting on it. Forces acting on an ice cover include current drag, wind drag, weight of the ice cover, and bank shear. The ice cover can collapse any time during the winter when the strength of the ice cover, together with the bank shear, cannot support the external forces acting along the direction of flow. During freeze-up, mechanical thickening or "shoving" will occur until the cover reaches a thickness that is capable of withstanding the external forces. The freeze-up of a thin solid ice cover in the granular surface ice accumulation can significantly increase the strength of the initial ice cover.

The surface ice that is swept under the ice cover can travel along the underside of the ice cover and be deposited downstream. This deposition, together with the similar deposition of frazil ice that remained in suspension when entering the ice-covered region, can lead to the formation of frazil hanging dams or frazil ice jams. Frazil hanging dams or frazil ice jams often occur under ice covers downstream of rapids. If the flow velocity increases at a later period, loosely accumulated frazil ice dams can be eroded and transported farther downstream.

These surface and under-cover ice accumulation processes have been presented in the context of ice cover

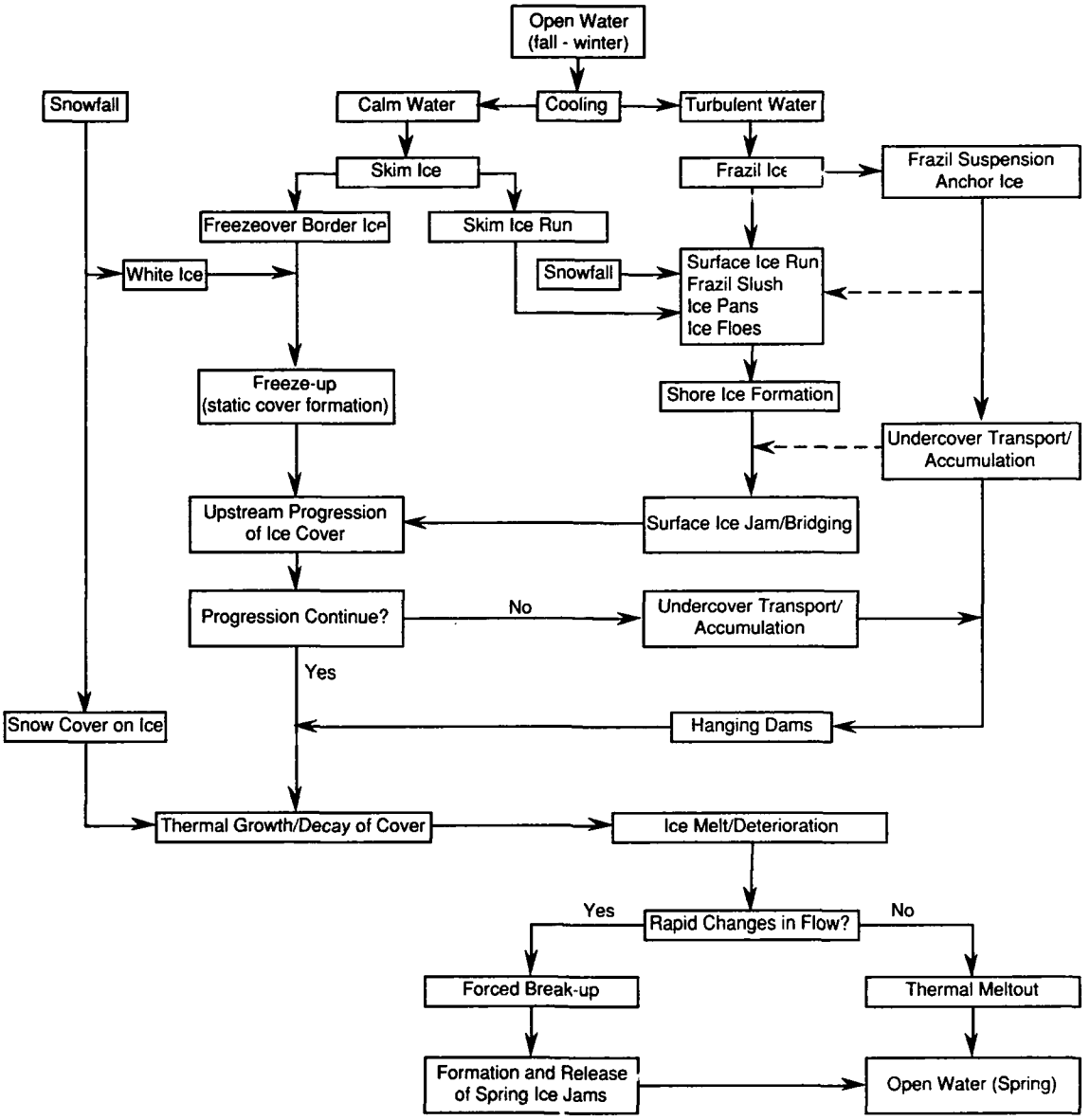

Figure 1. River ice processes.

formation during freeze-up. Similar processes can occur when a large volume of surface ice floes is released during the break-up of the ice cover upstream. In this case the leading edge of the intact downstream ice cover often acts as the obstacle that initiates the ice accumulation process. The dynamic process of the movement and accumulation of ice fragments after the break-up of the ice cover is similar to that of the surface ice run during freeze-up. Both of these processes involve relatively small time scales.

As heat exchange continues over a consolidated ice cover, water-filled voids in the granular ice mass will freeze from the water level downwards. This process is faster than black ice growth, and it can extend into the frazil layer if it exists. The existence of a snow cover can affect the thermal growth and decay of the ice cover. The snow cover provides an insulation layer that can retard the growth of the ice cover thickness. However, when the snow–ice interface submerges below the water level, the snow–ice growth on top of the cover can accelerate the growth of the ice cover thickness. Figure 1 shows a brief summary of these river ice processes.

Objective of the study

In this study a comprehensive one-dimensional river ice model called RICE was developed. The model includes submodels for river hydraulics, distributions of water temperature and ice discharge, formation of ice covers, formation and erosion of under-cover ice accumulations or hanging dams, thermal growth and decay of ice covers, and stability of ice covers. Existing theories on each ice process were reviewed and weaknesses identified. The model makes maximum use of the existing information, with improvements on analytical and mathematical formulations. Each ice process is modeled in a separate subroutine. With this arrangement the model can easily be modified to accommodate future improvements when new theories become available. The model can be used as a diagnostic tool to determine important factors that control the ice conditions in a river. This will provide guidelines for developing systematic field programs of data collection, designing of ice control projects and planning flow regulations. From the point of view of ice research, it is expected that by applying the model to rivers with existing field data, the shortcomings in the existing theories can be identified for future improvements. Together with weather forecasts, the model should also be able to forecast ice conditions in a river. Because of the limitations in the current knowledge on river ice, the model should first be calibrated with the field data before being used in forecasting.

UNSTEADY FLOW COMPUTATIONS

Governing equations

The hydraulics of one-dimensional river flow can be described by Saint Venant equations. These equations represent the conservation of mass and momentum in the river. For a river with a floating ice cover, the equation of conservation of mass is given as

$$\frac{\partial Q}{\partial x} + \frac{\partial A}{\partial t} = 0 \tag{1}$$

where Q = discharge
A = net flow cross-sectional area
x = distance
t = time.

The momentum equation is given as

$$\rho \frac{\partial Q}{\partial t} + \rho \left(\frac{2Q}{A} \frac{\partial Q}{\partial x} - \frac{Q^2}{A^2} \frac{\partial A}{\partial x} \right) + \rho g A \frac{\partial H}{\partial x} + (p_i \tau_i + p_b \tau_b) = 0 \tag{2}$$

where H = water surface elevation ($H = z_b + d_w + t_{sub}$)
g = gravitational acceleration
z_b = bed elevation
d_w = depth of flow
p_b = wetted perimeters formed by the channel bed
p_i = wetted perimeters formed by the ice cover
τ_b = shear stresses at the channel bottom
τ_i = shear stresses at the ice/water interface
t_{sub} = submerged thickness of the ice cover.

Numerical formulation

Finite-difference formulation of St. Venant equations

Finite-difference discretization for St. Venant equations requires the river to be divided into a sufficient number of reaches. The discretization should be done in such a manner that the average of the cross sections at the upstream and downstream ends of any reach closely represent the river reach. Junctions where different river branches meet have to be considered as nodes. Schematization of a river involves numbering river reaches and nodes. A method of numbering nodes and reaches for efficient computation is explained later.

The four-point implicit method (e.g. Amein and Chu 1975, Potok 1978, Potok and Quinn 1979) has many advantages over other methods, and it is capable of simulating a wide spectrum of wave types and river characteristics (Fread 1985). In this study the four-point implicit model for river networks developed by Potok and Quinn (1979) is used. The finite-difference formulation of St. Venant equations is presented in this section. In the finite-difference scheme, the river is discretized into a series of reaches. These reaches are connected by cross sections at their upstream and downstream ends. These cross sections are called nodes. The notation used is shown in Figures 2 and 3. The finite-difference grid on the x–t plane is shown in Figure 4. The finite-difference form of the continuity equation can be written as

$$\left[\theta\left(Q_d^p - Q_u^p\right) + (1-\theta)(Q_d - Q_u)\right]\frac{1}{\Delta x} + \left[T_d\left(H_d^p - H_d\right) + T\left(H_u^p - H_u\right)\right]\frac{1}{2\Delta t} = 0 \qquad (3)$$

where Q = discharge
H = stage
d, u = subscripts representing downstream and upstream ends of the reach
p = superscript indicating the solution at time level $t+\Delta t$
T = top width
θ = weighting factor = $\Delta t_m/\Delta t$

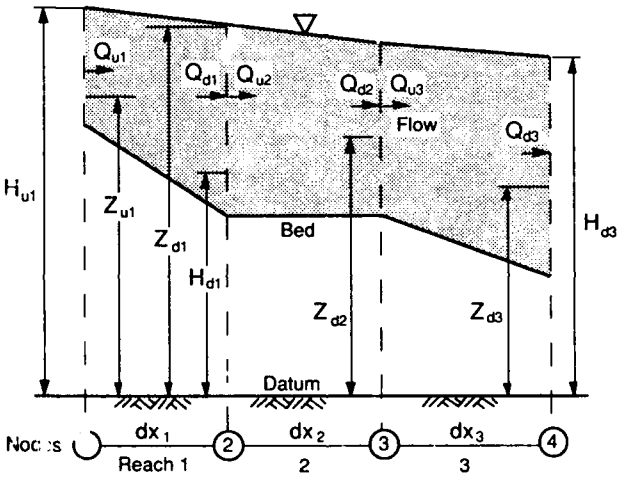

Figure 2. Example of finite-difference discretization.

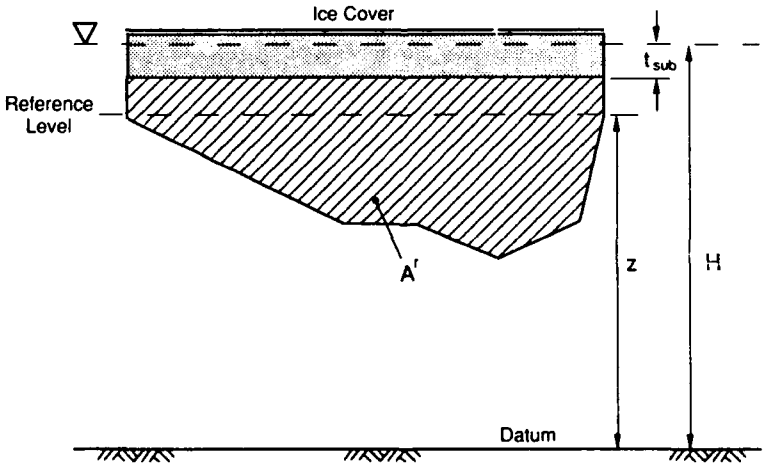

Figure 3. Channel cross section with an ice cover.

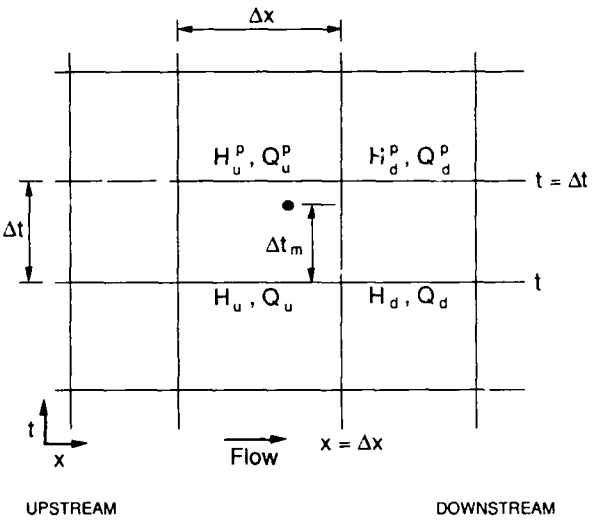

Figure 4. Implicit finite-difference scheme.

Δx = length of a reach
Δt = time step
Δt_m = fraction of Δt as shown in Figure 4 .

To ensure numerical stability and accuracy, the value of θ should be greater than 0.5 (Fread 1985). When $\theta = 1$, the scheme is fully implicit and unconditionally stable, except that the accuracy is reduced to $O(\Delta t)$. A value of 0.75 has been suggested to ensure stability and minimize loss of accuracy. The finite-difference form of the momentum equation can be written as

$$\left[\theta\left(Q_d^p - Q_u^p\right) + \left(1-\theta\right)\left(Q_d - Q_u\right)\right]\frac{2\overline{Q}^2}{\overline{A}\Delta x} - \frac{\overline{Q}^2}{\overline{A}^2}\left\{\theta\left[T_d\left(H_d^p - Z_d\right) - T_u\left(H_u^p - Z_u\right) + \Delta A^r\right]\right.$$

$$\left. + \left(1-\theta\right)\left[T_d\left(H_d - Z_d\right) - T_u\left(H_u - Z_u\right) + \Delta A^r\right]\right\}\frac{1}{\Delta x}$$

$$+ g\overline{A}\left[\theta\left(H_d^p - H_u^p\right) + \left(1-\theta\right)\left(H_d - H_u\right)\right]\frac{1}{\Delta x}$$

$$+ g n_e^2 \overline{Q}\left|\overline{Q}\right|\frac{\overline{P}^{4/3}}{\overline{A}^{7/3}} + \left[Q_d^p + Q_u^p - \left(Q_d + Q_u\right)\right]\frac{1}{2\Delta t} = 0 \qquad (4)$$

where $\Delta A^r = A_d^r - A_u^r - t_{sub}\left(T_d - T_u\right)$ (5)

$$\overline{Q} = 0.5\left[\theta\left(Q_d^p + Q_u^p\right) + \left(1-\theta\right)\left(Q_d + Q_u\right)\right] \qquad (6)$$

$$\overline{A} = 0.5\left\{A_d^r + A_u^r + \theta\left[H_u^p T_u + H_d^p T_d\right] + \left(1-\theta\right)\left[H_u T_u + H_d T_d\right] - \left(Z_u + t_{sub}\right)T_u - \left(Z_d + t_{sub}\right)T_d\right\} \qquad (7)$$

and z_u and z_d = reference elevations of upstream and downstream, respectively
A_u^r and A_d^r = cross-sectional area of the river below reference levels at upstream and downstream, respectively
g = gravitational acceleration
$\overline{P}$ = average wetted perimeter of the channel branch
n_e = equivalent Manning's roughness coefficient
t_{sub} = submerged depth of the ice cover thickness.

In eq 4, n_e represents the gross Manning's roughness coefficient of the river reach. It includes the effects of both the flow resistance of the channel bed and the resistance of the ice cover. In the absence of an ice cover,

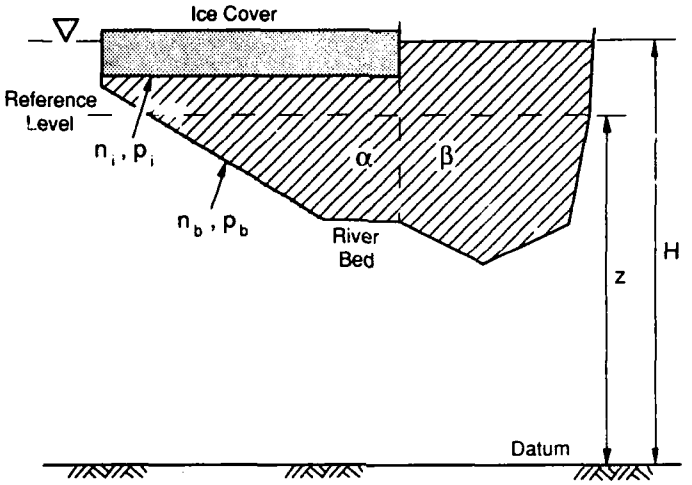

Figure 5. Partially ice-covered river cross section.

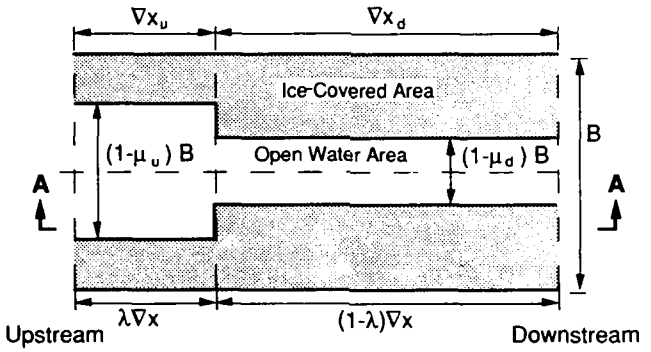

a. Top view.

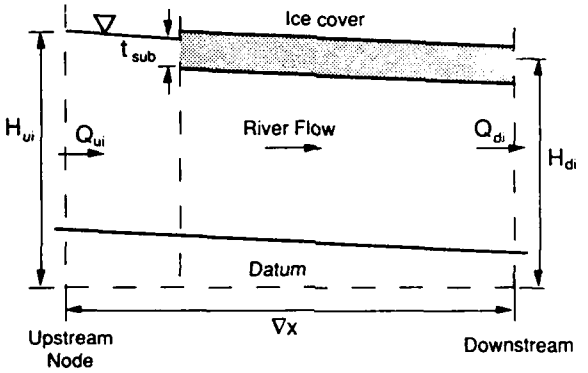

b. Longitudinal section.

Figure 6. Partially ice-covered river reach.

$n_c = n_b$. The derivation for a general expression of n_c is presented below. The present model considers the possibility of having border ice covering a fraction of the width and the main ice cover extending over a fraction of the length of a reach. Figure 5 shows a partially ice-covered river cross section. A typical plan area of an ice-covered reach considered in the model is shown in Figure 6, along with its longitudinal section. This river reach has a downstream fraction λ of length covered, except for a fraction $(1 - \mu_d)$ of the width. This type of partial ice cover can exist due either to the formation of border ice or to the erosion of the ice cover along a deep channel or thalweg in a river reach. The upstream fraction $(1 - \lambda)$ of the length is considered open, except for a fraction $(1 - \mu_u)$ of the width.

In the general case of a partially covered cross section as shown in Figure 5, the friction slope and shear resistance at any river cross section can be obtained using

$$S_f = \frac{p_b\tau_b + p_i\tau_i}{\rho g\bar{A}} = \frac{(p_b\tau_b)_O + (p_b\tau_b)_O + (p_i\tau_i)_I}{\rho g\bar{A}} \tag{8}$$

where the subscripts I and O represent covered and open portions of the cross section, respectively. When a fraction of the length of the river reach is covered with ice of a different width, the average energy slope of the river reach can be determined by considering the head loss h_f within a reach as the sum of the losses in the upstream and downstream sections of the reach. The total head drop over the length of the reach is given by

$$h_f = \bar{S}_f \Delta x = S_{fu}\Delta x_u + S_{fd}\Delta x_d \tag{9}$$

which reduces to

$$\bar{S}_f = (1-\lambda)S_{fu} + \lambda S_{fd} \tag{10}$$

where $\bar{S}_f$ = average friction slope over the length of the reach
S_{fu} = friction slope of the upstream $(1-\lambda)$ fraction of the reach
S_{fd} = friction slope of the downstream λ fraction of the river
$\lambda = \frac{\Delta x_d}{\Delta x}$.

Shen and Ruggles (1982) showed that

$$\rho_b\tau_b + p_i\tau_i = \rho g n_b^2 \left[\left(\frac{Q^2 p^{4/3}}{A^{7/3}}\right)_O + (1+F)^{4/3}\left(\frac{Q^2 p_b^{4/3}}{A^{7/3}}\right)_I\right] \tag{11}$$

where the subscripts I and O indicate ice-covered and open portions of the cross sections, respectively. F is defined as

$$F = \left(\frac{n_i}{n_b}\right)^{3/2}\left(\frac{p_i}{p_b}\right)_I \tag{12}$$

and n_i is the Manning coefficient for ice cover. The time-dependent variation of n_i can be related to an initial ice cover roughness n_{ini} and a final ice roughness n_{end} using the following formula (Nezhikhovskiy 1964, Shen and Yapa 1986):

$$n_i = n_{end} + (n_{ini} - n_{end})\, e^{-kt}. \tag{13}$$

Values of n_{ini} and n_{end} have to be calibrated prior to the application of the model.

In the case of a river with no ice cover, eq 8 and 11 give

$$S_f = \frac{P_b\tau_b}{\rho g A} = \frac{\rho g n_b^2 P_b^{4/3} Q|Q|}{\rho g A^{10/3}}. \tag{14}$$

If the ice cover extends over the entire width of the river, eq 11 reduces to

$$S_f = \frac{P_i\tau_i + P_b\tau_b}{\rho g A} = \frac{\rho g n_b^2 P_b^{4/3} Q|Q|(1+F)^{4/3}}{\rho g A^{10/3}}. \tag{15}$$

For a river reach that is fully covered over part of its length and fully open over the remaining part, S_{fu} is obtained using eq 14 and S_{fd} is obtained using eq 15. The average friction slope over the reach can be obtained using eq 10:

$$\bar{S}_f = Q^2 n_b^2 \left[(1-\lambda) \frac{P_u^{4/3}}{A_u^{10/3}} + \lambda (1+F)^{4/3} \frac{P_d^{4/3}}{A_d^{10/3}} \right]. \tag{16}$$

When the channel cross section is relatively uniform in a reach and the cross-sectional area occupied by the ice cover is small in comparison to the total cross-sectional area, both P_u and P_d can be replaced by an average value P for the reach. Similarly A_u and A_d can be replaced by the average cross-sectional area $\bar{A}$ for the reach. With these approximations, eq 16 reduces to

$$\bar{S}_f = \frac{Q^2 n_b^2 P_b^{4/3}}{\bar{A}^{10/3}} \left[(1-\lambda) + (1+F)^{4/3} \lambda \right]. \tag{17}$$

Using eq 17, an expression for n_e can be obtained to give an equivalent roughness in Manning's relationship (Yapa 1983):

$$n_e^2 = n_b^2 \left[\frac{\Delta x_o}{\Delta x} + (1+F)^{4/3} \frac{\Delta x_c}{\Delta x} \right]. \tag{18}$$

The same approach can be made to find the friction slope for a case where the ice extends over part of the width $(1-\mu)B$, assuming the channel to be a wide rectangular such that $p_\alpha \approx \mu B$, $A_\alpha \approx \mu A$, etc. Applying Manning's formula to the entire channel section and the ice-covered and open portions, respectively, and assuming the ice cover to be relatively thin in comparison to the flow depth, yields

$$Q = \frac{A R^{2/3} S_f^{1/2}}{n_e} \tag{19}$$

$$Q_\alpha = \frac{\mu A}{n_c} \left(\frac{\mu A}{2\mu B} \right)^{2/3} S_f^{1/2} = \frac{\mu A^{5/3}}{n_c 2^{2/3} B^{2/3}} S_f^{1/2} \tag{20}$$

$$Q_\beta = \frac{(1-\mu)A}{n_b} \left[\frac{(1-\mu)A}{(1-\mu)B} \right]^{2/3} S_f^{1/2} = \frac{(1-\mu)A^{5/3}}{n_b B^{2/3}} S^{1/2}. \tag{21}$$

The continuity condition gives

$$Q = Q_\alpha + Q_\beta. \tag{22}$$

Substituting Q_α, Q_β, p_α, p_β, A_α and A_β into eq 11 yields the following:

$$S_f = \frac{B^{4/3} n_b^2 Q^2}{A^{7/3}} \frac{(1+F)^{4/3}}{\left[\mu + (1-\mu)(1+F)^{2/3} \right]^2}. \tag{23}$$

Equation 23 can be used to obtain S_{fu} and S_{fd} of eq 10 by applying $S_f = S_{fu}$ when $\mu = \mu_u$ and $S_f = S_{fd}$ when $\mu = \mu_d$. A general expression for the average friction slope $\bar{S}_f$ can now be expressed as

$$\bar{S}_f = \frac{Q^2 B^{4/3} n_b^2}{A^{10/3}} \left(\frac{(1-\lambda)(1+F)^{4/3}}{\left[\mu_u + (1-\mu_u)(1+F)^{2/3}\right]^2} + \frac{\lambda(1+F)^{4/3}}{\left[\mu_d + (1-\mu_d)(1+F)^{2/3}\right]^2} \right). \quad (24)$$

The resistance term $(p_i\tau_i + p_b\tau_b)$ in eq 2 can now be determined by using eq 8. If the ice cover extends over the entire width in the downstream reach as a result of progression, $\mu_d = 1$. If there is no border ice, $\mu_u = 0$, and eq 24 reduces to eq 17.

Nodal equations

The equation governing the flow continuity at node k can be expressed as

$$\sum_{i=1}^{in} Q_{d,i}^p + q_k = \sum_{j=1}^{out} Q_{u,j}^p \quad (25)$$

where Q = discharge
i = incoming reaches
j = outgoing reaches
u and d = subscripts denoting upstream and downstream ends of each reach
q_k = external flow at node k.

The energy balance for the node k can be expressed using the following equations:

$$H_{d,1}^p = H_{u,i}^p + \Delta H_i \quad \text{for } i = 2,\ in + out \quad (26)$$

where H = water level
$(in + out)$ = total number of incoming and outgoing reaches for the node
ΔH_i = head loss between reaches 1 and i due to control structures at the node.

The variable ΔH_i is a function of $Q_{d,1}$, $H_{d,1}$ and $H_{u,1}$ etc. There are a total of $(in + out - 1)$ such equations at each internal node.

External boundary conditions

Three types of boundary conditions are common in practice. They are the discharge, the water level and the control structure type. In the case of a control structure, a functional relationship between the discharge and the water level is necessary. Only one time history or stage–discharge relationship is required at each boundary. Special treatment may be needed when a downstream control structure is not available in a long river. In such a case the downstream boundary can be treated by satisfying the uniform flow condition at the downstream boundary as presented by Viessman et al. (1972). An alternative method is to use an approximate rating curve developed from the channel characteristics as suggested by Gunaratnam and Perkins (1970). In the case of a boundary node connected to a reservoir having a known inflow and plan area, the continuity condition for the reservoir can be used as the boundary condition (Potok and Quinn 1979).

The general functional form of an upstream and a downstream boundary conditions can be expressed as

$$F_u\left(H_u^p, Q_u^p\right) = 0 \quad (27)$$

and

$$F_d\left(H_d^p, Q_d^p\right) = 0 \quad (28)$$

where F_u and F_d represent known functions. When the head is known at the upstream boundary,

$$F_u\left(H_u^p, Q_u^p\right) = H_{u,1}^p - H_{ub} \tag{29}$$

where H_{ub} is the known head at the upstream boundary. When the discharge is known,

$$F_u\ \left(H_u^p, Q_u^p\right) = Q_{u,1}^p - Q_{ub} \tag{30}$$

where Q_{ub} is the known discharge at the upstream boundary. Similar expressions can be obtained for the downstream boundary. When the rating curve $Q = f(H)$ is used, then for the downstream boundary,

$$F_d\ \left(H_d^p, Q_d^p\right) = Q_d^p - f\left(H_d^p\right) = 0. \tag{31}$$

Initial condition

If the initial conditions of the problem are known, the simulation can start with known initial values given in the input. Otherwise, the steady state solution is commonly used as the initial condition. To obtain a steady state solution, the program can be made to run starting from assumed flow and depth conditions close to those existing in the field. A sufficient number of iterations have to be used to bring the solution to the steady state.

Fread (1985) suggested the use of a backwater computation to determine H and Q values. In this study the method suggested by Potok and Quinn (1979) is used. The initial water surface profile and discharge distributions are obtained by first setting a zero discharge and an assumed constant water level for the entire study reach. The boundary conditions are then changed to those corresponding to the first time step. The flow simulation is then run until the river profile becomes steady. The resulting profile is then used as the initial condition.

Method of solution

In eq 3 and 4, the unknowns are Q_u^p, Q_d^p, H_u^p and H_d^p for each branch. For a river system with *NR* branches, *NB* nodes (including boundary nodes) and *NBND* boundary conditions, 4*NR* equations are needed to solve the 4*NR* unknowns. A breakdown of the number of equations is given in Table 1.

Table 1. Number of equations available in the system of equations.

Type	*Number of equations*
River reach continuity condition	*NR* (number of reaches)
River reach momentum condition	*NR* (number of reaches)
Nodal continuity condition	*NB–NBND* (total no. of nodes–no. of boundary nodes)
Nodal energy condition	sum of (in–out–1) at *NB–NBND* nodes
Boundary conditions	*NBND* (no. of boundary nodes)

The finite-difference form of the Saint Venant equations, along with the nodal and boundary conditions, form a system of nonlinear equations of the form

$$\mathbf{F}(\boldsymbol{x}) = 0 \tag{32}$$

where $\boldsymbol{x} = (x_1, x_2, \ldots x_n)^t$ is the vector containing the unknown variables Q^p and H^p, and $f_1, f_2, \ldots f_n$ are the coordinate functions of **F**. Using Newton's method, the iterative procedure to find **x** at the time step k is given as (Burden and Faires 1985)

$$J[x^{(k-1)}]\ [x^{(k)} - x^{(k-1)}] = -F(x)^{(k-1)} \tag{33}$$

where $J(x)$ is the Jacobian matrix. For computational efficiency, **x** is solved as a system of linear equations. The (i,j) element of the Jacobian matrix can be written as

Table 2. Arrangement of a Jacobian matrix and the right side of eq 30 for the case shown in Figure 2.

	Reach 1				*Reach 2*				*Reach 3 (NR)*				
Equation	H_u	Q_u	H_d	Q_d	H_u	Q_u	H_d	Q_d	H_u	Q_u	H_d	Q_d	*RHS*
Upstream boundary	A	B	0	0	0	0	0	0	0	0	0	0	C
Continuity: reach 1	X	X	X	X	0	0	0	0	0	0	0	0	X
Momentum: reach 1	X	X	X	X	0	0	0	0	0	0	0	0	X
Continuity: node 2	0	0	0	X	X	0	0	0	0	0	0	0	X
Energy: node 2	0	0	X	0	X	0	0	0	0	0	0	0	X
Continuity: reach 2	0	0	0	0	X	X	X	X	0	0	0	0	X
Momentum: reach 2	0	0	0	0	X	X	X	X	0	0	0	0	X
Continuity: node 3	0	0	0	0	0	0	0	X	0	X	0	0	X
Energy: node 3	0	0	0	0	0	0	X	0	X	0	0	0	X
Continuity: reach 3	0	0	0	0	0	0	0	0	X	X	X	X	X
Momentum: reach 3	0	0	0	0	0	0	0	0	X	X	X	X	X
Downstream boundary	0	0	0	0	0	0	0	0	0	0	D	E	F
	(Jacobian matrix, 12*12)												(RHS, 12*1)

Key: X = Variables taken care of by the program.
A,B,C,D,E,F = Variables defined by user in subroutines UPBOUND and DNBOUND to take care of boundary conditions.

$$J_{i,j}(\mathbf{x}) = \frac{\partial f_i(\mathbf{x})}{\partial x_j}. \tag{34}$$

At each computational time step, the above iterative procedure is followed to obtain the unknowns $\mathbf{x}$, which are the H and Q values of the river reaches. The selection of initial values $\mathbf{x}^0$ is explained later. An alternative method for solving a system of nonlinear equations is available when the analytical expression of $J(\mathbf{x})$ cannot be obtained easily (Broyden 1965).

By selecting a suitable numbering system for nodes and reaches, the bandwidth of the Jacobian matrix can be reduced to a minimum. This is a very useful technique to reduce computing time and obtain accurate results (Potok 1978). In the method used, nodes have to be numbered *along the river* from the upstream end of the river to the downstream end of the downstream boundary reach. By doing this, external boundary conditions would not come into the center of the Jacobian matrix. Also, the difference between two neighboring reaches and nodes has to remain at a minimum, which is a condition for minimum bandwidth. Reach numbers should follow node numbers. It is preferable to have the reach number be the same as the node number at the upstream end of the reach. This condition is not possible in the case of river networks. Table 2 shows an example of a numbering system for a river divided into three reaches.

Calibration of resistance coefficients

A river system consisting of many river reaches can be considered as a discrete system, and the Manning coefficient of each section can be calibrated using influence coefficient methods (Beck and Arnold 1977, Lal and Shen 1990b). Since influence coefficients can be obtained numerically, the calibration methods do not require any manipulation of the governing equations. The numerical model for simulating the unsteady flow can be used without further modification. Observed and simulated values of any number of state variables (water levels) can be used to calibrate a number of parameters equal to the number of state variables.

The calibration uses observations of the state variable Y_k, for each of $i = 1, 2, \ldots n$ sensors (water level gauges) at time steps $k = 1, 2, \ldots m$. The data are used to calibrate the parameters, θ_i, $i = 1, 2, \ldots n$ (Manning's roughness coefficients). Three influence coefficient methods, depending on the selection of the objective function, can be used. These methods are the least-square method, the minimax method and the minimum bias method. The objective function used when applying the principle of least squares is the minimization of the error sum of squares S over all the sensors and all the time steps. The expression for S is

$$S = \sum_{i=1}^{n} \sum_{k=1}^{m} (y_i^k - Y_i^k)^2 \tag{35}$$

where y_i^k is the simulated value of the i^{th} state variable at time k. The objective function of the minimax method is to minimize the sum of maximum errors in the simulation:

$$\min e_1 + e_2 + \ldots + e_n \tag{36}$$

where $e_1, e_2, \ldots e_n$ are the maximum errors at gauges $1, 2, \ldots n$. The objective function of the minimum bias method is to minimize the absolute value of the overall bias of simulated values at all the gauging stations. The overall bias at any gauge i is given by

$$B_i = \sum_{k=1}^{m} \left(y_i^k - Y_i^k \right). \tag{37}$$

The objective is to minimize $|B_i|$ for each $i = 1, 2, \ldots n$. This objective is achieved by making each element zero. The current study uses the minimum bias method to obtain values of Manning's coefficients, since the method is more efficient and gives accurate results.

WATER TEMPERATURE AND ICE CONCENTRATION DISTRIBUTIONS

Governing equations

In a well-mixed river, distributions of water temperature and depth-averaged frazil concentration along the river can be described by the one-dimensional advection–diffusion equation (Fischer et al. 1979). The equation for the cross-section-averaged water temperature T_w of a river is

$$\frac{\partial}{\partial t}\left(\rho C_p A T_w\right) + \frac{\partial}{\partial z}\left(Q \rho C_p T_w\right) = \frac{\partial}{\partial x}\left(A E_x \rho C_p \frac{\partial T_w}{\partial x}\right) - B\phi_T \tag{38}$$

where A = cross-sectional area of the river
B = river width
Q = discharge
ρ = density of water
C_p = specific heat of water
E_x = longitudinal dispersion coefficient
ϕ_T = total heat loss rate per unit surface area of the river.

Two boundary conditions and an initial condition are needed to solve this equation.

If the river does not have large temperature gradients in the longitudinal direction, the longitudinal dispersion term

$$\frac{\partial}{\partial x}\left(A E_x \rho C_p \frac{\partial T_w}{\partial x}\right)$$

can be neglected. An analysis of the water temperature data in the upper St. Lawrence River shows that typical values of $\partial T_w/\partial t$, $\partial T_w/\partial x$ and $\partial^2 T_w/\partial x^2$ are on the orders of 10^{-6}, 10^{-5} and 10^{-8}, respectively. Without the dispersion term, the solution procedure simplifies. When flow is unidirectional, only one boundary condition is needed at the upstream end:

$$T_w(0, t) = T_1(t) \tag{39}$$

where $T_1(t)$ is the time history of the water temperature at the upstream boundary. If the initial condition $T_w(x,0)$ is not available, a steady state solution can be used as in the case of the hydraulics computation.

When the water temperature drops below the freezing point, frazil ice will be produced. The one-dimensional equation governing the transport of frazil ice is (Shen and Chiang 1984)

$$\frac{\partial}{\partial t}(\rho_i L_i A C_i) + \frac{\partial}{\partial x}(Q\rho_i L_i C_i) = \frac{\partial}{\partial x}\left(AE_x\rho_i L_i \frac{\partial C_i}{\partial x}\right) - B\phi_T + \Sigma S \tag{40}$$

where C_i = ice concentration
L_i = latent heat of fusion of water
ρ_i = density of ice
B = width of the river
ΣS = additional source or sink terms due to ice cover progression, erosion, deposition and melting.

The total heat flux term ϕ_T may be approximated by the surface heat flux ϕ^*. Since eq 40 is in the same form as eq 38, both the ice concentration and the water temperature can be obtained from the solution of a single equation by considering that $C_i\rho_i L_i = -\rho C_p T_w$ and letting the water temperature in the heat exchange term ϕ_T in eq 40 be equal to the freezing point of water (Shen and Chiang 1984).

Heat exchanges

During open water conditions the total heat flux at the free surface is equal to the sum of the net short- and long-wave radiations, the sensible heat exchange and the heat transfers due to evaporation and precipitation. Some of these components, especially the long-wave radiation, are nonlinear functions of air and water temperatures. In this model, linear relationships using constant heat exchange coefficients are used to express the net heat exchange. These relationships can be obtained using multiple linear regression of computed heat exchange and weather parameters (Lal and Shen 1990a).

The net heat exchange rate at the water surface can be approximated by the following linear relationship (Ashton 1986)

$$\phi^* = h_{wa}(T_w - T_a) \tag{41}$$

where ϕ^* = net rate of heat loss from the water surface
T_a = air temperature
T_w = water temperature
h_{wa} = heat exchange coefficient.

Since the short-wave radiation is independent of the water temperature T_w and the air temperature T_a and varies with latitude and cloud cover, a modified form of eq 41 may be used (Dingman and Assur 1969):

$$\phi^* = -\phi_R + \alpha' + \beta'(T_w - T_a) \tag{42}$$

where α' and β' are heat exchange parameters and ϕ_R is the short-wave radiation, which has to be computed separately making use of the latitude and cloud cover. Linear models cannot completely describe the heat exchange process. However, for rivers where extensive weather data are not available, linear models provide a sufficiently accurate alternative for computing the surface heat exchange.

When there is an ice cover in the river, the turbulent heat exchange taking place between water and the underside of the ice cover ϕ_{wi} may be represented by

$$\phi_{wi} = h_{wi}(T_w - T_m) \tag{43}$$

where h_{wi} is the turbulent heat exchange coefficient between ice and water in W m^{-2} °C^{-1}. Considering the ice-covered river as a closed conduit, the following relationship can be used to explain the heat exchange coefficient (Ashton 1973):

$$h_{wi} = C_{wi}\frac{U^{0.8}}{d_w^{0.2}} \tag{44}$$

where U = average flow velocity (m s^{-1})
d_w = depth of flow (m)
C_{wi} = constant ≈ 1622 W $s^{0.8}$ $m^{-2.6}$ $°C^{-1}$.

Laboratory and field investigations indicate that the coefficient C_{wi} may vary with the resistance of the cover (Haynes and Ashton 1979, Calkins 1984, Marsh and Prowse 1987).

In river reaches where the heat exchange at the river bed and the heat flux from thermal effluents may be significant, these terms have to be considered in the source term. For most rivers the bed heat flux can either be neglected or lumped into the surface heat exchange in the thermal analysis.

Numerical solution

Many numerical methods have been introduced to solve the transport equations. Most of these methods are based on Eulerian schemes. The method suggested by Leendertse (Cunge et al. 1980) is capable of reducing artificial diffusion but introducing artificial dispersion. It produces oscillatory behavior in the solution. Holly and Preissman (1977) introduced a method aimed at reducing both numerical diffusion and dispersion but at the expense of computational efficiency.

The difficulties in using Eulerian schemes to model convection without causing instabilities, inaccuracies and oscillations led to the use of Lagrangian or Eulerian–Lagrangian schemes (Fischer et al. 1979, Jobson 1987). The Lagrangian scheme uses marked parcels of water moving along the channel at the flow velocity. Lagrangian schemes are stable at any Courant number, and if there is no need for the values of the concentration in the moving parcel to be interpolated to the Eulerian grid, numerical diffusion is virtually nonexistent.

In the present model a Lagrangian–Eulerian scheme is developed to solve the transport equation. The following Lagrangian equation can be obtained from eq 38 or 40 using the continuity equation and neglecting the dispersion term:

$$\frac{DT_w}{Dt} = -\frac{\phi}{\rho C_p d_w}. \tag{45}$$

In the computation, marked parcels of water with known water temperature or ice concentration are released from the upstream boundary and nodal points at each time step. The parcels are followed along the river with known flow velocities from the hydraulic computation. The temperature or concentration values of each moving parcel can be determined at any time during the movement. When the parcel velocities are numerically integrated over the time step Δt, the new position of a parcel originally located at the i^{th} node with distance x_i from node 1 can be obtained:

$$S_i = x_i + \sum_{k=i}^{j-1} \Delta x_k + u_j \left(\Delta t - \sum_{k=i}^{j-1} \frac{\Delta x_k}{u_k} \right) \tag{46}$$

where Δt = time increment
Δx_k = length of the k^{th} reach
S_i = distance to the particle from node 1 at the end of the time step
x_i = distance to node i from node 1
$j-1$ = number of the last reach completely passed by the moving parcel before the time step is complete
u_k = average flow velocity in reach k at time t^n
i, j, k = dummy integer variables.

The movement and positions of parcels can be illustrated by an x–t plot as shown in Figure 7. In the figure, $\delta t_i = \Delta x_i / u_i$ within any reach i. A parcel a_1 at node 1 will go through b_1, c_1 and end up at d_1 at time t^{n+1}. Similarly parcels starting at a_2, a_3, . . . move during the time step Δt along the paths shown.

The temperature of the i^{th} parcel at time t^{n+1} can be obtained by integrating eq 45 over time:

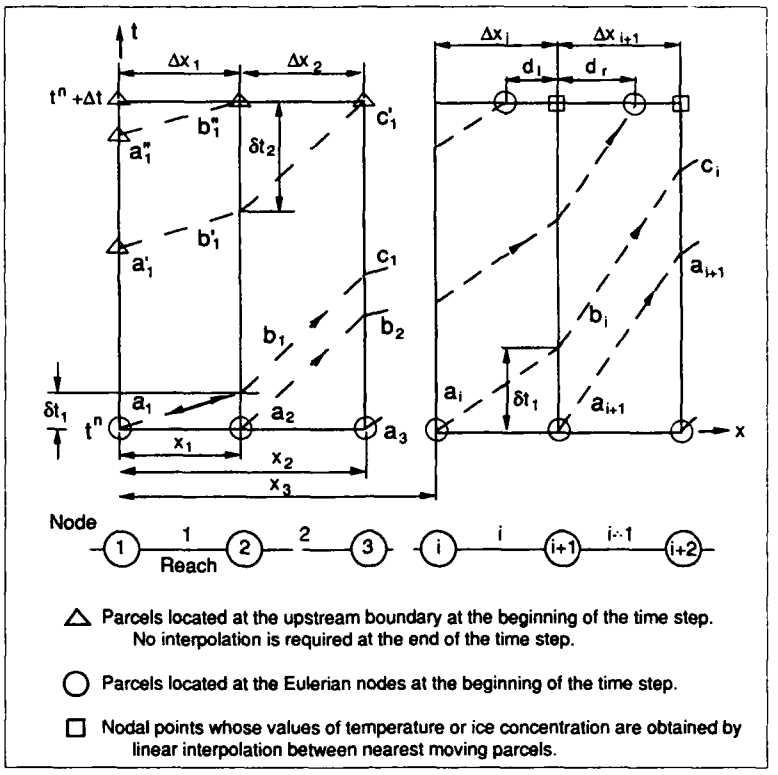

Figure 7. Lagrangian–Eulerian scheme.

$$T_{w,j}^{(n+1)} = T_{w,i}^{n} - \sum_{k=i}^{j-1} \frac{\phi_k}{\rho C_p d_{wk}} \frac{\Delta x_k}{u_k} - \frac{\phi_j}{\rho C_p d_{wj}} \left(\Delta t - \sum_{k=i}^{j-1} \frac{\Delta x_k}{u_k} \right) \tag{47}$$

where $T_{w,i}^{n+1}$ = T_w at node i at time t^{n+1}
$T_{w,i}^{(n+1)}$ = T_w of a Lagrangian parcel i at time t^{n+1}
d_{wk} = mean depth of the reach k
ϕ_k = heat loss rate in reach k.

For large values of Δt, the above procedure cannot determine the water temperature distribution in the vicinity of the upstream boundary, e.g. at nodes 2 and 3 in Figure 7. The values at these nodes can be determined by backtracking moving parcels to the upstream boundary. For example, parcels that arrive at nodes 2 and 3 at time t^{n+1} are originated at a_1' and a_1'. The positions of a' and a'' can be determined by drawing $a_1'b_1'$ and $a_1''b_1''$ parallel to a_1b_1, and $b_1'c_1'$ parallel to a_2b_2. The values of the water temperature or ice concentration at the boundary node at any time can be determined by linearly interpolating between values at the time levels t^n and t^{n+1}. Using this procedure, temperatures at the nodes near the upstream boundary can be determined using the following expression:

$$T_{w,i}^{n+1} = \frac{T_{w,1}^{n}}{\Delta t} \left(\sum_{k=1}^{i-1} \frac{\Delta x_k}{u_k} \right) + \frac{T_{w,1}^{n+1}}{\Delta t} \left(\Delta t - \sum_{k=1}^{i-1} \frac{\Delta x_k}{u_k} \right) - \sum_{k=1}^{i-1} \frac{\phi_k}{\rho C_p d_{wk}} \frac{\Delta x_k}{u_k}. \tag{48}$$

Equation 47 does not give the values of temperature or concentration directly at the fixed Eulerian nodes. For the convenience of bookkeeping, the information carried by Lagrangian parcels are interpolated to the fixed Eulerian nodal points at the end of each Δt time step. These interpolated nodal values are then used as the starting

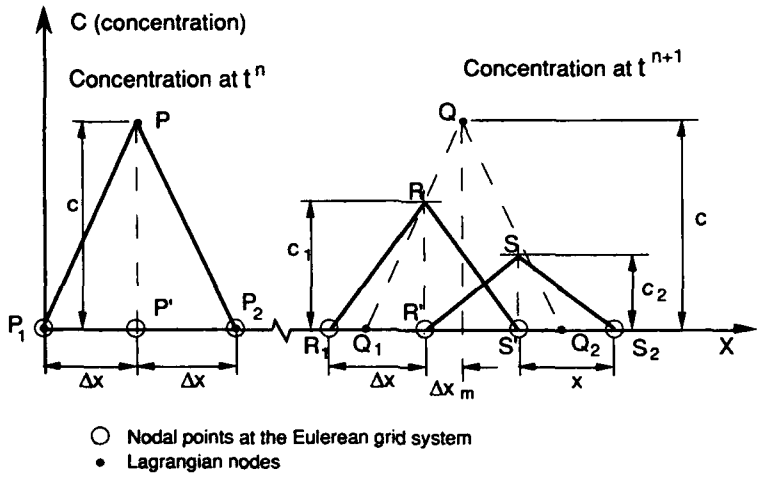

Figure 8. Definition sketch for the analysis of numerical diffusion.

points for the Lagrangian computation in the next time step. The nodal temperature values are interpolated from the closest moving parcels upstream and downstream of each node, using the following approximation:

$$T_{w,j}^{n+1} = \frac{T_{w,j}^{(n+1)} d_r + T_{w,j+1}^{(n+1)} d_\ell}{d_\ell + d_r} \tag{49}$$

where d_ℓ and d_r are the distances from the fixed node to moving parcels. In the case of ice transport, the additional sink and source terms in eq 40 should be considered. These terms are due to the consumptions of the ice in the initial ice cover formation and frazil deposition and the addition of ice into the stream due to the ice cover failure and the erosion of frazil accumulations. Modeling of these phenomena will be discussed later.

Numerical diffusion is introduced when interpolating temperature or frazil concentration from the moving parcels to the Eulerian grid system. Numerical diffusion can be minimized either by using higher-order interpolation schemes (e.g. Cheng et al. 1984, Holly and Usseglio-Polatera 1984) or by simply introducing more Lagrangian parcels where the concentration gradient is large. Since gradients of water temperature or ice concentration distribution in natural rivers are small, linear interpolation is used for numerical efficiency.

A single moving parcel P of unit mass moving in a uniformly spaced grid system is used to examine the magnitude of artificial diffusion. As shown in Figure 8, a concentration slug of triangular spatial distribution P_1PP_2 at time t^n will move to Q_1QQ_2 at time t^{n+1}. Based on the linear interpolation formula, eq 49, the concentration distribution at the Eulerian grid system after interpolation becomes R_1RSS_1. The concentration distribution can be replaced by the linear superposition of two triangles R_1RS' and $R'SS_2$.

For these two triangles the condition for the conservation of mass gives

$$c_1\Delta x + c_2\,\Delta x = c\Delta x. \tag{50}$$

The conservation of the first moment around R–R (or any other point) gives

$$c\Delta x\,\Delta x_m = c_2\Delta x^2. \tag{51}$$

Equations 50 and 51 give

$$c_1 = \frac{\Delta x - \Delta x_m}{\Delta x}\,c \tag{52}$$

and

$$c_2 = \frac{\Delta x_m}{\Delta x} c. \tag{53}$$

This indicates that the interpolation procedure satisfies both the conservation of mass and the conservation of first moment. The total mass of the dispersant is $c\Delta x = 1$. The variance of the mass concentration σ^2 is given as (Fischer et al. 1979)

$$\sigma^2 = \int_{-\infty}^{\infty} (x-\bar{x})^2 c \, dx. \tag{54}$$

For the original triangular concentration distribution centered at P at time t^n,

$$\sigma^2 = \frac{1}{6} \Delta x^2. \tag{55}$$

Substituting eq 52 and 53 into eq 50 gives σ^2 for the concentration around the axis Q–Q' due to the two triangles at R and S:

$$\sigma^2 = \frac{1}{6} \Delta x^3 c_1 + \Delta x \Delta x_m^2 c_1 + \frac{1}{6} \Delta x^3 c_2 + \Delta x (\Delta x - \Delta x_m)^2 c_2. \tag{56}$$

The change of σ^2 during the period t^n to t^{n+1} is determined from eq 55 and 56, while noting that $c\Delta x = 1$:

$$\Delta\sigma^2 = \Delta x_m (\Delta x - \Delta x_m). \tag{57}$$

If the parcel has passed j grid points during time Δt to come to Q, the Courant number is given by

$$C_r = U \frac{\Delta t}{\Delta x} = \frac{j \Delta x + \Delta x_m}{\Delta x}$$

$$= j + \frac{\Delta t_m}{\Delta x}. \tag{58}$$

Using the value of $\Delta x_m/\Delta x$ obtained from eq 58 in eq 57, the numerical diffusion K_n is computed as

$$K_n = \frac{1}{2} \frac{d\sigma^2}{dt} = \frac{1}{2} \frac{\Delta x^2}{\Delta t} (C_r - j)(j + 1 - C_r) \tag{59}$$

$$= \frac{1}{2} \frac{\Delta x_m (\Delta x - \Delta x_m)}{\Delta t} \tag{60}$$

$$\approx O \left(\frac{\Delta x^2}{\Delta t} \right) \tag{61}$$

where C_r is the Courant number ($U\Delta t/\Delta x$) and j is the largest integer smaller than the Courant number (zero included).

The following observations, which are useful in selecting time steps and grid spacing, can be made about numerical diffusion K_n:

- K_n is zero for integer values of C_r;
- K_n is at its maximum when $C_r = n + 0.5$ where n is zero or a positive integer;
- K_n averages to 0.083 ($\Delta x^2/\Delta t$) for random values of C_r;
- K_n is proportional to Δx^2; K_n can be reduced by dividing the river into more sections;
- K_n can be reduced by increasing the time step Δt.

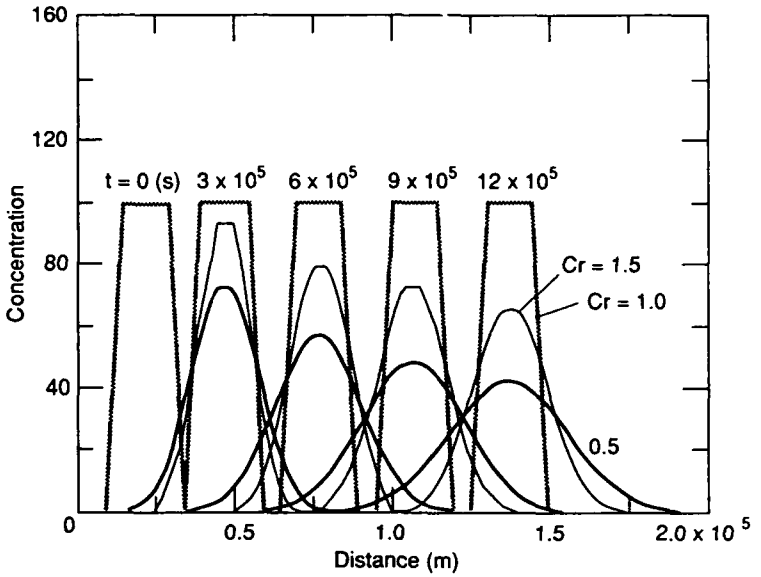

Figure 9. Effect of the Courant number on numerical diffusion.

The effect of the Courant number on numerical diffusion is illustrated in Figure 9. The parameters used are as follows:

Space discretization, Δx	5,000 m
Velocity, u	0.1 m s^{-1}
Cross-sectional area, A	10,000 m^2
Width, B	2,000 m
Time step length, Δt ($C_r = 1.0$)	50,000 s
Time step length, Δt ($C_r = 0.5$)	25,000 s
Time step length, Δt ($C_r = 1.5$)	75,000 s.

An imaginary dispersant with a rectangular concentration distribution is used, and simulations are carried out with the Lagrangian schemes using Courant numbers of 1.0, 0.5 and 1.5. Figure 9 shows the concentration distribution plotted at 0.0; 300,000; 600,000; 900,000 and 1,200,000 s. The curve for $C_r = 1$ shows no numerical diffusion. $C_r = 0.5$ gives the maximum numerical diffusion for this problem. The curve for $C_r = 1.5$ shows that numerical diffusion is reduced by taking a larger time step. Values Δx and Δt can be selected for a numerical scheme such that numerical diffusion would not become excessive. Numerical diffusion can be made approximately equal to the physical dispersion coefficient to reduce its effect.

The numerical procedure for simulating the water temperature distribution was verified by comparing the numerical solution with a steady-state analytical solution. The steady-state solution for eq 38 with constant values of A, B and u, neglecting dispersion and unsteady terms, is

$$T_w = (T_o - T_a) \exp(-kx) + T_a \tag{62}$$

where $k = (h_{wa}B)/(\rho C_p u A)$ and T_o is the temperature at the upstream boundary at $x = 0$. Analytical and numerical solutions for $C_r = 4.32$ are shown in Figure 10. Values of the parameters used are given below:

Time step length, Δt	216,000 s
Space discretization, Δx	5,000 m
Velocity, u	0.1 m s^{-1}
Cross-sectional area, A	10,000 m^2
Width, B	2,000 m
Heat exchange coefficient , h_{wa}	20.0 W m^{-2} °C
Specific heat of water, C_p	4.1855 × 103 J kg^{-1}.

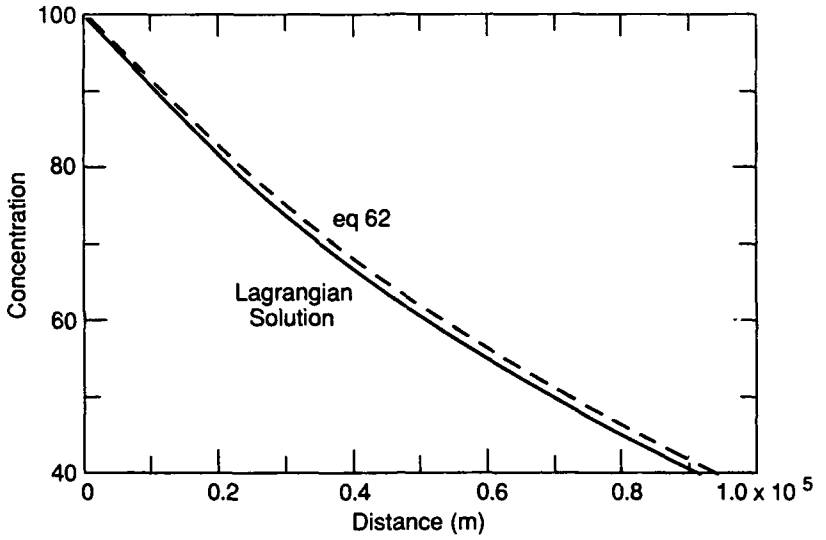

Figure 10. Comparison of the numerical and analytical solutions.

The error shown in Figure 10 is due to the linear interpolation of values between nodes and the error in the finite-difference discretization. In this example, where numerical diffusion is not important, a larger time step $\delta t = \Delta x/u$ as chosen to show that although numerical diffusion can be reduced by taking larger values of Δt, the discretization error, which is on the order of δt, increases to give a larger deviation between the observed and simulated results. This error can be reduced by reducing δt in the simulation.

Stratification effect

Temperature and density stratification is common in lakes located in temperate regions. This stratification can persist for some distance if the flow velocity is too low for rapid mixing. In the case of the upper St. Lawrence River, as the water comes out of Lake Ontario, the temperature remains between 0° and 4°C. In the upstream portion of the river, the flow velocity is low, and the river stratifies due to lack of mixing and intense surface heat loss. This stratification makes the one-dimensional assumption invalid. Modeling stratification requires two-dimensional models. Verifying and applying such a model require observed temperature variations with depth. When temperature observations over the depth are not available and the effects of temperature stratification have to be considered in a one-dimensional model, a simplified two-layer formulation may be used.

Lagrangian formulation for stratified flow

The governing equation for the vertical distribution of water temperature in a river with weak density stratification can be expressed as

$$\frac{\partial T_w}{\partial t} + u\frac{\partial T_w}{\partial x} + v\frac{\partial T_w}{\partial y} = \frac{\partial}{\partial x}\left(\varepsilon_x \frac{\partial T_w}{\partial x}\right) + \frac{\partial}{\partial y}\left(\varepsilon_y \frac{\partial T_w}{\partial y}\right) + \frac{\phi_v}{\rho C_p} \tag{63}$$

where T_w = water temperature
ρ = density of water
C_p = specific heat of water
ε_x, ε_y = turbulent mixing coefficients in x and y directions
ϕ_v = time rate of absorption of energy from short-wave radiation per unit volume of water.

The short-wave radiation ϕ_v decays exponentially from the top surface with increase in depth (Tennessee Valley Authority 1972).

For flows with small longitudinal temperature gradients and low vertical velocities, eq 63 reduces to

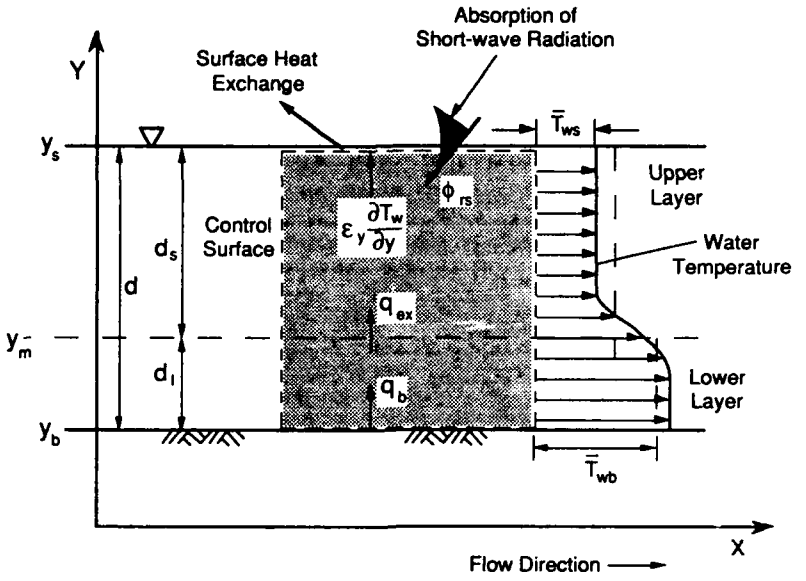

Figure 11. Definition sketch for the formulation of stratified flow.

$$\frac{\partial T_w}{\partial t} + u\frac{\partial T_w}{\partial x} = \frac{\partial}{\partial y}\left(\varepsilon_y \frac{\partial T_w}{\partial y}\right) + \frac{\phi_v}{\rho C_p}. \tag{64}$$

By dividing the river water into a colder upper layer and a warmer lower layer as shown in Figure 11, a two-layer formulation can be developed. Integrating eq 64 over the assumed upper layer from level $y = y_m$ to $y = y_s$ yields

$$\frac{\partial \bar{T}_{ws}}{\partial t} + \bar{u}\frac{\partial \bar{T}_{ws}}{\partial x} = \frac{1}{d_s}\left[\varepsilon_y \frac{\partial T_w}{\partial y}\right]_{y=y_m}^{y=y_s} + \frac{\phi_{vs}}{\rho C_p d_s} \tag{65}$$

where

$$\bar{T}_{ws} = \frac{1}{d_s}\int_{y_m}^{y_s} T_w\, dy \tag{66}$$

$$d_s = y_s - y_m \tag{67}$$

and d is the river depth $y_s - y_b$ and ϕ_{vs} is the total rate of absorption of short-wave radiation by the surface layer. At the top boundary the heat exchange with the atmosphere, as given by eq 42, is

$$\varepsilon_y \frac{\partial T_w}{\partial y}\Big|_{y=y_s} = -\frac{\phi_s}{\rho C_p} \tag{68}$$

where ϕ_s is the total heat loss at the top surface of water excluding the absorption of short-wave radiation within the depth. Heat exchange at $y = y_m$ can be expressed using a simple relationship

$$q_{ex} = \varepsilon_y \frac{\partial T_w}{\partial y}\Big|_{y=y_m} = \frac{\varepsilon_y'}{\delta_d \rho C_p}\left(\bar{T}_{ws} - \bar{T}_{wb}\right) \tag{69}$$

where q_{ex} = rate of heat exchange at the interface $y = y_m$

$\bar{T}_{wb}$ = average temperature of the lower layer
ε_y' = average turbulent mixing coefficient across the mixing zone
δd = thickness of the mixing zone between two layers.

Substituting eq 69 into eq 65 yields

$$\frac{\partial \bar{T}_{ws}}{\partial t} + \bar{u}\frac{\partial \bar{T}_{ws}}{\partial x} = -\frac{\phi_s}{\rho C_p \alpha_m d} - \frac{\varepsilon_y'(\bar{T}_{ws} - \bar{T}_{wb})}{\delta d \rho C_p} + \frac{\phi_{vs}}{\rho C_p d_s} \tag{70}$$

where $\alpha_m = d_s/d$. In Lagrangian form, this reduces to

$$\frac{D\bar{T}_{ws}}{Dt} = -\frac{-\phi_s + \phi_{vs}}{\rho C_p \alpha_m d} - \frac{\varepsilon_y'(\bar{T}_{ws} - \bar{T}_{wb})}{\delta d \rho C_p}. \tag{71}$$

Assuming all the short-wave radiation is absorbed in the upper layer, the following relationship is derived using eq 41:

$$\frac{D\bar{T}_{ws}}{Dt} = -\frac{h_{wa}(\bar{T}_{ws} - \bar{T}_a)}{\alpha_m \rho C_p d} + \frac{E_y(\bar{T}_{wb} - \bar{T}_{ws})}{\rho C_p d} \tag{72}$$

where $E_y = \varepsilon_y'/\delta$. Similarly the following equation is obtained for the bottom layer:

$$\frac{D\bar{T}_{wb}}{Dt} = \frac{E_y(\bar{T}_{ws} - \bar{T}_{wb})}{\rho C_p}. \tag{73}$$

Equations 72 and 73 are depth-averaged equations for water temperatures in the upper and lower layers, respectively. The parameters E_y and α_m have to be determined before these equations can be solved. In the case of the St. Lawrence River, only one observation, $\bar{T}_{ws}$, is available, and hence only one parameter can be calibrated. E_y is calibrated by further assuming $\bar{T}_{wb} = 4°C$ and $\alpha_m = 0.5$.

An alternate method of modeling the average water temperature using only one calibration constant is to lump the parameters of eq 72 as

$$\frac{D\bar{T}_{ws}}{Dt} = -\frac{1}{\rho C_p}\left(\frac{h_{wa}}{\alpha_m d} + E_y\right)(\bar{T}_{ws} - T_a) - \frac{E_y}{\rho C_p}(T_a - \bar{T}_{wb}). \tag{74}$$

Assuming $\bar{T}_{wb}$, α_m, δ and E_y to be constants, eq 74 can be written using two unknown parameters, α_{wa} and β_{wa}:

$$\frac{D\bar{T}_{ws}}{Dt} = -\frac{\beta_{wa}(\bar{T}_{ws} - T_a)}{\rho C_p d} + \alpha_{wa}. \tag{75}$$

When there are no data available for evaluating α_{wa} and β_{wa}, eq 75 needs to be simplified:

$$\frac{D\bar{T}_{ws}}{Dt} = -\frac{\beta_w(T_{ws} - T_a)}{\rho C_p d}. \tag{76}$$

The parameters α_{wa}, β_{wa} and β'_{wa} are unknown. To model $\bar{T}_{ws}$ using eq 76, β'_{ws} has to be calibrated. Equation 76 is similar to eq 45 and 41 except that the heat exchange coefficient is modified for the stratification effect.

Relatively large values of β'_{wa} observed in the upper St. Lawrence River can be expected due to stratification. From eq 74, it can be seen that larger values of β'_{wa} can be attributed to $\alpha_m < 1.0$ and $E_y > 0$. Since β'_{wa} varies with T_a, eq 72 is used in the present model instead of eq 76.

Calibration of heat exchange coefficient

Calibration of E_y for a river reach is carried out based on a least-square error criterion. It is possible to minimize the sum of square errors by using an iterative scheme (Beck and Arnold 1977). Assume an initial guess value of E_{y0} for E_y, and let T_i, t_i be the n pairs of observed and simulated temperatures at the downstream ends of the reach. The predicted value for E_y in the next iteration is

$$E_y = E_{y0} - \frac{\Sigma_{i=1}^{n} (t_i - T_i) a_i}{\Sigma_{i=1}^{n} a_i^2} \tag{77}$$

where a_i is obtained numerically by simulating t_i using two close but different values of E_y:

$$a_i = \frac{\partial t_i}{\partial E_y} \approx \frac{t_i(E_y + \Delta E_y) - t_i(E_y)}{\Delta E_y} . \tag{78}$$

The difference used was $\Delta E_y = 0.01 E_y$. Two to three iterations are usually sufficient to obtain a minimum value for $\Sigma_{i=1}^{n} (t_i - T_i)^2$. The period of data used for calibration is 21 December 1979 to 16 January 1980. This period is selected because the river is ice free and the water temperature is below 4°C. When the water temperature is above 4°C, warm water stays in the upper layer relative to colder water. Calibration is first done for reaches 1–4, using known water temperature record at Kingston, to minimize the sum-of-square errors at node 5. Using these values of E_y, calibration is then continued for reaches 5–22, using the same upstream end water temperature at 1, to minimize errors at node 23. Stratification with $\alpha_m = 0.5$ was assumed only up to reach 11, because the downstream reaches are well mixed. The same procedure is continued over the entire river. Calibrated E_y values are given in Table 3. The value of $h_{wa} = 19.71$ W m^{-2} °C^{-1} used in the model was obtained from linear regression of the computed heat exchange for the St. Lawrence River with weather data (Lal and Shen 1990b).

The constants α_{wa} and β_{wa} in eq 75 or β'_{wa} in eq 76 can be calibrated using regression or any other method if data are available. Since β'_{wa} changes with air temperature, its value has to be determined for different temperature ranges for better results. Table 4 shows the values of β'_{wa} obtained for the St. Lawrence River using

Table 3. Calibrated heat exchange coefficient E_y for the St. Lawrence River.

	Location		E_y	α_m	h_{wa}
Reaches	*Starting*	*Ending*	*(W m^{-2} °C^{-1})*	*(W m^{-2})*	*(W m^{-2} °C^{-1})*
1–4	Kingston	Clayton	43.46	0.5	19.71
5–11	Clayton	Waddington	6.00	0.5	19.71
12–22	Waddington	Ogdensburg	0.00	1.0	19.71
23–32	Waddington	Massena	0.00	1.0	19.71

Table 4. Modified heat exchange coefficients for the St. Lawrence River.

	Location		β'_{wa}
Reaches	*Starting*	*Ending*	*(W m^{-2} °C^{-1})*
1–4	Kingston	Clayton	29.80
5–22	Clayton	Waddington	30.84
23–32	Waddington	Ogdensburg	19.00

the least-squares method given by eq 77 and 78. The heat exchange coefficient in the well-mixed reach between Waddington and Massena in Table 3 agrees well with that in Table 4.

ICE COVER FORMATION

Ice covers form on rivers when the water surface cools to 0°C and the heat loss over the surface continues. There are two types of ice cover formations: static ice cover formation and dynamic ice cover formation. The static formation of ice covers occurs in lakes and slow-flowing regions of rivers. In this case, ice crystals form in the supercooled surface layer and remain on the surface to form a stationary or moving skim ice cover. The formation, growth and decay of this type of ice covers are dominated by thermal effects rather than mechanical effects (Matousek 1984b). Since it can affect the frazil ice production by reducing the open water area, it is important to consider the skim ice formation in a river ice model.

Dynamic ice cover formation is dominated by the interaction of surface ice particles with each other under the influence of hydraulics and wind conditions. This type of ice cover forms due to the accumulation of the surface ice discharge. The surface ice discharge consisting of slush ice and ice floes is developed from the frazil ice that is suspended throughout the depth of the flow. Once an ice cover accumulates, surface heat loss can freeze the voids and lead to a rapid increase in strength. Dynamic ice cover formation can take place in the form of particle juxtaposition, hydraulic thickening or mechanical thickening (Pariset and Hausser 1961). Unlike the static case, dynamic formation needs an existing leading edge or an obstacle on the water surface to impede the ice movement. The thickness of the initial ice cover is governed by channel geometry, hydraulic conditions and ice properties. Formulations used to model ice cover formation are discussed in this section.

Static ice cover formation

In addition to the weather conditions the formation of skim ice is related to the turbulent intensity of the flow, which affects both the degree of supercooling of the surface water temperature in relation to the depth-averaged water temperature and the entrainment of the frazil ice crystals. Current understanding of static ice formation is limited. According to field observations in River Ohre, Czechoslovakia, Matousek (1984b) obtained the following empirical relationship:

$$T_{w,s} = T_w - \frac{\phi}{1130u + bW} \tag{79}$$

where b = 15.0 when $B \leq 15.0$ m

b = $-0.9 + 5.87 \ln B$ when $B > 15.0$ m

ϕ = rate of heat loss from the water surface to the atmosphere (W m^{-2})

$T_{w,s}$ = temperature of the water surface (°C)

T_w = depth-averaged water temperature

u = local depth-averaged flow velocity (m s^{-1})

W = wind velocity at an elevation of 2.0 m above the water surface

B = surface width in the wind direction (m).

The value of $T_{w,s}$ obtained from eq 79 is used to decide the mode of skim ice formation on the surface during the beginning of freeze-up. According to Matousek (1984b), the following criteria may be used:

- When $T_{w,s} \geq 0$°C, no ice phenomena will occur.
- When $T_w > 0$°C, a skim ice run will occur if $T_{cr} < T_{w,s} < 0$°C and $v_b > v_z$. The skim ice run will change to a frazil ice run if $v_b > v_z$
- When $T_w > 0$°C, a static skim ice cover will form if $T_{w,s} \leq T_{cr}$.
- When $T_w \leq 0$°C, a frazil ice run will occur, which will lead to dynamic cover formation.

In the above discussion v_b is the buoyancy velocity of frazil ice (m s^{-1}), v_z' is the vertical component of the turbulent fluctuation velocity and T_{cr} is the supercooled surface temperature below which static skim ice will

form. The value of T_{cr} is site dependent. Matousek obtained a value of –1.1°C for River Ohre. In the current model, T_{cr} = –0.5°C was found to describe the skim ice formation in the upper St. Lawrence River. This discrepancy may be partly caused by the use of one-dimensional velocity in eq 79.

The above formulation reflects the effect of turbulent intensity on the river ice formation process. The stability of frazil ice crystals formed in the supercooled surface layer is governed by the relative magnitudes of the vertical component of the turbulent fluctuation v_z' and the buoyant velocity of ice crystals v_b (Matousek 1984b). When $v_z' > v_b$, ice crystals formed in the surface layer are entrained into the depth of the flow. If $T_w > 0$°C, ice crystals melt into the flowing water. If $T_w < 0$°C, ice crystals grow and will be transported as frazil suspension. The equations developed by Ramseier (1970) and Zacharov et al. (1972) are used to obtain an expression for v_b (Matousek 1984b):

$$v_b = -0.025T_{w,s} + 0.005. \tag{80}$$

Matousek (1984b) used the equation developed by Makaveyev to obtain v_z' (Karaushev 1969):

$$v_z' = \frac{\sqrt{g}}{5\sqrt{(0.7C + 6)C}}\, u \tag{81}$$

where u = depth-averaged velocity of the water flow (m s^{-1})
v_z' = vertical fluctuating component of water velocity (m s^{-1})
C = Chezy's coefficient (m$^{0.5}$ s^{-1})
g = gravitational acceleration (m s^{-2}).

Equation 81 is valid for $10 < C < 60$. Figure 12 illustrates freeze-up and ice run types obtained for a given set of T_w, b and W values by Matousek. For lack of a better analytical formulation, Matousek's empirical formulation is used in the present model to determine skim and static shore ice formation. Equation 81 does not include the effect of wind on the turbulent fluctuation velocity. It gives a very low value for the turbulence fluctuation velocity on the water surface. Following is a simple derivation for turbulent velocity, similar to the one presented in Fischer et al. (1979) for vertical mixing under the influence of wind. In this method the resultant turbulent velocity fluctuation due to both wind and bed shears is obtained by assuming that the input powers of both effects can be added linearly.

To find the turbulent fluctuation velocity due to wind, the rate of work done by wind on the water surface

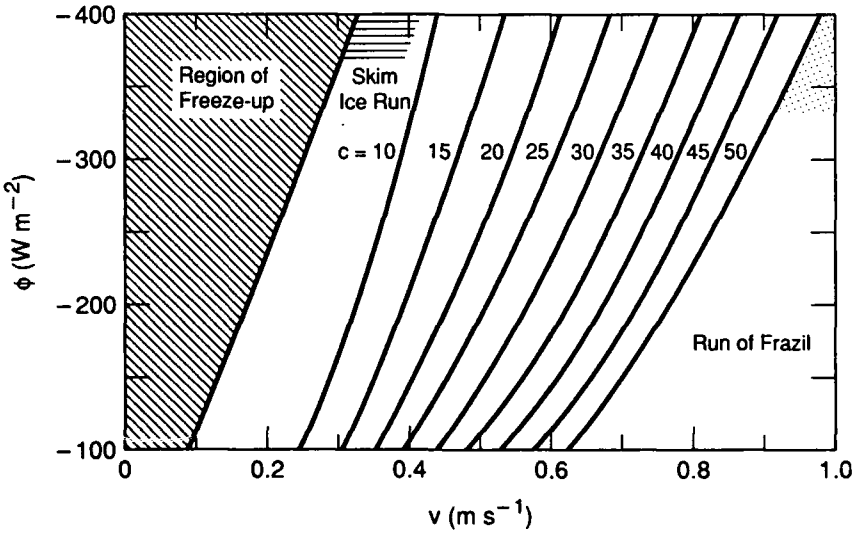

Figure 12. Relationship between ice run types, freeze-up mode and ϕ, u *and* C *at* $T_w = 0$, $b = 27$ *and* $W = 0.5$ *m s*$^{-1}$ *(Matousek 1984).*

To find the turbulent fluctuation velocity due to wind, the rate of work done by wind on the water surface P is

$$P = \tau_w u_w \tag{82}$$

where u_w is the velocity of water near the surface and τ_w is the shear stress of wind. Then,

$$\tau_w = C_D \rho_a W^2 \tag{83}$$

where W = wind velocity (m s^{-1}) at 10 m above the water surface
ρ_a = density of air (1.22×10^3 kg m^{-3})
C_D = drag coefficient.

$C_D = 1.3 \times 10^3$ is used with wind velocities measured 10 m above the water surface. The shear velocity due to wind w_* can be obtained by using

$$\tau_w = \rho w_*^2 \tag{84}$$

where ρ is the density of water. After combining with eq 83, it gives

$$w_* = \left| C_D \frac{\rho_a}{\rho} W^2 \right|^{1/2}. \tag{85}$$

Assuming u_w is of the same order of magnitude as w_*, and using τ_w of eq 84 in eq 82,

$$P \approx \rho w_*^3. \tag{86}$$

The second source of turbulence at the river surface is due to the shear at the river bed. The turbulent fluctuation velocity v' at the channel surface due to bed shear has been related to the shear velocity u_* by Rodi (1980) using plots that give the ratio C_*. This relationship can be expressed as

$$\frac{v'^2}{u_*^2} = C_* . \tag{87}$$

Rodi's experimental results show that the ratio C_* lies between 0.2 and 0.3. An expression for u_* can be obtained using the following equations:

$$u = \frac{1}{n_b} R^{2/3} S_f^{1/2} \tag{88}$$

$$\tau_o = \rho g R S_f \tag{89}$$

$$\tau_o = \rho u_*^2 \tag{90}$$

where u = average flow velocity
n_b = Manning's roughness coefficient
R = hydraulic radius
S_f = energy slope.

Equations 88–90 give

$$u_* = g^{1/2} \frac{u n_b}{R^{1/6}} . \tag{91}$$

Assuming that the input powers of bed shear and wind shear can be added, a measure of the turbulent fluctuating velocity q due to both effects can be obtained using

$$q^3 = \left(v'^3 + C_{w*} w_*^3\right) \tag{92}$$

where C_{w*} is a constant explaining the efficiency of wind energy utilization. $C_{w*} = 1$ was selected in the current study after considering different experimental observations (Fischer et al. 1979). Equations 87 and 91 are then used to obtain v', when eq 85 is used to obtain w_*. Equation 92 can now be expressed as

$$q^3 = \left(C_*^{1/2} g^{1/2} \frac{un}{R^{1/6}}\right)^3 + C_{w*}\left(C_D \frac{\rho_a}{\rho}\right)^{3/2} W^3 \tag{93}$$

where q is an indicator of the magnitude of the turbulent fluctuation velocity. In the current study, q obtained using eq 93 is used to replace the turbulent fluctuation velocity v_z of eq 81. When the condition in a given reach favors skim ice formation, the rate of growth across the width is assumed to be infinite. The maximum width up to which skim ice can form is given as input data because it depends on the distribution of flow across the width. A variable μ is used to represent the fraction of width that can be covered by skim ice. In this section, plausible empirical formulations are used for simulating static ice formations. Further studies are needed to improve the formulation.

Dynamic border ice formation

In addition to the static thermal mode, dynamic border ice can form due to the accumulation of surface ice along the shore or edges of existing border ice. This type of lateral growth is limited by the stability of surface ice particles in contact with the existing edge of the border ice. The rate of growth of the width of the border ice will also be governed by the surface concentration of the frazil ice run. The stability of the ice particles that are in contact with the edge of existing border ice is governed by the drag force acting on the particle, the component of the gravity force along the water surface, and forces from neighboring ice particles. These forces are resisted by the friction or strength at the contact point. A theoretical model that is capable of describing the above phenomena is yet to be developed. An empirical model has been proposed by Michel et al. (1980), and this study uses that model.

Based on the border ice development in the St. Anne River, Canada, Michel et al. (1980) obtained the following empirical relationship for the rate of lateral growth of border ice:

$$R = 14.1 V_*^{-0.93} N^{1.08} \tag{94}$$

where $R = \dfrac{\rho L_i \Delta W}{\Delta \phi}$

$V_* = \dfrac{u}{V_c}$

u = depth-averaged flow velocity in the open water adjacent to edge of the existing border ice (m/s^{-1})

V_c = maximum velocity at which a surface ice particle can adhere to the border ice

ρ = density of water

L_i = latent heat of fusion of ice

ΔW = growth of border ice per unit time

$\Delta \phi$ = heat exchange per unit area per unit time

$N = \dfrac{Q_i^s}{u t_i B}$ = aerial concentration of the surface ice

Q_i^s = surface ice transport rate

t_i = ice floe thickness

B = width of the reach.

According to Michel et al. (1980), only the static mode exists when $N < 0.1$, and eq 48 should be used with $N = 0.1$.

Michel et al. (1980) indicated that eq 94 is valid for $0.167 < V_* < 1.0$. When $V_* < 0.167$, static ice or skim ice formation occurs; when $V_* < 1.0$, only thermal growth occurs because frazil cannot adhere to the border ice. The rate of thermal growth is negligible. In the present study, since the static ice formation is modeled using the formulation given earlier, the lower limit is not used. For the St. Anne River, Michel et al. (1980) found that the critical velocity V_c is 1.2 m s^{-1}. According to the preceding discussion, however, this value is governed by gravity, drag and friction forces acting on the surface particle, and it will vary accordingly. For the upper St. Lawrence River, the V_c value is about 0.4 m s^{-1} for typical flow conditions (Shen and Van DeValk 1984).

Dynamic ice cover formation

When the ice run occurs, an ice cover may be formed due to the accumulation of surface ice on the river surface. If conditions are favorable, this type of ice cover can extend upstream with the accumulation of surface ice. In the present study, existing quasi-static ice jam theories (Pariset and Hausser 1961, Uzuner and Kennedy 1976) are used by taking into consideration the interaction between flow and ice conditions to determine the rate of ice cover progression. The present model is capable of simulating ice cover formation by particle juxtaposition, hydraulic thickening (commonly known as a narrow river jam) and mechanical thickening (commonly known as a wide river jam).

Particle juxtaposition

In regions with a relatively low flow velocity, an ice cover can form by the juxtaposition of ice floes. For an ice cover to progress in this mode, a stability condition for incoming ice floes must be satisfied. The stability of an ice floe when the leading edge thickness of the ice cover equals that of the ice floe can be determined by an equilibrium analysis of an arriving ice floe.

Pariset and Hausser (1961) and Pariset et al. (1966) suggested that the critical stability criterion can be expressed in terms of the Froude number of the flow:

$$F_{rc} = \frac{V_c}{\sqrt{gH}} = F\left(\frac{t_i}{l_i}\right)\left(1 - \frac{t_i}{H}\right)\sqrt{2g\left(1 - \frac{\rho_i}{\rho}\right)(1 - e)\frac{t_i}{H}} \tag{95}$$

where F_{rc} = Froude number of the river
V_c = critical velocity upstream of leading edge for underturning and submergence
t_i = thickness of the ice floe
H = upstream flow depth
h = H–t_i
g = acceleration of gravity
$F(t_i/l_i)$ = form factor that varies between 0.66 and 1.30
l_i = length of the ice floe.

Ashton (1974) pointed out that it is more appropriate to express the stability criterion in terms of the particle Froude number. For ice floes with $0.1 < t_i/l_i < 0.5$, the following analytical expression derived by Ashton (1974) compared well with laboratory data:

$$F_{rc}^{p} \equiv \frac{V_c}{\sqrt{\left[gt_i\left(1 - \frac{\rho_i}{\rho}\right)\right]}} = \frac{2\left(1 - \frac{t_i}{H}\right)}{\sqrt{\left[5 - 3\left(1 - \frac{t_i}{H}\right)^2\right]}} \tag{96}$$

where F_{rc}^{p} is the critical value of the particle Froude number. The effect of porosity in the ice particle is not considered in this equation. Equations 95 and 96 are identical if

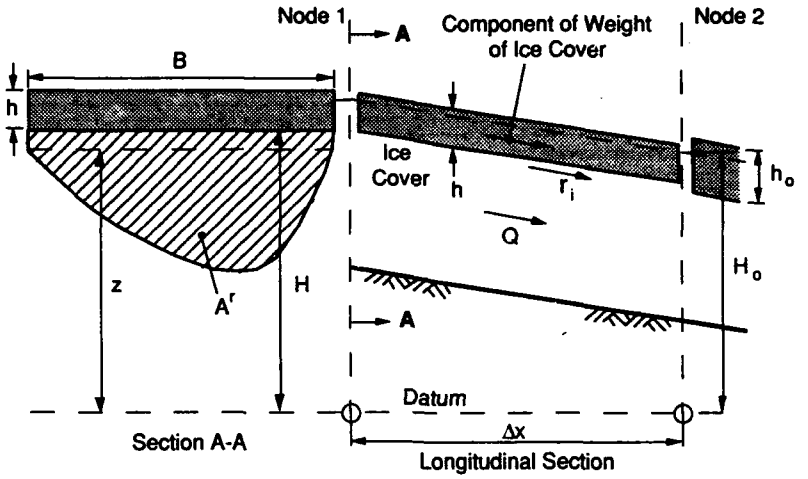

Figure 13. Definition sketch of an ice-covered river section.

$$F\left(\frac{t_i}{l_i}\right) = \frac{\sqrt{2}}{\left[5 - 3\left(\frac{t_i}{H}\right)\right]^{1/2}}.$$

The term $(1 - e)$ is introduced into eq 95 when the effect of porosity is considered.

Under the criteria given by eq 95 or 96, an ice cover of one floe thickness will form by juxtaposition. At higher velocities, ice floes will accumulate into a cover of more than one floe thick. Equations 95 and 96 require ice floe dimensions to determine the critical velocity. Since no reliable analytical method is available to determine these dimensions, field observations or calibrated V_c or F_{rc} values are used in the present model. Most laboratory data lie between $F_{rc} = 0.08$ and 0.13, while field data lie between $F_{rc} = 0.06$ and 0.08 (Kivisild 1959, Ashton 1986). For an ice floe 6.0 thick and 10.0 ft in diameter and when $F(t_i/l_i) = 1.2$ with $e = 0.5$, V_c is about 1.4 ft s^{-1}. For a flow depth of 30.0 ft, this is equivalent to $F_{rc} = 0.055$.

During the progression of an ice cover in a river reach, a simultaneous change in hydraulic conditions takes place. To improve the accuracy of the numerical computation, this change must be considered so that a reasonably large time step can be used in the simulation. The present model assumes that the local hydraulic conditions can be approximated by a backwater profile over the discretized river reach or reaches where progression takes place during the current time step.

Consider the case of ice cover progression by juxtaposition in the river reach shown in Figure 13. The ice cover is assumed to have reached node 2 at time t^n, so that conditions at node 2 are known. Energy balance between sections 1 and 2 gives

$$H + \frac{Q^2}{2gA^2} = H_o + \frac{Q^2}{2gA_o^2} + \bar{S}_f \Delta x \tag{97}$$

where $\bar{S}_f$ is the average friction slope over the reach. The subscript o denotes a variable at the downstream section whose values are known. In a typical cross section of the river, the water level H and the net flow cross area A are related by

$$A = A^r + B\left(H - z - \frac{\rho_i}{\rho} h_o\right) \tag{98}$$

where h_o is the thickness of the ice cover, which is equal to the thickness of the ice floes t_i. The friction slope $\bar{S}_f$ is obtained using eq 17. Substituting eq 98 into eq 97, the following equation can be obtained:

$$F_1(A) = \frac{A - A^r}{B} + z + t_i \frac{\rho_i}{\rho} + \frac{Q^2}{2gA^2} - H_o - \frac{Q^2}{2gA_o^2}$$

$$- 2^{1/3} Q^2 n_c^2 \Delta x \left\{ \frac{B^{4/3}}{A^{10/3}} \left[1 + \left(\frac{A}{B^2} \right)^{4/3} \right] + \frac{B_o^{4/3}}{A_o^{10/3}} \left[1 + \left(\frac{A_o}{B_o^2} \right)^{4/3} \right] \right\} = 0. \tag{99}$$

Since the thickness t is known, the flow area A can be solved by the Newton–Raphson method (Burden and Faires 1985). In eq 99 it is assumed that the entire length of Δx of the reach will be covered.

When the solution A is known, H is determined using eq 98, and the water surface profile is updated locally to take the effect of ice cover into account. If progression continues to the next reach upstream, eq 99 has to be applied to that reach using the A and t values just determined. The process continues until either the surface ice supply for the time step is used up or the Froude number exceeds F_{rc}. It should be noted that A and H values computed according to the above procedure are only the approximate values to be used to determine the ice conditions during the current time step. These values will be replaced by the solutions of the St. Venant equations at the time level t^{n+1} obtained from the hydraulic routine.

Hydraulic thickening

When the Froude number is greater than F_{rc}, the juxtaposition mode cannot exist. The ice cover will then form in the hydraulic thickening mode. The accumulation process responsible for this mode of ice cover formation is commonly known as narrow river jam formation. The equation for the narrow jam thickness was derived by Pariset and Hausser (1961) using a simple non-submergence or "no spill" condition. With a modification proposed by Michel (1971), the equation for narrow jam thickness is

$$\frac{V}{\sqrt{gH}} = \left[2 \frac{h_o}{H} (1 - e_c) \left(1 - \frac{\rho_i}{\rho} \right) \right]^{1/2} \left(1 - \frac{h_o}{H} \right) \tag{100}$$

where

$$e_c = e_p + (1 - e_p)e \tag{101}$$

and V = velocity upstream of the leading edge
h_o = equilibrium initial thickness of the ice cover
H = upstream flow depth
e_p = porosity in the accumulation representing the space between ice floes ≈ 0.4
e = porosity of an ice floe ≈ 0.2
e_c = overall porosity ≈ 0.5.

Equation 100 gives a maximum critical Froude number for progression F_{rc}^* at $(h_a/H) = (1/3)$ (Pariset and Hausser 1961):

$$F_{rc}^* = \frac{V_c}{\sqrt{gH}} = 0.158 \sqrt{(1 - e_c)} \ . \tag{102}$$

Field observations (Kivisild 1959) indicated that F_{rc}^* varies between 0.05 and 0.1. Recent studies indicated that this value is approximately equal to 0.9 in the St. Lawrence River (Shen et al. 1984) and the Yellow River (Sun and Shen 1988). Equation 100 is used to compute the initial ice cover thickness. In the hydraulic thickening case, the interaction between the ice cover formation and the hydraulics is considered using a procedure similar to that used earlier. This procedure is as follows.

For the convenience of formulation, eq 100 may be written as

$$\frac{V_u^2}{2g} = (1 - e_c)\left(1 - \frac{\rho_i}{\rho}\right) h_o \tag{103}$$

or

$$F_2(A, h_o) = Q^2 - 2gA^2\left(1 - \frac{\rho_i}{\rho}\right) h_o = 0 \tag{104}$$

where A = net cross-sectional area of flow under the cover
h_o = thickness of the initial ice cover
V_u = velocity under the ice cover
Q = $V_u A$ = river discharge.

In addition to eq 104, the energy equation (eq 99) for the flow is needed to solve for the unknowns A and h_o.

Eliminating h_o from eq 104 and 99, with t_i replaced by h_o, a nonlinear equation in the form of $F_3 = 0$ can be obtained:

$$F_3(A) = \frac{A - A^r}{B} + z + \frac{Q^2}{2gA^2\left(1 - \frac{\rho_i}{\rho}\right)}\frac{\rho_i}{\rho} + \frac{Q^2}{2gA^2} - H_o - \frac{Q^2}{2gA_o^2}$$

$$-2^{1/3}Q^2 n_c^2 \Delta x\left[\frac{B^{4/3}}{A^{10/3}}\left(1 + \frac{A}{B^2}\right) + \frac{B_o^{4/3}}{A_o^{10/3}}\left(1 + \frac{A_o}{B_o^2}\right)\right] = 0. \tag{105}$$

This equation can be solved using the Newton–Raphson algorithm.

Once A is obtained from eq 105, the value of h_o can then be obtained from eq 104. Progression will continue to the next river reach upstream from cross section 2 if more surface ice supply is available. This solution procedure should continue until the ice supply is exhausted.

A study of the behavior of eq 99 and 104 indicates that there can be two roots of A and h_o in a given river reach. This is similar to the solution of Pariset and Hausser (1961), which neglected the interaction between the ice cover formation and the hydraulic condition. In addition, there exists a Froude number beyond which no root for A or h_o exists. This Froude number corresponds to the critical Froude number for progression given by eq 102.

To obtain the correct root of A, an appropriate initial value of A has to be chosen in the Newton–Raphson procedure. As pointed out by Pariset and Hausser (1961), the smaller positive root of h_o, which occurs at a Froude number less than F_{ic}^*, is the physically correct solution. Since smaller h_o values correspond to larger A values, a larger initial trial value of A should be used in the Newton–Raphson procedure.

Mechanical thickening

In a wide or steep river the increase in streamwise forces acting on the ice cover may exceed the increase in bank resistance. In this case the internal resistance of the ice accumulation may not be able to resist the increasing stress as the cover extends upstream. If the stress in the ice accumulation exceeds its internal strength, the cover will collapse and thicken until an equilibrium thickness is reached (Pariset and Hausser 1961). This process of mechanical thickening is commonly known as shoving, and an accumulation of this kind is often called a wide river jam. When shoving occurs, a relatively long reach of ice cover will collapse, and the leading edge will move a long distance downstream before new progression occurs.

The formula for equilibrium wide jam thickness is given by Pariset and Hausser (1961) as

$$\frac{BV_u^2}{\mu C^2 H^2}\left(1 + \frac{\rho_i h_o}{\rho R_H}\right) = \frac{2\tau_c h_o}{g\rho\mu H^2} + \frac{\rho_i}{\rho}\left(1 - \frac{\rho_i}{\rho}\right)\frac{h_o}{H^2} \tag{106}$$

where B = width of the river
V_u = velocity under the cover
μ = ice-over-ice friction coefficient, approximately equal to 1.23
H = depth of water
C = Chezy coefficient
R_H = hydraulic radius of the water passage under the cover
h_o = thickness of the ice cover
ρ, ρ_i = densities of water and ice
τ_c = cohesion term in the bank shear.

According to Pariset and Hausser, $\tau_c h_o$ has an approximate range of 75–91 lbf ft^{-1} during freeze-up. The current model uses $\tau_c = 0.98$ kPa (100 kgf m^{-2} or 20.48 lbf ft^{-2}). During the break-up period τ_c is usually negligible.

Equation 106 has two roots for h_o. The smaller root is considered to be the physically correct solution for thickness. There exists a maximum discharge in the river beyond which a solution does not exist and a stable ice cover cannot exist (Pariset and Hausser 1961). For $\tau_c = 0$, when the interaction with flow is neglected, this condition is given by

$$\frac{Q^2}{BC^2H^4} \leq 2.8 \times 10^{-3}. \tag{107}$$

Based on the analysis of Uzuner and Kennedy (1976) and Pariset and Hausser (1961), the following modified form of eq 107 can be obtained for steady-state flow (Shen and Yapa 1984):

$$\left[f_i + \frac{\rho_i}{\rho}(f_b + f_i)\frac{h_o}{d_w}\right]\frac{V_u^2 B}{8g} = \frac{2\tau_c h_o}{\rho g} + \mu(1 - e_c)\left(1 - \frac{\rho_i}{\rho}\right)\frac{\rho_i h_o^2}{\rho} \tag{108}$$

where f_1 and f_2 = Darcy–Weisbach friction factors related to the ice covers and the channel bed, respectively
d_w = depth of the flow under the ice cover
V_u = flow velocity under the cover
e = porosity of the ice accumulation.

Equation 106 and eq 108 were obtained by treating the ice cover as an accumulation of granular material.

Both eq 106 and 108 were derived by assuming that the flow condition when the ice cover reaches the equilibrium thickness is known. In practice, however, only the flow condition before shoving is known. A solution procedure taking into consideration the interaction between the flow condition and the cover formation is needed. The following discussion presents a method that considers the interaction of wide jam formation with the hydraulics within a reach of the river. The method involves solving the coupled backwater and jam equations simultaneously for each reach where ice cover progression takes place, starting from the position of the existing leading edge. This method is based on the Newton–Raphson procedure similar to that presented for hydraulic thickening.

The following force balance equation can be written for the case of an equilibrium ice jam within a discretized river reach:

$$2(\tau_c h_o + \mu_1 f)\Delta x = (\tau_i + \tau_g + \tau_a)B\,\Delta x \tag{109}$$

where f = longitudinal force of ice
τ_i = shearing stress of flowing water on the underside of the cover
τ_g = component of the weight along the cover
$\tau_a = C_a \rho_a |\vec{V}_a| V_a \cos\theta_a$ = wind stress along the cover
ρ_a = density of air
V_a = wind speed
θ_a = angle between wind direction and downstream direction of the river

C_a = resistance coefficient depending on surface roughness
μ_1 = bank friction coefficient
τ_c = cohesive component of the bank shear.

Assuming complete mobilization of the granular mass, the balance between the passive resistance of the ice cover and the net longitudinal force f gives

$$f = \rho_i K_2 \left(1 - \frac{\rho_i}{\rho}\right) \frac{g h_o^2}{2} \tag{110}$$

where $K_2 = \tan^2\left(\frac{\pi}{4} + \frac{\phi}{2}\right)(1 - e_c)$
e_c = porosity of the cover
$\tan \phi$ = internal friction coefficient of the granular ice accumulation.

Before using eq 109, τ_i and τ_g have to be determined using known variables. An expression for τ_i is determined by first assuming that Manning's equation can be applied for the average flow condition prevailing in the river:

$$V = \frac{1}{n_i} R_i^{2/3} S_f^{1/2} = \frac{1}{n_c} R^{2/3} S_f^{1/2} \tag{111}$$

where R_i = hydraulic radius for the portion of the flow affected by the resistance on the underside of the ice cover
R = hydraulic radius of the entire flow cross section
V = average flow velocity
S_f = friction slope of the flow
n_c = composite Manning's coefficient.

The following expression is obtained from eq 111 for the shear stress due to flow:

$$\tau_i = \rho g R_i S_f = \rho g \left(\frac{n_i}{n_c}\right)^{3/2} R S_f . \tag{112}$$

The weight component of the ice cover in the direction of river flow τ_g is obtained by taking the weight of ice and water in the voids into account:

$$\tau_g = \rho_i g h_o S_f. \tag{113}$$

An expression for $\bar{S}_f$ is obtained using Manning's equation and approximating R as $A/2B$:

$$S_f = 2^{4/3} Q^2 n_c^2 \left[\frac{B^{4/3}}{A^{10/3}}\right]. \tag{114}$$

Substituting the expressions for τ_g, τ_i and S_f in eq 109 and using a new variable μ for $\mu_1 K_2$,

$$F_4(A, h_o) = \mu \frac{\rho_i}{\rho}\left(1 - \frac{\rho_i}{\rho}\right) h_o^2 + \frac{2\tau_c h_o}{\rho g} - 2^{1/3} \frac{Q^2 n_c^2 B^{4/3}}{A^{7/3}} \left[\left(\frac{n_i}{n_c}\right)^{3/2} + 2 \frac{\rho_i}{\rho} \frac{h_o B}{A} + B C_a \frac{p_a}{p} V_a |V_a| \cos\theta_a\right] = 0. \tag{115}$$

Equation 99 is the second equation required in the procedure. Solutions of A and h_o are obtained by solving the two nonlinear equations $F_1(A,h_o) = 0$ and $F_4(A,h_o) = 0$ simultaneously.

The solution of eq 99 and eq 115 can give two sets of roots for A and h_o. The two roots of h_o correspond to those obtained in the derivation by Pariset and Hausser (1961). In both cases the smaller root of h_o gives the correct solution.

Equation 107 for wide jams derived by Pariset and Hausser (1961) gives the condition for the existence of roots in the wide jam equation. A similar condition exists for the present analysis. When the flow rate is larger than a certain critical value, no solution exist for eq 99 and 115. This indicates that there is a critical Froude number beyond which progression will not occur. This is similar to eq 4.32 obtained by Pariset and Hausser (1961).

The interaction between ice cover progression and river flow is more significant in shallow rivers than in deep rivers, due to the large relative thickness $h_o A/B$ in a shallow river. The present procedure has an additional length parameter Δx in the formulation. Values of thickness and water depth obtained by this procedure are more accurate for smaller values of Δx.

Effect of freezing and cover stability

Michel (1986) pointed out that it takes only a little freezing to form a solid crust near the top surface of the ice cover. This can prevent shoving. Shoving can take place at any time after formation when the internal strength is not capable of withstanding the external forces. Conditions of failure of an ice cover due to shoving can be formulated by considering the force balance of a section of ice cover along the longitudinal direction.

Assuming steady uniform flow and uniform cover thickness, a force balance can be expressed using eq 109. For shoving to occur, the condition to be satisfied is given by

$$2(\tau_c h_o + \mu_1 f)\Delta x < (\tau_i + \tau_g + \tau_a)B\Delta x. \tag{116}$$

Considering that the ice cover consists of a granular accumulation with a solid ice crust near the top surface and a frazil deposit on its underside, the maximum longitudinal force f that can be exerted by the ice cover per unit width can be expressed in terms of maximum stresses in the ice cover layers:

$$f = f_i + f_n + f_f \tag{117}$$

where the subscripts i, n and f represent contributions from the solid crust, the granular layer and the frazil ice layer, respectively. Then

$$f_i = \sigma t_i \tag{118}$$

$$f_n = \rho K_2 \left(1 - \frac{\rho_i}{\rho}\right) g \left[\frac{1}{2}\frac{(1-e_n)}{(1-e_c)} t_n^2 + \left(\frac{1-e_f}{1-e_c}\right) t_f t_n\right] \tag{119}$$

$$f_f = \rho K_2' \left(1 - \frac{\rho_i}{\rho}\right) g \frac{1}{2}\frac{(1-e_f)}{(1-e_c)} t_f^2 \tag{120}$$

where t_i, t_f and t_n = thicknesses of the solid ice layer, frazil ice layer, and the granular layer, respectively
e_f and e_n = porosities of frazil ice and initial cover, respectively
σ = strength of the solid ice crust.

According to Michel (1986), $\sigma \approx 0.8$ MPa. The weight component of the ice cover in the direction of the flow is

$$\tau_g = [\rho_i g t_i + \rho_i g t_n (1 - e_n) + \rho g t_n e_n + \rho_i g t_f (1 - e_f) + \rho g t_f e_f] S_f \tag{121}$$

$$= [\rho_i (t_i + t_n + t_f) + (\rho - \rho_i)(t_f e_f + t_n e_n)] g S_f. \tag{122}$$

Using eq 112 to express τ_i and assuming $\tau_a = 0$, the right side of eq 116 can be expressed as

$$(\tau_i + \tau_g)B = \rho g S_f B \left\{\left(\frac{n_i}{n_c}\right)^{3/2} R + \frac{\rho_i}{\rho}[t_i + (1 - e_n)t_n + (1 - e_f)t_f] + e_n t_n + e_f t_f\right\} \tag{123}$$

and the left side can be expressed assuming $K_2' = K_2$:

$$2(\tau_c h_o + \mu_1 f) = 2\tau_c(t_i + t_n + t_f) + 2\mu_1\left\{\sigma t_i + \frac{\rho g K_2}{(1-e_c)}\left(1 - \frac{\rho_i}{\rho}\right)\left[\frac{1}{2}(1-e_n)t_n^2 + (1-e_f)t_n t_f + \frac{1}{2}(1-e_f)t_f^2\right]\right\}. \tag{124}$$

K_2 is defined as in eq 110. Further study is needed for estimating the value of K_2. The failure of an ice cover in a river reach can be checked using eq 116 because all ice and hydraulic conditions in eq 123 and 124 are known. Equation 124 can also be written as

$$(2\tau_c t + \mu_1 f) = 2\tau_c(t_i + t_n + t_f) + 2\sigma\mu_1 t_i + \frac{2\mu\rho g}{(1-e_c)}\left[\frac{1}{2}(1-e_n)t_n^2 + (1-e_f)t_n t_f + \frac{1}{2}(1-e_f)t_f^2\right] \tag{125}$$

in which $\mu = K_2\mu_1$. The values of the physical constants μ, K_2, and τ_c used in the wide jam case can be used in this case too. The strength of the ice cover against shoving mostly depends on the strength of the crust. The strength of the crust depends on the air temperature and the amount of solar radiation absorbed. The conditions of shoving can be more accurately predicted if the strength of crust is modeled accurately.

ICE TRANSPORT AND COVER PROGRESSION

Two-layer model for frazil suspension and surface ice transport

Ice cover progression starts with the formation of frazil ice in a river. In supercooled turbulent water, frazil ice crystals are produced over the entire flow depth. Suspended frazil particles will grow in size, may cluster together, and move up to the water surface to form surface ice runs. This upward movement is governed by the buoyant velocity and the turbulent mixing. Surface ice flocs can collect into ice pans and floes when traveling along the river. Water in the interstices can freeze to decrease the porosity of the surface ice pieces. The thickness of the surface ice pieces can increase due to the accumulation of frazil ice particles on the underside of these ice pieces and the downward freezing caused by surface heat losses.

Besides buoyant velocity and turbulent mixing, the amount of ice in the surface layer depends on the travel time and the rate of surface heat exchange. When the travel time increases, the fraction of ice discharge on the surface increases. A complete formulation for the process of frazil transport and the evolution of surface ice discharge does not exist, although the vertical transport of frazil ice suspension in a river may be described by the following advection–diffusion equation (Shen and Harden 1978):

$$\frac{\partial c}{\partial t} + u\frac{\partial c}{\partial x} + V_b\frac{\partial c}{\partial y} = \frac{\partial}{\partial x}\left(\varepsilon_x\frac{\partial c}{\partial x}\right) + \frac{\partial}{\partial y}\left(\varepsilon_y\frac{\partial c}{\partial y}\right) - \frac{\phi_v}{\rho_i L_i d} \tag{126}$$

where c = volumetric concentration of the frazil suspension
u = longitudinal velocity
V_b = buoyant velocity of frazil ice
ε_x and ε_y = horizontal and vertical mixing coefficients
d = depth of flow
ρ_i = density of ice
L_i = latent heat of fusion of ice
ϕ_v = net rate of heat gain per unit volume due to absorption of short-wave radiation.

The variable ϕ_v is a function of the distance from the water surface and the characteristics of the surface ice layer. In this study a simplified two-layer approach is used.

In the following discussion the ice discharge in the river is considered to consist of a surface layer and a suspended layer, as shown in Figure 14. The thickness of the surface layer, although it varies with time and distance, is considered to be negligible compared to the flow depth. The suspended layer is assumed to extend approxi-

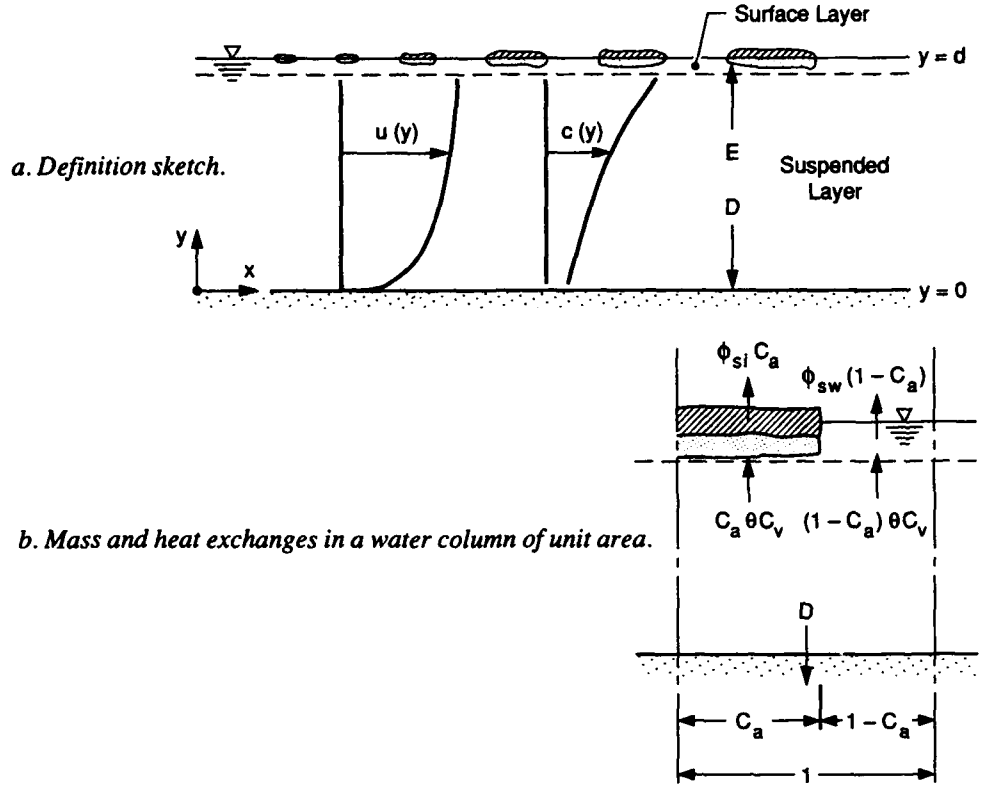

Figure 14. Two-layer system for ice transport.

mately over the entire depth. In the present model the influence of moving ice on the flow, as well as the dynamic interactions between ice particles, is neglected. Volumetric rates of ice transport in these two layers are given by the following expressions:

$$Q_s^i = [h_i + (1 - e_f)h_f]C_a B u \tag{127}$$

$$Q_d^i = C_v A u \tag{128}$$

where Q_s^i and Q_d = volumetric rates of ice discharges in the surface and in the suspended layers, respectively
h_i = solid ice thickness in the floating ice pans
e_f = porosity of the frazil ice in the surface layer
h_f = thickness of frazil ice on the underside of floating ice pans
C_a = area concentration, or the fraction of water surface area covered by floating ice particles
C_v = average volumetric concentration of frazil ice in the suspended layer
u = cross-sectional average flow velocity in the river
B = top width of the channel
A = cross-sectional area of the channel.

The velocity of ice floes in the surface layer is assumed to be the same as the mean flow velocity u.

For the surface layer, the equation of mass conservation can be written as the following:

$$\frac{\partial}{\partial t}\{[h_i + (1 - e_f)\, h_f]C_a B\} + \frac{\partial}{\partial x}\{[h_i + (1 - e_f)\, h_f]C_a B U\} = \frac{BC_a\phi_{si}}{\rho_i L} + E. \tag{129}$$

Similarly, for the suspended layer, the equation of mass conservation is:

$$\frac{\partial}{\partial t}(C_v A) + \frac{\partial}{\partial x}(C_v A u) = \frac{B(1 - C_a)\,\phi_{sw}}{\rho_i L} - D - E \tag{130}$$

where ρ_i = density of ice

L = latent heat of fusion of ice

ϕ_{si} = net rate of heat loss per unit area over the portion of the water surface covered by ice

ϕ_{sw} = net rate of heat loss per unit area over the open water portion of the water surface

D and E = net exchanges of ice flux at the bed and the interface between the surface and the suspended layers, respectively.

Longitudinal dispersion of both volumetric and surface concentrations is neglected, assuming concentration gradients are small.

The rate of mass exchange at the interface between the two layers can be expressed as

$$\frac{E}{B} = \left(-\varepsilon_y \frac{\partial C_v}{\partial y} + V_b C_v\right)_{\text{at } y = d}$$

$$= (\alpha V_b c)_{\text{at } y = d} - \gamma\left[h_i + (1 - e_f)h_f\right] C_a \tag{131}$$

where α is a coefficient representing the probability that frazil reaching the surface layer will remain there and γ is a coefficient representing the speed at which the surface ice is re-entrained into the suspension. Since ε_y is small near the water surface, it is expected that α has a value close to 1.0 and γ should be close to zero, except in rapid reaches. If we further assume that the rate of the exchange between the surface and the suspended layers E/B can be represented by $\theta V_b C_v$, and neglect the exchange at the bed D, eq 129 and 130 become

$$A \frac{DC_v}{Dt} = \frac{B\phi_{sw}(1 - C_a)}{\rho_i L} - \theta V_b C_v B \tag{132}$$

and

$$C_a B \frac{D}{Dt}\left[h_i + (1 - e_f)h_f\right] + \left[h_i + (1 - e_f)h_f\right] \frac{D}{Dt}(C_a B)$$

$$= \frac{BC_a\phi_{si}}{\rho_i L} + \theta V_b C_v B - \left[h_i + (1 - e_f)h_f\right] C_a B \frac{\partial u}{\partial x}. \tag{133}$$

By assuming that the heat loss over floating ice pans is responsible for the growth of solid ice thickness, the rate of change of solid ice thickness can be obtained using a quasi-steady-state finite-difference calculation:

$$\frac{Dh_i}{Dt} = \frac{\phi_{si}}{e_f \rho_i L}. \tag{134}$$

Expressing surface heat exchange in the form of $\phi_{si} = \alpha + \beta(T_s - T_a)$, in which T_s is the temperature at the ice surface, the rate of thermal growth of thickness can be determined.

For $h_f = 0$, and no frazil supply to the underside of ice pans,

$$\frac{Dh_i}{Dt} = \frac{1}{\rho_i L} = \frac{\alpha + \beta(T_m - T_a)}{\left(1 + \frac{\beta h_i}{K_i}\right)}. \tag{135}$$

For $h_f > 0$,

$$\frac{Dh_i}{Dt} = \frac{1}{e_f \rho_i L} = \frac{\alpha + \beta(T_m - T_a)}{\left(1 + \frac{\beta h_i}{K_i}\right)} \tag{136}$$

where T_m = melting point of ice
T_a = air temperature
K_i = thermal conductivity of ice
α and β = known constants in the heat exchange model.

Equation 136 is valid only when the solid ice does not grow beyond the bottom of the frazil accumulation at the end of the time step.

The rate of change of frazil ice thickness depends on the rate of frazil ice deposition on the underside of ice pans and the rate of downward growth of solid ice into the frazil ice deposit:

$$\frac{Dh_f}{Dt} = \frac{\theta V_b C_v}{(1-e_f)} - \frac{Dh_i}{Dt} . \tag{137}$$

Substituting eq 136 into eq 137 yields

$$\frac{Dh_f}{Dt} = \frac{\theta V_b C_v}{(1-e_f)} - \frac{1}{e_f \rho_i L} \frac{\alpha + \beta(T_m - T_a)}{\left(1 + \frac{\beta h_i}{K_i}\right)} . \tag{138}$$

As with eq136, eq 138 is valid only when the solid ice does not grow beyond the bottom of the frazil ice accumulation at the end of the time step. Since during the time step Δt the thickness of frazil deposited on the underside is

$$\frac{\theta V_b C_v}{(1-e_f)} \Delta t ,$$

the time required for the solid ice grow to the bottom of the frazil ice accumulation is

$$\Delta t' = \frac{\theta V_b C_b \Delta t}{(1-e_f)} \left[e_f \rho_i L \frac{1 + \frac{\beta h_i}{K_i}}{\alpha + \beta(T_m - T_a)} \right] . \tag{139}$$

If $\Delta t' < \Delta t$, i.e.

$$\frac{\theta V_b C_v}{(1-e_f)} < \frac{\alpha + \beta(T_m - T_a)}{e_f \rho_i L \left(1 + \frac{\beta h_i}{K_i}\right)}$$

then additional solid ice growth will occur during a period $\Delta t - \Delta t'$ according to the rate described in eq 135. Then the overall rate of growth of solid ice can be expressed as

$$\frac{Dh_i}{Dt} = \theta V_v C_v + \frac{1}{\rho_i L} \frac{\alpha + \beta(T_m - T_a)}{\left(1 + \frac{\beta h_i}{K_i}\right)} . \tag{140}$$

Equation 138 is valid only if $\Delta t' > \Delta t$.

Using eq 135 and 137 (or their equivalent), eq 133 can be further reduced to

$$\left[h_i + (1-e_f)h_f\right] \frac{D}{Dt}(C_a B) = (1-C_a)\theta V_b C_v B - \left[h_i + (1-e)h_f\right] C_a B \frac{\partial u}{\partial x} . \tag{141}$$

This equation describes the increase of ice area concentration in the surface layer due to lateral accretion and flow convergence. Solutions of variables h_i, h_f, C_v and C_a can be obtained using equations discussed above. The model has one calibration constant, θ. Since there is no analytical means to determine V_b accurately, and V_b always appears with θ, calibration can be done by considering θV_b as a single parameter. In river channels, both the ice pieces in the surface layer and the frazil ice in the suspended layer are mixtures of particles of different sizes. These size distributions are not considered in the present model. Values of h_f, h_i and θV_b can be considered as weighted average values for the mixture.

Solutions for two-layer model equations

An analytical solution for the governing equations for the two-layer model cannot be obtained. A simplified solution for the surface layer, neglecting the existence of the suspended layer, was obtained by Hausser et al. (1984) to examine the effect of floating ice on river ice production. Their solution used the following assumptions: a) all the surface heat exchange over the open water area contributes to the lateral growth of floating ice, and b) the thickness of floating ice is computed by assuming that the surface temperature of ice floes is equal to the air temperature.

The presence of surface ice floes on the water surface reduces the surface heat exchange and the total ice production rate in the river. The present model uses a quasi-steady-state finite-difference solution to estimate the effect of a surface ice layer on the reduction of heat exchange and the fraction of ice discharge in the surface layer. The parameters $\bar{\alpha}_c$ and $\bar{\alpha}_a$, which account for the effect of a surface layer, are computed separately from the main river ice model at each time step for each reach. The overbar represents the average value for a river reach. Definitions of these parameters are given by eq 142 and 143:

$$\alpha_c = \frac{Q_s^i}{Q^i} = \frac{Q_s^i}{Q_s^i + Q_d^i} \tag{142}$$

and

$$\alpha_a = \frac{Q^i}{Q_o{}^i}. \tag{143}$$

Q_s^i and Q_d are as defined in eq 127 and 128, and Q_o is the rate of ice discharge if the effect of surface ice on ice production is neglected. The value of Q_o can be calculated from $Q_o{}^i = QC_o$ and

$$\frac{DC_o}{Dt} = \frac{h_{wa}(T_m - T_a)}{\rho_i L} \tag{144}$$

where C_o is the volumetric concentration of ice calculated by neglecting the effect of surface ice.

In the present study the variation of ice conditions is solved using the Euler method (Burden and Faires 1985). By assuming a quasi-steady condition, DF/Dt in eq 132, 134, 137 and 141 can be replaced by $u(\partial F/\partial x)$. The terms on the right side are computed using values of the previous time step. A sample simulation for a steady-state case is presented below for a channel with uniform flow. The parameters used are

Air temperature	T_a	–20.0°C
Buoyancy velocity	V_b	0.001 m s^{-1}
Width	B	100.0 m
Frazil porosity	e_f	0.5
Cross sectional area	A	500 m^2
Step length	Δx	100.0 m
Initial solid ice thickness	$(h_i)_{init}$	0.005 m
Average flow velocity	$\bar{u}$	0.5 m s^{-1}.

Initial values of h_f, C_a and C_v are assumed as zero at $t = 0$. The results are shown in Figures 15–18. The Euler method was used instead of a second-order Runge Kutta method (Burden and Faires 1985) since Dh_i/Dt is discontinuous between $h_f = 0$ and $h_f > 0$.

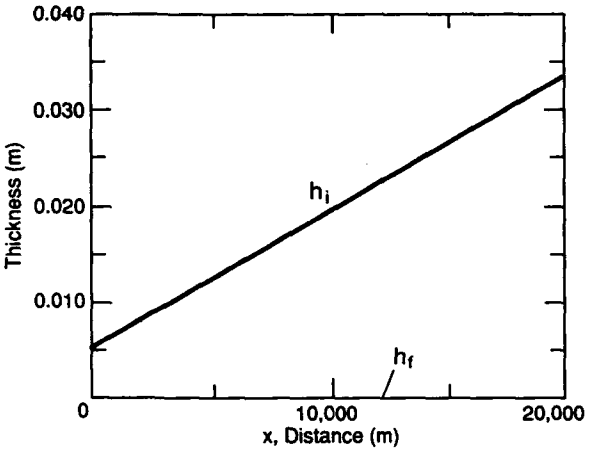

Figure 15. Variation of solid and frazil thickness with distance.

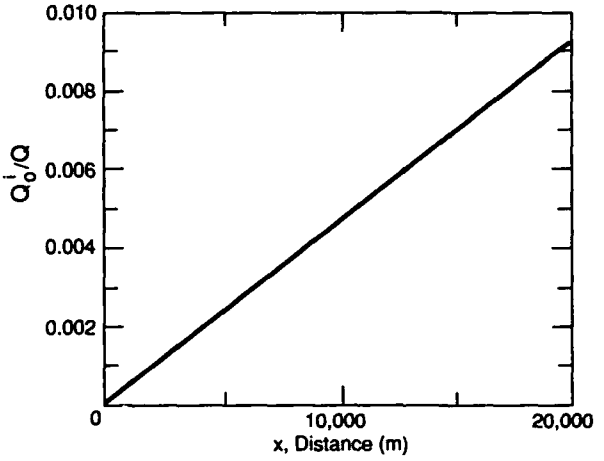

Figure 16. Ice concentration, neglecting the effect of surface ice.

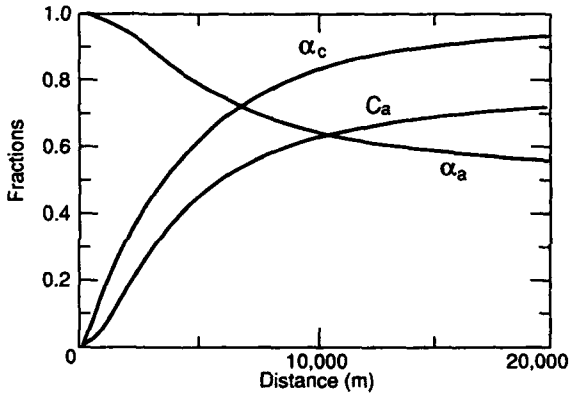

Figure 17. Variations of α_c, α_a and C_a with distance.

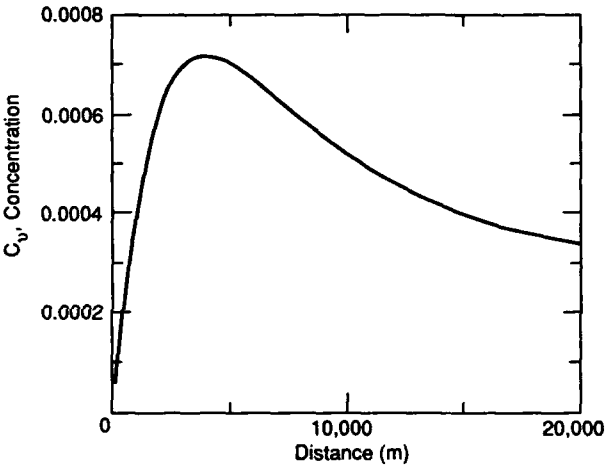

Figure 18. Variation of C_v with distance.

Figure 15 shows that the frazil ice thickness remains at zero due to the thermal growth of the solid ice. Figure 16 shows that when the effect of surface ice is neglected, the rate of ice production remains constant if the air temperature remains constant. Figure 17 shows that the rate of increase in surface area concentration C_a decreases with the travel distance due to reductions in free surface area and the suspended concentration C_v, as shown in Figure 18. The surface fraction of the ice discharge α_c increases with the increase in C_a. The ratio α_a between the total ice discharge and the ice discharge calculated by neglecting the surface ice effect decreases with increasing C_a.

Parameters α_a and α_c are used to modify the quantities of ice discharge computed in the main program, neglecting the effect of surface ice. In applying the parameter α_a, the main program is first used to compute the ice production assuming no surface ice effect. The result is then multiplied by α_a to obtain the correct ice discharge. The amount of ice in the surface layer that contributes to the cover progression is obtained by multiplying the ice discharge rate by a factor α_c.

Values of $\overline{\alpha}_c$ and $\overline{\alpha}_a$ are computed by applying the two-layer governing equations separately for each reach as described earlier. Computations are carried out reach by reach along the river starting from the upstream end of the most upstream reach having 0°C water temperature or zero isotherm. These computations are continued up to the nearest leading edge and commenced again at the zero isotherm in the next open water area. Values of variables at the downstream end of a reach are used as the upstream boundary conditions for the next reach

downstream. The longitudinal element length in this computation is obtained by dividing a reach into 20–40 equal sections to ensure the stability of the numerical scheme. Variables u, A and B are assumed to be constant in a reach. Reach-averaged values of α_c and α_a are calculated by

$$\overline{\alpha}_c = \frac{\alpha_c^u + \alpha_c^d}{2} \tag{145}$$

and

$$\overline{\alpha}_a = \frac{Q_d^i + Q_u^i}{Q_{o,d}^i + Q_{o,u}^i} \tag{146}$$

where u and d represent values at the upstream and downstream ends of the reach. Reach-averaged values of thicknesses h_i and h_f are computed in a similar manner. These values are used as the minimum ice thickness in the ice cover formation computation.

Two-layer model for skim ice run

Skim ice runs can occur in a river reach when the underlying water temperature is above freezing. In this case the lower layer does not have frazil ice suspension, and the surface ice concentration is assumed to be approximately 100%. Assuming that the entire water surface area is covered by skim ice that is free to drift with the flow, the rate of transport of skim ice is

$$Q_s^i = B\, h_i \overline{u} \tag{147}$$

where h_i is the skim ice thickness. The cross-section-averaged "water temperature" is

$$T_w = -\frac{Bh_i}{A}\frac{\rho_i L}{\rho C_p} + T_d \tag{148}$$

where T_d is the average water temperature over the flow cross section underneath the surface layer.

The rate of growth of skim ice thickness can be calculated from

$$\frac{Dh_i}{Dt} = \frac{1}{\rho_i L}\left[\frac{\alpha + \beta(T_m - T_a)}{\left(1 + \frac{\beta h_i}{K_i}\right)} - h_{wi}(T_d - T_m)\right]. \tag{149}$$

The convergence and divergence effects caused by the changing river width are neglected. The rate of change of water temperature in the lower layer can be expressed as

$$\frac{DT_d}{Dt} = \frac{h_{wi}(T_d - T_m)}{\rho C_p A}. \tag{150}$$

Equations 149 and 150 can be solved for h_i and T_d using the Lagrangian method. In the current model, quasi-steady-state solutions of the equations are obtained using the Euler method discussed earlier. Reach-averaged values of h_i are used in the model for ice cover progression.

Progression of the initial ice cover

The initiation of an ice cover occurs as a result of the obstruction of a surface ice run by natural or artificial obstacles. Natural obstacles are usually surface ice bridges formed by the congestion of surface ice runs. Static ice covers formed across the river in a slow-flow region can also act as a natural obstruction to ice runs. The most common artificial obstructions to ice runs are ice control structures, ice booms, weirs, bridges and dams.

The phenomenon of ice bridging is not well understood, even though ice bridges usually form at the same location of a river each winter. The formation of an ice bridge at a river section is related to the ice transport capacity of the section and the rate of ice discharge from upstream. The maximum rate of ice discharge that can pass through a river section not forming an ice bridge is dependent on the flow discharge, the channel top width between banks or shore ice, the surface slope, and the size and concentration of the surface ice layer, among other things (Shen et al. 1988).

When the hydraulic conditions permit, the leading edge of an ice cover will progress upstream due to the accumulation of surface ice against the leading edge. This type of ice cover progression depends on the rate of ice supply and the thickness of the ice cover formed. The conservation of surface ice mass at the leading edge gives

$$(Q_s^i - Q_u)\frac{(V_s + V_{cp}^i)}{V_s} = Bh_o(1-e)(1-e_p)V_{cp}. \tag{151}$$

The rate of progression of the leading edge V_{cp} can be obtained from

$$V_{cp} = \frac{(Q_s^i - Q_u)}{Bh_o(1-e)(1-e_p) - \dfrac{(Q_s^i - Q_u)}{V_s}} \tag{152}$$

where V_{cp} = rate of progression of the leading edge
Q_u = volumetric rate of ice entrainment under the cover at the leading edge
B = width of the ice cover
e = porosity of individual ice floes
e_p = porosity in the accumulation representing voids between floes
h_o = initial cover thickness calculated using the method discussed earlier
V_s = average velocity of the incoming surface ice particles.

Equation 152 is valid when

$$Bh_o(1-e_p)(1-e) > \frac{(Q_s^i - Q_u)}{V_s};$$

otherwise the progression will take place at an infinite speed with a larger thickness h_o' given by

$$h_o' = \frac{Q_s^i - Q_u}{B(1-e_p)(1-e)V_s}. \tag{153}$$

Further discussion of this case is given in the next section. When

$$Bh_o(1-e_p)(1-e) >> \frac{(Q_s^i - Q_u)}{V_s}$$

i.e., $V_{cp} << V_s$, eq 151 reduces to

$$V_{cp} = \frac{(Q_s^i - Q_u)}{(1-e)(1-e_p)h_o B}. \tag{154}$$

Computational procedure

Due to the advection of ice in the river, ice upstream from the leading edge at the beginning of a time step can reach the leading edge before the end of that time step. This leads to a continuous change in the rate of ice

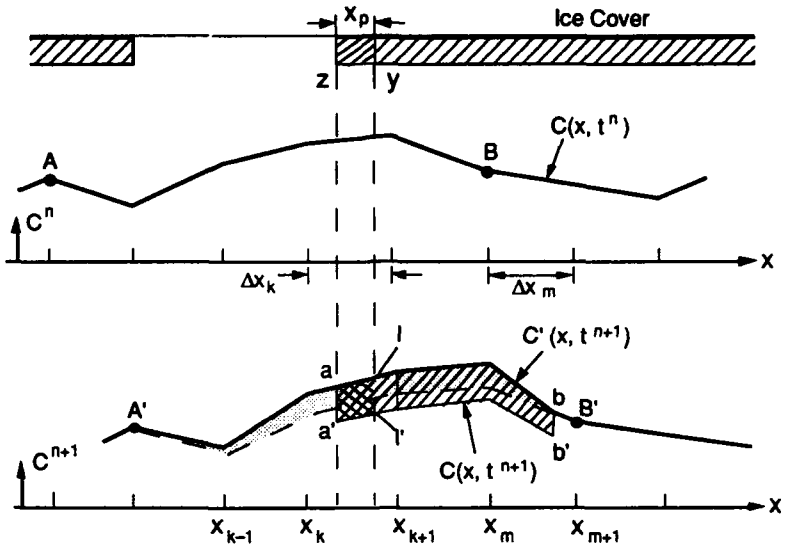

Figure 19. Definition sketch for the computation of ice cover progression.

supply at the leading edge during a time step. This effect is included in the model using a Eulerian–Lagrangian numerical procedure, similar to the water temperature simulation discussed earlier. This procedure may be considered to be a generalized upwind scheme commonly used in simulating transport processes.

The numerical procedure used in modeling ice cover progression is formulated by considering the following phenomena:

- The ice discharge that passes the leading edge during the time interval Δt will contribute to the leading edge progression during that time interval;
- The ice discharge includes contributions from the production due to surface heat exchanges and the ice volume that will be added to the ice discharge if there is a collapse of the existing ice cover;
- Only ice in the surface layer, which is assumed to be equal to an α_c fraction of the ice discharge, will contribute to the volume of ice supply for cover progression;
- The leading edge position will migrate upstream during time Δt; and
- If the leading edge progression stops before the end of the time step due to the effect of the hydraulic condition, the ice discharge passing through the leading edge after the cessation of progression will not contribute to the cover progression.

Consider the progression of the leading edge of an ice cover as shown in Figure 19. The leading edge progresses from Y to Z during the time interval between t^n and t^{n+1}. The Lagrangian scheme will first compute the ice concentration profile $C'(x,t^{n+1})$ assuming no ice cover progression. This concentration profile includes the ice production and the contribution from the collapsed surface ice cover. During this time step, ice particles located at A and B will move to A' and B'. The amount of ice passing the leading edge Y that can contribute to ice cover progression is given by the shaded area $ll'b'b$. The volume of the ice is given as

$$V_c = \overline{\alpha}_k r_k \overline{C}_k \Delta x_k A_k + \sum_{i=k+1}^{m-1} \overline{\alpha}_i \overline{C}_i \overline{A}_i \Delta x_i + \Delta t' \overline{u}_m \overline{C}_m \overline{A}_m \tag{155}$$

$$\text{where } \Delta t' = \Delta t - \left(\frac{r_k \Delta x_k}{u_k} + \sum_{i=k+1}^{m-1} \frac{\Delta x_i}{u_i} \right) \tag{156}$$

r_k = fraction of the ice-covered length in the k^{th} reach
$\overline{\alpha}_c$ = fraction of the total ice discharge contributing to cover formation
$\overline{u}_i$ = average flow velocity in i^{th} reach
$\overline{C}_i$ = average of concentration $C'(x,t^{n+1})$ of ice in i^{th} reach
$\overline{A}_i$ = average cross-sectional area of the i^{th} reach

Δx_i = length of the i^{th} reach
k = index number of the reach that contains the leading edge Y at time t^n
m = reach number where a parcel starting at the leading edge Y at time t^n is located at the end of time step Δt.

If progression ceases before the end of the time interval, then the portion of the ice volume that passed the leading edge after the cessation of progression should not be included in eq 155. This part of the concentration profile $C'(x,t^{n+1})$ is restored to its original shape.

When the volume of the ice supply V_c is known, the length of progression x_p during Δt is computed using

$$Bh_o x_p(1 - e_c) = V_c + \overline{\alpha}_c x_p \overline{C}_p \overline{A}_p \tag{157}$$

which gives

$$x_p = \frac{V_c}{Bh_o(1 - e_c) - \overline{\alpha}_c \overline{C}_p \overline{A}_p} \tag{158}$$

where h_o = average thickness of the initial cover
B = width of the new ice cover
A = average cross-sectional area of the river section
e_c = effective porosity of the ice cover
C_p = average ice concentration
p = subscript representing the reach containing the newly formed ice cover.

The case $Bh_o(1 - e_c) \leq \alpha_c \overline{C}_p \overline{A}_p$ implies that a large amount of surface ice exists in the river. This large quantity of surface ice is more than enough to form the initial cover of thickness h_o. Although rare in the field, this case is treated by assuming that the initial cover in the reach will form at a thickness larger than h_o. This thickness depends on the ice supply and is calculated by

$$h' = \frac{V_c + \overline{\alpha}_c x_p' \overline{C}_p \overline{A}_p}{B x_p'(1 - e_c)} \tag{159}$$

where $x_p' = x_k - x_Y$.

When the volume V_c is removed from the concentration profile $C'(x,t^{n+1})$, the remaining concentration profile cannot be correctly represented by only the remaining nodal point concentrations. An interpolation procedure is used to obtain equivalent nodal concentrations for $C(x,t^{n+1})$, so that the total volume of the ice and the center of mass of the ice contained in each reach remain unchanged. The latter restriction is introduced to avoid artificial advection. This procedure was discussed in detail earlier.

The ice cover cannot progress beyond a cross section where the maximum local Froude number along the width of the cross section exceeds the critical Froude number. In a one-dimensional model a considerable amount of geometrical information is lost during the schematization. It is possible for a reach having an average Froude number less than F_{rc}^* to have a cross section that has a local Froude number exceeding F_{rc}^*. In the present model, locations of possible critical cross sections, and the ratio between the local Froude number and the average Froude number of the schematized reach, are determined from the hydrographic charts. When these values are provided as input conditions, local Froude numbers can be computed from the average Froude number of the river reach. The control on the progression of ice cover can then be modeled correctly.

UNDERCOVER DEPOSITION AND EROSION

Transport and deposition of ice particles in ice-covered reaches are discussed in this section. The transport of ice particles in an ice-covered channel is similar to the transport of sediments in an alluvial river, except that ice particles move up due to buoyancy whereas sediment particles settle down. Based on this analogy, the trans-

port of ice along the river can be considered to consist of a cover load and a suspended load. Ice particles traveling on the underside of the cover at a given location can have a number of origins. They include:

- Frazil ice produced in the upstream reaches remaining in suspension (this ice will add to the undercover accumulation when it floats to the ice cover);
- Ice particles eroded from an undercover accumulation of an upstream reach or from the collapse of an existing ice cover; and
- Surface ice discharge that was swept under the ice cover at the leading edge due to unfavorable conditions for progression.

Laboratory and field studies of frazil ice transport are difficult due to the effect of thermal regimes and adverse field conditions. The present understanding of the undercover transport is rather limited. Large accumulations of ice particles on the underside of an ice cover are commonly known as hanging dams. Hanging dams may be classified into two categories depending on the formation process (Shen et al. 1983). The first type of hanging dams, referred to as surface ice hanging dams, are accumulations of large plates or frazil ice pans, which were surface ice particles underturned at the leading edge during ice cover progression. Surface ice hanging dams are formed near the leading edge of an ice cover, usually during its upstream progression. The second type of hanging dams, referred to as frazil ice hanging dams or frazil ice jams, are formed by the accumulation of suspended frazil ice particles on the underside of an ice cover.

There are two mechanisms by which surface ice hanging dams are formed. In the first mechanism, ice floes that are released from upstream reach the leading edge of an ice cover, submerge, move along the undersurface of the cover, and get arrested at some point downstream. These floes can accumulate until a hanging dam is formed. In the second mechanism the external forces acting on the ice cover exceed its strength, causing the ice cover to collapse upon itself and subsequently thicken. This second type of hanging dam is essentially a localized ice jam. Both mechanisms can occur either at the beginning of the winter during the formation of the new cover or during the spring break-up period when ice floes are generated from the fragmentation of ice covers.

Frazil ice particles suspended in a river are subjected to the buoyancy force, which tends to move ice particles upward, and turbulent mixing, which tends to disperse the particles and effectively move them from high- to low-concentration regions. Undercover deposition requires a net upward movement of particles to bring them to the underside of the cover. As the effective size of ice particles increases with time, buoyancy overcomes turbulent mixing to create a net upward movement. This upward movement can also take place when ice particles move into a slow-flow area where turbulence intensity is low. Deposition or erosion of frazil ice particles on the underside of the ice cover can change the size of a frazil ice jam.

A critical velocity, or Froude number, criterion has long been accepted as a means of determining frazil ice jam or hanging dam thicknesses (Kivislid 1959, Michel and Drouin 1975, Tesaker 1975, Ashton 1986). In the critical velocity concept, ice particles will be deposited on the underside of the ice cover if the local flow velocity is low. Changes in hanging dam size can change the flow condition. When the thickness of a hanging dam increases, the flow velocity will also increase due to the reduction in flow cross section. Deposition will cease when the velocity is high. Ice erodes from frazil ice deposits when the flow velocity is high and ice particles can no longer resist the hydrodynamic force exerted on them.

Field observations have indicated that the critical velocity varies not only from river reach to river reach but also from time to time in a given reach. We believe that the undercover deposition or erosion is governed by the ice transport capacity of the flow. Deposition will occur when the ice discharge exceeds the transport capacity of the river flow. Similarly, deposits that are not frozen onto the cover will erode when the ice discharge is less than the ice transport capacity of the flow. Unfortunately a theory does not exist that can determine the ice transport capacity of a river. Simplified critical deposition and erosion criteria will be used in the study. Erosion and deposition can take place in different parts of a river at the same time. This section describes the one-dimensional formulation used in the present model.

Deposition and erosion criteria

Because of the lack of understanding of the detailed mechanics of undercover transport and hanging dam formation, a simple critical velocity criterion is used to determine the location and size of hanging dams. Both

critical velocity and critical Froude number criteria have been suggested in the literature (Kivislid 1959, Tesaker 1975). Using the laboratory data of Filippov (1974), Ashton (1975) obtained empirical relationships for undercover travel distance of ice floes:

$$\frac{L}{l} = f\left(\frac{V}{\sqrt{gl\frac{\Delta\rho}{\rho}}}, n_i, \frac{t_i}{l}\right) \tag{160}$$

where L = undercover travel distance of an ice floe before its rest
V = mean velocity upstream of the cover
$\Delta\rho = \rho - \rho_i$
l = length of an ice block
ρ and ρ_i = densities of ice and water.

Equation 160 gives some insight into the possible patterns of ice deposition near the leading edge.

Particle stability theories can also be used to calculate accumulation thickness by determining the critical conditions for local velocity, depth and ice characteristics that allow the deposition or erosion of ice particles. Tatinclaux and Gogus (1981) carried out a laboratory study aimed at determining the re-entrainment criterion of an ice block resting under the ice cover. The following equation was developed by considering the rotational stability of an ice floe along with laboratory experiments using simulated floes:

$$F_e \equiv \frac{V_c}{\left[\left(1-\frac{\rho_i}{\rho}\right)gh\right]^{1/2}} = \frac{1}{\left[c_1\left(\frac{h}{L}\right)^2 + c_2\left(\frac{h}{L}\right) + c_3\right]} \tag{161}$$

where F_e = densimetric Froude number
V_c = critical velocity under the cover for erosion
ρ = density of water
ρ_i = density of ice
h = block thickness
L = length of the block
c_1 = −2.26
c_2 = 2.14
c_3 = 0.015.

At velocities greater than V_c, thickening should not occur. These laboratory studies are not sufficient to make them usable in field applications.

Field studies in the upper St. Lawrence River suggested that the critical velocity for ice deposition is around 3.0 ft s^{-1} (Shen et al. 1983). These studies also show that hanging dams are affected by the transverse distribution of the river flow. Once deposited in a hanging dam, frazil ice undergoes morphological and structural changes, and the critical velocity can change accordingly.

Based on observations in the LaGrande River, Michel and Drouin (Ashton 1986) suggested the following critical velocities for ice deposition:

- In narrow sections the critical velocity ranges from 0.9 m s^{-1} at the beginning of the winter to 0.5 m s^{-1} at the end.
- In wide sections the critical velocity ranges from 0.8 m s^{-1} at the beginning of the winter to 0.5 m s^{-1} at the end.
- After making corrections for back eddies and low flows, the local velocity of deposition is 0.9 m s^{-1}.

In a recent study in the Yellow River near Hequ, Sun and Shen (1988) obtained an empirical relationship between the thickness of frazil accumulation and the Froude number. They pointed out the inadequacy of the critical velocity criterion. However, in view of the lack of a better method, the critical velocity criterion is used in the present model.

Simulation of undercover deposition

Both ice cover progression and undercover erosion and deposition depend on the frazil ice concentration distribution in the river. As explained earlier, progression takes place when surface ice reaches the leading edge of an existing ice cover. Similarly, deposition can take place when frazil ice reaches the bottom surface of an ice cover. Surface ice that is swept under the cover at the leading edge will also contribute to the undercover deposition.

The rate of undercover deposition depends on the rate of ice supply reaching the underside of the ice cover. The distribution of frazil ice under an ice cover can be represented by the following transport equation, which is similar to eq 126:

$$\frac{\partial c}{\partial t} + u\frac{\partial c}{\partial x} = \frac{\partial}{\partial x}\left(\varepsilon'_x \frac{\partial c}{\partial x}\right) + \frac{\partial}{\partial y}\left(\varepsilon'_y \frac{\partial c}{\partial y} - V_b c\right) \tag{162}$$

where ε'_x and ε'_y are turbulent mixing coefficients for flow under the ice cover. The source term is not considered in this equation, assuming short-wave radiation does not penetrate the ice cover. The boundary condition at the top boundary is

$$\varepsilon_y \frac{\partial c}{\partial y} - v_s(1-\alpha)c = 0 \quad \text{at } y = d_w \tag{163}$$

where d_w is the depth of flow measured from the channel bottom to the bottom of the ice accumulation and α is an adsorption coefficient or the probability that a particle reaching the top surface will remain at the surface. At the channel bottom, assuming there is no bottom heat exchange or anchor ice formation,

$$\varepsilon_y \frac{\partial c}{\partial y} - v_s c = 0 \quad \text{at } y = 0. \tag{164}$$

In a one-dimensional model, only depth-averaged concentrations can be considered.

Transport of frazil ice

The ice volume that can deposit in a given reach can be computed in a manner similar to the case of progression. The fraction of the total ice discharge β that can contribute to deposition in a given reach is determined first. Since the total ice discharge is known at the end of a Lagrangian step, the volume of ice supply to the deposit can be obtained by multiplying it by β.

In one-dimensional form the mass conservation of the ice in suspension can be written as

$$\frac{\partial}{\partial t}(C_v A) + \frac{\partial}{\partial x}(C_v A u) = B\left[\left(\varepsilon_y \frac{\partial c}{\partial y} - V_b c\right)_{y=d_w} - \left(\varepsilon_y \frac{\partial c}{\partial y} - V_b c\right)_{y=0}\right] \tag{165}$$

where C_v is the depth-averaged ice concentration. Assuming no exchange at the bed and replacing the square bracket term on the right side by $\theta_1 V_b C_v$, eq 165 becomes

$$\frac{\partial}{\partial t}(C_v A) + \frac{\partial}{\partial x}(C_v A u) = -B\theta_1 V_b C_v \tag{166}$$

where $\theta_1 V_b C_v$ represent the rate of deposition of the frazil ice accumulation. Assuming steady uniform flow, this equation can be approximated by

$$Au\frac{dC_v}{dx} = -B\theta_1 V_b C_v. \tag{167}$$

The variation of C_v along the river becomes

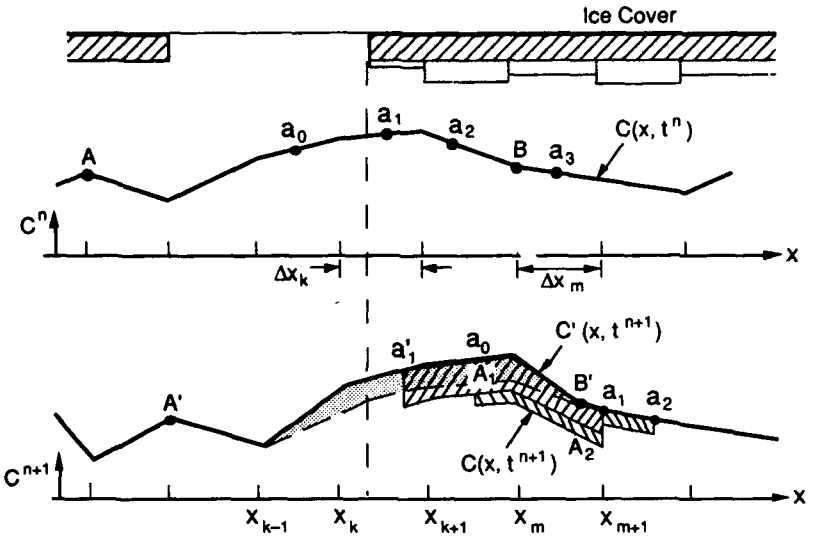

Figure 20. Definition sketch for the computation of under-cover deposition.

$$C_v(x) = C_0 \exp\left(-\frac{\theta_1 V_b B x}{Au}\right) + \text{constant} \tag{168}$$

where C_0 is the concentration at the upstream end. For a reach of length Δx, eq 168 gives

$$C_2 = C_1 \exp\left(-\frac{\theta_1 V_b \Delta x}{Au}\right) \tag{169}$$

where C_1 is the average concentration at the beginning of the reach and C_2 is the average concentration at the end of the reach. Let the coefficient β represent the factor of the reduction of ice concentration over the distance Δx. Then

$$\beta = \frac{C_1 - C_2}{C_1} \tag{170}$$

and

$$\beta = 1 - exp\left(\frac{\theta_1 V_b B \Delta x}{A\bar{u}}\right). \tag{171}$$

The concentration of ice remaining in the suspension after deposition is $(1-\beta)C_1$. The parameter $\theta_1 V_b$ is to be determined by calibration against field data.

Computation of the ice supply that is available for deposition is similar to that for ice cover progression explained earlier. Consider the longitudinal frazil ice concentration profiles at times t^n and t^{n+1} as shown in Figure 20. Parcels A and B at time t^n move to A' and B' at time t^{n+1}. In the computation, ice particles are first transported to new positions at the end of the time step, as shown by $C'(x,t^{n+1})$, ignoring deposition. The volume of ice that is available for deposition to each reach is then calculated and deducted from $C'(x,t^{n+1})$ at the end of the time step.

Concentrations at the center of each reach, as represented by a_0, a_1 a_2, and a_3 in Figure 20, are considered to be representative for the reach. The volumes of ice that are available for deposition in reaches Δx_k and Δx_{k+1} are represented by A_1 and A_2 in Figure 20. The volume corresponding to A_1 is

$$V_d = \frac{r_k}{2} \beta_k \bar{C}_k \bar{A}_k \Delta x_k + \sum_{i=k+1}^{m-1} \beta_1 \bar{C}_i \bar{A}_i \Delta x_i + \Delta t' \bar{u}_m \bar{C}_m \tag{172}$$

where

$$\Delta t' = \Delta t - \left(\frac{1}{2} \frac{r_k \Delta x_k}{\bar{u}_k} + \sum_{i=k+1}^{m-1} \frac{\Delta x_i}{\bar{u}_i} \right) \tag{173}$$

and r_k = fraction of ice covered length in the k^{th} reach
β_i = fraction of total ice discharge in the reach that can contribute to deposition
$\bar{u}_i$ = average flow velocity in the i^{th} reach
$\bar{C}_i$ = average volumetric concentration of ice in the i^{th} reach determined by interpolation
$\bar{A}_i$ = average cross-sectional area of reach
Δx_i = length of the i^{th} reach
k = number of the reach that contains the leading edge at time t^n
m = number of the reach where the particle B (starting at the leading edge at time t^n) would be located at the end of the time step.

Ice deposition proceeds reach by reach from the leading edge of the ice cover downstream. A particle moving under the ice cover is to be deposited under the first ice-covered reach it meets unless the flow velocity is above the critical limit. If all the ice volume available cannot be accommodated in a given reach due to the limitation imposed by the critical velocity criterion, the excess ice will remain in the concentration profile and be deposited downstream. The final concentration profile $C(x,t^{n+1})$ at the end of the time step is obtained by removing all the ice deposited under the ice-covered section from the ice concentration profile $C'(x,t^{n+1})$. The final concentration profile is shown by the unshaded area in Figure 20. Conversion of the final shape into a shape that can be expressed using single nodal values is done by interpolation.

Thickness of a frazil deposit

The thickness of a frazil deposit under an ice cover depends on the amount of frazil ice that is available for deposition and the hydraulic conditions that determine the limiting condition for deposition. As ice deposits under the ice cover, the hydraulic conditions are affected due to the reduction in the flow cross section. The following derivation assumes that the hydraulic conditions do not change significantly during a time step and that the water level remains unchanged before and after deposition. Based on the critical velocity criterion, the condition for deposition of frazil ice under the ice cover can be expressed as

$$\frac{Q}{A} \le v_d \tag{174}$$

where v_d = critical velocity for ice deposition
A = net area of flow
Q = flow rate in the river.

Assuming that the ice cover is floating freely, the following expression is obtained by equating the river cross-sectional areas under the water level before and after deposition during a time step:

$$A_o + B\left(\frac{\rho_s}{\rho_w} h_s + \frac{\rho_i}{\rho_w} h_i + \frac{\rho_n}{\rho_w} h_n + \frac{\rho_f}{\rho_w} h_{fo}\right) = A + B\left(\frac{\rho_s}{\rho_w} h_s + \frac{\rho_i}{\rho_w} h_i + \frac{\rho_n}{\rho_w} h_n + \frac{\rho_f}{\rho_w} h_f\right) \tag{175}$$

where ρ_w, ρ_s, ρ_i, ρ_n and ρ_f = densities of water, snow, solid ice, initial cover formed by ice fragments and frazil ice layers, respectively, as defined earlier
h_{fo} and h_f = frazil ice thicknesses before and after deposition
B = average width of the river

Substituting A of eq 174 into eq 175, the following equation is obtained for the maximum thickness of frazil deposition:

$$h_{fc} = h_{fo} + \frac{\rho_f}{\rho_w}\left(\frac{A_o}{B} - \frac{Q}{Bv_d}\right) \tag{176}$$

where h_{fc} is the maximum allowable thickness of a frazil deposit. The maximum volume of ice that can be deposited with a uniform thickness is given as

$$V_{fm} = B\, r\Delta x(1 - e_f)\,(h_{fc} - h_{fo}) \tag{177}$$

where r is the fraction of the ice-covered length in Δx and e_f is the porosity of the frazil deposit. Since a simplified formulation is used in treating the interaction between the ice deposition and hydraulics during a time step, the allowable frazil deposit thickness calculated is not precise. The interaction effect can be considered more accurately by a formulation similar to that for ice cover formation described earlier. However, since the rate of deposition is generally small and the interaction will be accounted for in the next time step, the simplification used in the present model is acceptable.

Erosion of frazil ice

Frazil ice is assumed to erode when the local flow velocity over frazil ice increases beyond a critical value v_e. The critical velocity of erosion can be expected to be higher than the critical velocity of deposition because the bond between frazil particles in the deposit may have been increased due to sintering and freezing. The incipient condition for frazil ice erosion has some similarity with the incipient conditions for sediment erosion, but modeling in the case of frazil ice is more difficult because of the effects of metamorphism of ice. The model needs v_e as an input, which can be obtained from field observations or calibrated using observed flow and ice conditions.

As shown in Figure 20, if the k^{th} reach is subjected to erosion, eroded ice particles will be re-entrained into the flow and distributed between a_1' and a_1 during the time step Δt. Since there is no theory available for estimating the rate of erosion, the current model assumes a rate of erosion that will add a concentration equal to the current concentration in the river.

When the water temperature is above freezing, part of the eroded frazil ice will first absorb the latent heat of water to melt and bring the water temperature down to 0°C. This concentration can be computed by distributing the remaining volume of ice in the flow passing over the section. Erosion in warm water (above freezing) is possible during break-up.

The maximum thickness of a frazil deposit that can remain after erosion h_{fc} is governed by the following critical velocity criterion:

$$\frac{Q}{A} \le v_e \tag{178}$$

where v_e is the critical velocity of erosion. An expression for h_{fc} is

$$h_{fc} < h_{fo} + \frac{\rho_f}{\rho_w}\left(\frac{A_o}{B} - \frac{Q}{Bv_e}\right). \tag{179}$$

The volume of ice that enters the stream as a result of erosion is given by

$$V_{fm} = Br\Delta x\,(h_{fo} - h_{fc})\,(1 - e_f). \tag{180}$$

THERMAL GROWTH AND DECAY OF ICE COVERS

The thickness of an ice cover can be changed by thermal growth and decay as a result of heat exchange with the atmosphere and the river water. Determining the ice cover thickness is important in river ice modeling. The ice cover thickness can affect the flow cross-sectional area and hence the velocity of the flow. The ice cover thickness is also important in determining the stability of an ice cover and its break-up. A solid ice cover can

consist of layers of black ice and white ice in addition to a snow cover and frazil accumulations. When repeated cycles of heavy snowfalls and cooling take place, the formation of slush layers sandwiched between white ice layers can occur.

The rate of thermal growth and decay of an ice cover is governed by the heat exchange at the top and bottom surfaces and the heat conduction in the ice cover. Heat exchange across the top surface depends on air temperature, wind velocity, humidity, short- and long-wave radiation, albedo and cloud cover. Heat exchange at the bottom surface depends on water temperature and flow velocity. Heat conduction depends on the thermal conductivities of ice, snow or white ice, which are functions of porosity. Since the horizontal extent of the ice cover is much larger than its thickness, the growth or decay of an ice cover can be treated as a one-dimensional problem. Many methods have been used to model the thickness of ice covers.

Although a numerical solution of the full unsteady equations is possible, simple steady-state solutions are commonly used in river ice problems because the thicknesses involved are small. The current model assumes a quasi-steady state and uses a finite-difference method to model the variation of black and white ice thicknesses with time. A linear heat transfer model is used to compute the heat exchange at the top surface, and a turbulent heat exchange coefficient is used to model the heat exchange at the bottom.

The degree-day method (Stefan 1891) has long been used for predicting ice cover thicknesses in lakes and rivers. In this method the ice thickness h is given as

$$h = \alpha_h \sqrt{S} \tag{181}$$

where $S = \int_{t_0}^{t} (T_m - T_a)dt$ = cumulative freezing degree-days of air temperature since the formation of the cover at time t_0

t = time from the formation of the ice cover

T_m = freezing temperature of water

T_a = air temperature

α_h = empirical degree-day constant.

Typical values of α that have been used for ice covers of different conditions are shown in Table 5. Equation 181 cannot be used to simulate the melting of an ice cover.

Table 5. Typical values of α_h (from Michel 1971).

Ice cover condition	α_h *(cm °C$^{-1/2}$ day$^{-1/2}$)*
Windy lake with no snow	2.7
Average lake with snow	1.7–2.4
Average river with snow	0.4–0.5
Sheltered small river with rapid flow	0.7–1.4

Bilello (1980) suggested the use of accumulated thawing degree-days to describe the decay and break-up of ice covers. In his model the ice thickness is given as

$$h = h_{max} - \alpha_o S_T \tag{182}$$

where h_{max} = maximum ice thickness at the beginning of decay

S_T = accumulated thawing degree-days

α_o = empirical constant.

Shen and Yapa (1985) developed a unified degree-day method for simulating the thermal growth, decay and break-up of river ice covers in the St. Lawrence River. In this model the variation of the ice cover thickness was related to the ambient air temperature using the formula

$$h = (h_0^2 + \alpha_r S)^{1/2} - \beta t^{\theta} \tag{183}$$

where h = ice cover thickness
h_o = initial ice cover thickness
α_t, β, θ = empirical constants.

The coefficient α_t is a function of time.

A number of finite-difference models were developed to determine the ice cover thickness in lakes and seas. Maykut and Untersteiner (1971) presented a one-dimensional model for sea ice that included the effect of snow cover, salinity and internal heating due to short-wave radiation. The model was applied to the central Arctic to simulate the thicknesses of young sea ice when the thickness was on the order of a few meters. In the model, heat exchange at the top surface, ocean heat flux, snow accumulation, ice salinity and albedo were treated as inputs that change with time.

Simulation models for sea or lake ice covers have undergone many improvements over the years (Maykut 1978, Sydor 1978, Wake and Rumer 1979, Miller 1980, Gabison 1987). Ashton (1979) developed models describing the suppression of river ice by a thermal effluent. In Ashton's model the convection of thermal energy in the river water was simulated numerically using a Lagrangian scheme. Surface heat exchange across the air/ice interface and the air/water interface were expressed using simple equations and heat transfer coefficients. Greene (1981) developed a numerical model and an analytical model. These models were used to simulate ice cover thicknesses in the upper St. Lawrence River. A detailed numerical model by Shen and Chiang (1984) treated the river as a coupled air–ice–water–bed system by taking into account the heat exchange at all the interfaces in the system. Simulated results for the St. Lawrence River were in good agreement with observed data.

Leppäräntä (1983) and Bengtsson (1984) considered the effect of snow ice formation. In Leppäräntä's model, snow slush was directly transformed to snow ice, completely neglecting the thermal process. The snow surface temperature was assumed to be the same as the air temperature. The packing of the snow layer was included using an empirical formulation. Bengtsson considered the effect of the surface thermal resistance and the conductivity of white ice in calculating black ice growth. Unfrozen snow slush between layers of white ice was directly converted to snow ice. The existence of the capillary fringe in the snow slush was neglected in both these studies.

Shen and Lal (1986) included the effects of capillary rise and the layered formation of white ice in a thermal growth and decay simulation model. The insulating effect of the snow layer and the presence of frazil ice were also considered in this model. Heat exchanges at the top and bottom surfaces were computed using a linear model and a turbulent heat exchange coefficient, respectively. The model can simulate thickness variations of black ice, white ice, snow and slush, if the weather conditions, snowfall, frazil thickness and porosities are given. The simulation of thermal growth and decay in the present study is based on a simplified version of the model of Shen and Lal (1986). It is capable of simulating both black and white ice thickness as well as snow and snow slush thicknesses.

All of the previous river ice models assumed quasi-steady-state thermal conditions in the cover. This approximation is justified in view of the small river ice thickness with respect to the time step used in the computation (Greene 1981).

Surface heat exchanges

The turbulent heat exchange at top and bottom surfaces of an ice cover governs the rate of change of the ice cover thickness. In the present model the heat exchange at the top surface is expressed using a linearized model similar to eq 43 proposed by Dingman and Assur (1969):

$$\phi_T = -\phi_R + \phi_n \tag{184}$$

and

$$\phi_n = \alpha_i + \beta_i(T_s - T_a) \tag{185}$$

where ϕ_T = net heat flux to the atmosphere from ice or snow surface (W m^{-2})
ϕ_n = net heat flux to the atmosphere excluding short-wave radiation (W m^{-2})
ϕ_R = net short-wave radiation (W m^{-2})

T_s = surface temperature (°C)
T_a = air temperature (°C)
α_i and β_i = coefficients that can be derived from the complete heat exchange process including long-wave radiation, evaporation and sensible heat transfer.

To further simplify the analysis, the solar radiation is sometimes lumped into the linear model:

$$\phi_T = \alpha_i' + \beta_i' (T_s - T_a). \tag{186}$$

Since ϕ_R varies with latitude, α_i' and β_i' values depend on the latitude. Coefficients α_i, β_i, α_i' and β_i' are functions of wind velocity, cloud cover and relative humidity. The following heat exchange models were obtained from multiple linear regression analysis of weather data at Massena, New York, for five years (Lal and Shen 1990b).

For heat exchange from the snow surface to the atmosphere,

$$\phi_n = 25.21(T_s - T_a) \qquad (s = 128.1, r = 0.72) \tag{187}$$

$$\phi_n = 83.65 + 18.64(T_s - T_a) \qquad (s = 108.8, r = 0.72) \tag{188}$$

$$\phi_T = 23.36(T_s - T_a) \qquad (s = 75.7, r = 0.84) \tag{189}$$

$$\phi_T = 54.92 + 19.64(T_s - T_a) \qquad (s = 69.4, r = 0.84). \tag{190}$$

For heat exchange from the ice surface to the atmosphere,

$$\phi_n = 17.38(T_s - T_a) \qquad (s = 77.9, r = 0.79) \tag{191}$$

$$\phi_n = 64.41 + 12.32(T_s - T_a) \qquad (s = 58.0, r = 0.79) \tag{192}$$

$$\phi_T = 13.31(T_s - T_a) \qquad (s = 44.0, r = 0.85) \tag{193}$$

$$\phi_T = 32.55 + 12.19(T_s - T_a) \qquad (s = 36.9\ r = 0.87). \tag{194}$$

Statistical indicators obtained from linear regression are the standard error estimate s and the coefficient of correlation r.

Turbulent heat transfer from the flowing river water to the ice cover has been studied by Ashton (1973), Calkins (1984) and Marsh and Prowse (1987), among others. In the present study the formulation by Ashton (1973) is used. In this formulation the turbulent heat transfer is expressed as

$$\phi_{wi} = h_{wi}(T_w - T_m) \tag{195}$$

where ϕ_{wi} = heat exchange (W m^{-2})
T_w = water temperature (°C)
T_m = freezing point of water.

The coefficient h_{wi} can be evaluated by the formula (Ashton 1973)

$$h_{wi} = C_{wi} U_w^{0.8} D_w^{-0.2} \tag{196}$$

where C_{wi} = 1662 (W s$^{0.8}$ m$^{-2.6}$ °C^{-1})
D_w = flow depth (m)
U_w = average flow velocity (m s^{-1}).

The coefficient C_{wi} may be increased by up to 50% when relief features form on the underside of the cover.

Simulation of thermal growth and decay

The equation governing the one-dimensional temperature distribution in an ice cover is given by (Shen and Chiang 1984)

$$\rho_i C_i \frac{\partial T}{\partial t} = \frac{\partial}{\partial z}\left(k_i \frac{\partial T}{\partial z}\right) + \phi_v(z,t) \tag{197}$$

where t = time
z = distance measured downward from the top surface
T = temperature in the cover
k_i = conductivity of ice
ρ_i = density of ice
C_i = specific heat of ice
$\phi_v(z,t)$ = rate of internal heating of the ice cover due to the absorption of penetrated short-wave radiation.

The boundary condition at the top surface is

$$\rho_i L \frac{dh}{dt} = \phi_T - k_i \frac{\partial T}{\partial z} \quad \text{at } z = 0 \tag{198}$$

where L = latent heat of fusion of ice
h = thickness of the ice cover
ϕ_T = net heat loss at the air/ice interface.

Any water on the top surface of the ice cover is assumed to drain through the cover. In this study $dh/dt = 0$ when the cover surface temperature is below freezing. The boundary condition at the bottom boundary is

$$\rho_i L \frac{dh}{dt} = -\phi_{wi} + k_i \frac{\partial T}{\partial z} \quad \text{at } z = h \tag{199}$$

where ϕ_{wi} is the net heat flux from the water to the ice cover.

Rate of growth in the absence of frazil accumulation

Time-dependent ice growth and decay can be determined by assuming one-dimensional quasi-steady-state calculations at each time step. At steady state the solution to the governing eq 197 gives a linear temperature distribution if the rate of internal heating of the ice cover $\phi_v(z,t)$ is neglected. The quasi-steady-state assumption has been shown to be acceptable for river ice covers because of the relatively small thickness (Greene 1981, Ashton 1982). At steady state the heat flux across different layers of the ice cover is the same if there is no water in the snow cover. As shown in Figure 21, the heat flux in each layer can be obtained using $\phi = k(\partial T/\partial z)$:

$$\phi_i = \frac{k_i}{h_i}(T_m - T_2) = \phi_s \tag{200}$$

$$\phi_s = \frac{k_w}{h_w}(T_2 - T_1) = \phi_a \tag{201}$$

$$\phi_a = \frac{k_s}{h_s}(T_1 - T_s) \tag{202}$$

where k = thermal conductivity
h = thickness
i, w and s = subscripts denoting black ice, white ice and snow, respectively.

The boundary condition at the ice/water interface is obtained using eq 199 and 200:

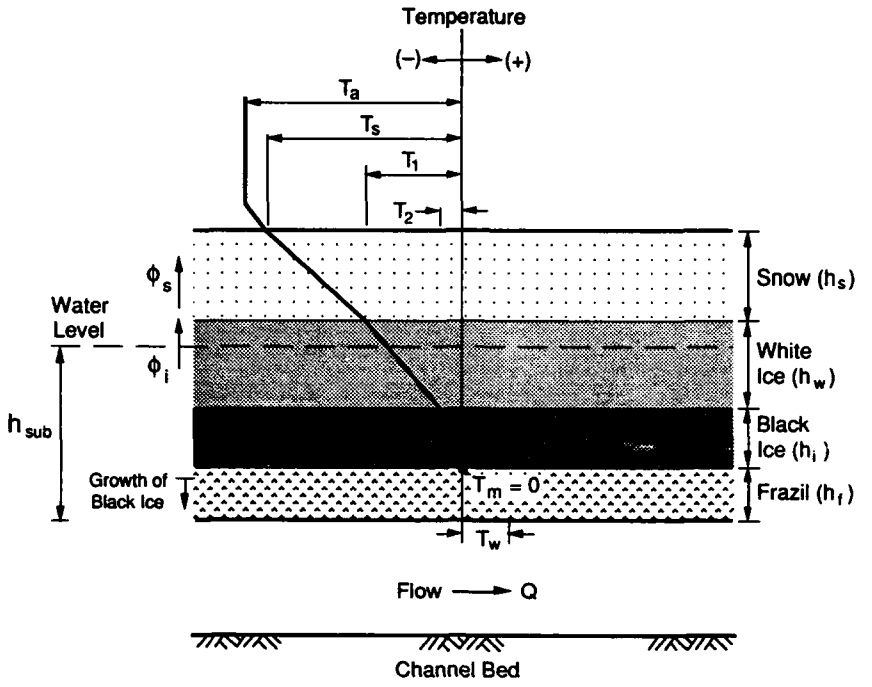

Figure 21. Thermal growth of an ice cover.

$$\phi_a - \phi_{wi} = \rho_i L \frac{dh_i}{dt} \tag{203}$$

where ϕ_{wi} is the heat flux from water to ice. In the absence of melting, the boundary condition at the top surface is obtained using eq 198 and 202:

$$\phi_a = \phi_T \tag{204}$$

where ϕ_T is the net heat exchange at the top surface. The rate of growth dh_i/dt given by eq 203 can be determined if ϕ_a or ϕ_T is known. The latter can be determined in terms of T_s using eq 184 or 186, and eq 195.

$$\rho_i L \frac{dh_i}{dt} = -\phi_R + \alpha + \beta(T_s - T_a) - h_{wi}(T_w - T_m). \tag{205}$$

T_s can be determined explicitly when a linear heat exchange model is used. Linear models given by eq 184 or 186 can be used with eq 200, 201 and 202 to eliminate T_1, T_2 and ϕ_a and obtain the following expression for T_s:

$$T_s = \frac{\left[\left(T_a + \frac{\phi_R - \alpha}{\beta}\right)\left(\frac{h_s}{k_s} + \frac{h_w}{k_w} + \frac{h_i}{k_i}\right) + \frac{T_m}{\beta}\right]}{\frac{h_s}{k_s} + \frac{h_w}{k_w} + \frac{h_i}{k_i} + \frac{1}{\beta}}. \tag{206}$$

Equation 205 is valid only if $T_s < T_m$. When there is no frazil ice accumulation, black ice growth takes place on the underside of the ice cover at a rate given by this equation.

An alternative expression for the rate of growth can be obtained by substituting eq 206 into eq 205:

$$\frac{dh_i}{dt} = \frac{-\phi_R + \alpha + \beta(T_m - T_a)}{\rho_i L \beta\left(\frac{1}{\beta} + \frac{h_s}{k_s} + \frac{h_w}{k_w} + \frac{h_i}{k_i}\right)} - \frac{h_{wi}}{\rho_i L}(T_w - T_m). \tag{207}$$

Equation 207 is also valid only when $T_s < T_m$. Under steady-state conditions, $T_s < T_m$ is synonymous with $T_a < T_m$ except when $\phi_R < \alpha$. This shows that ice cover growth takes place on most occasions when the air temperature is below freezing. Equation 207 gives the steady-state governing equation for the rate of growth of black ice. Equation 207 is valid only for $-\phi_R + \alpha + \beta (T_m - T_a) > 0$.

The condition for ice cover growth starting from skim ice of nearly zero thickness can be determined by obtaining the limiting condition for dh_i/dt to be positive as $h_i \rightarrow 0$. Using eq 207, it can be shown that the latter condition is equivalent to

$$T_a < T_m - \frac{[\phi_R + h_{wi}(T_w - T_m)]}{\beta}. \tag{208}$$

This shows that skim ice growth can start in turbulent water only if the condition in eq 208 is satisfied.

It can also be shown from eq 207 that for a given set of weather conditions, there exists an equilibrium thickness h_{ie} that has zero growth and decay or $dh_i/dt = 0$:

$$h_{ie} = -k_i \left(\frac{1}{\beta} + \frac{h_w}{k_w} + \frac{h_s}{k_s}\right) + \frac{k_i}{\beta} \frac{[-\phi_R + \alpha + \beta (T_m - T_a)]}{h_{wi}(T_w - T_m)}. \tag{209}$$

Analytical expressions for ice thickness can be obtained by solving eq 207 for h as shown below. Neglecting bottom heat transfer, the rearranged equation can be integrated as shown below:

$$\int_{h_i^o}^{h_i} \left(\frac{1}{\beta} + \frac{h_s}{k_s} + \frac{h_w}{k_w} + \frac{h_i}{k_i}\right) dh_i = \frac{1}{\rho L \beta} S \tag{210}$$

where

$$S = \int_t^{t+\Delta t} [-\phi_R + \alpha + \beta (T_m - T_a)] dt \tag{211}$$

and h_i^o and h_i are the black ice thicknesses at times t and $t+\Delta t$, respectively. The solution of the quadratic equation obtained from eq 210 is

$$h_i = -\left(\frac{k_i}{\beta} + \frac{k_i h_s}{k_s} + \frac{k_i h_w}{k_w}\right) + \left[\left(\frac{k_i}{\beta} + \frac{k_i h_s}{k_s} + \frac{k_i h_w}{k_w} + h_i^o\right)^2 + \frac{2 k_i S}{\rho_i L_i \beta}\right]^{1/2}. \tag{212}$$

The degree-day formula is a simplified form of eq 212 (Shen and Yapa 1985). This explicit expression for h_i is possible only when the heat transfer from the river flow is neglected. When heat transfer at the ice/water interface is included, eq 207 can be solved to obtain the following expression:

$$\Delta t = \frac{b}{d}(h_i - h_o) + \frac{ad - bc}{d^2} \ln\left(\frac{c + dh_i}{c + dh_i^o}\right) \tag{213}$$

where

$$a = \rho_i L \left(1 + \frac{\beta h_s}{k_s} + \frac{\beta h_w}{k_w}\right) \tag{214}$$

$$b = \frac{\rho_i L \beta}{k_i} \tag{215}$$

$$c = \phi_R + \alpha + \beta (T_m - T_a) - h_{wa}(T_w - T_m) \left(1 + \frac{\beta h_s}{k_s} + \frac{\beta h_w}{k_w}\right) \tag{216}$$

and

$$d = -\frac{h_{wa}\,\beta}{k_i}. \tag{217}$$

Since h_i cannot be expressed explicitly, eq 213 is not commonly used.

A solution to eq 205 or 207 can be obtained using a numerical procedure for solving initial value problems. Euler's algorithm provides a simple approach for solving for h_i with first-order accuracy (Burden and Faires 1985):

$$h_i = h_i^o + h_i' \Delta t \tag{218}$$

where

$$h_i' = \frac{dh_i}{dt}.$$

The error in the rate of growth for the simplified case with no snow and white ice can be shown as

$$\varepsilon = \left(\frac{dh_i}{dt}\right)_{fd} - \left(\frac{dh_i}{dt}\right)_{ex}$$

$$= \frac{1}{2}\frac{h'^2 \Delta t}{\left(h_o + \frac{k_i}{\beta}\right)}$$

$$= \frac{1}{2}\frac{\left[-\phi_R + \alpha + \beta\,(T_m - T_a)\right]^2 k_i^2}{\rho_i^2 L^2 \beta^2 \left(h_i^o + \frac{k_i}{\beta}\right)^3} \tag{219}$$

where $(dh/dt)_{fd}$ is the finite-difference approximation of (dh/dt) based on h_i^o, with $h_s = h_w = 0$. It can also be shown that the finite-difference algorithm of eq 218 is accurate only if $\varepsilon << (dh_i/dt)$, or

$$h' \Delta t << \frac{1}{2}\left(h_i^o + \frac{k_i}{\beta}\right). \tag{220}$$

Equation 220 is useful in selecting a time step for the finite-difference formulation. The error ε decreases with an increase of $(h_i^o)^3$ and will be negligible unless the thickness is very small. The accuracy of the thickness determination for very small values of h_i can be improved by using the analytical formula eq 212 until h_i becomes large enough to satisfy the condition given in eq 220.

Decay of ice cover thickness

When T_s (computed using eq 206) is greater than T_m, melting of the top surface of ice cover takes place, and the surface temperature T_s is equal to T_m. When melting takes place at the top surface, the temperature inside the ice, snow and frazil layers remains isothermal at 0°C, and thermal growth is not possible at any part of the ice cover at steady-state conditions. When a snow layer is present on the top surface of the solid ice cover, the rate of decay of the snow thickness takes place at a rate given by

$$(1 - e_s)\rho_i L \frac{dh_s}{dt} = -\phi_R + \alpha + \beta(T_m - T_a). \tag{221}$$

The rate of decay of solid ice in the absence of snow cover is

$$\rho_i L \frac{dh_{is}}{dt} = -\phi_R + \alpha + \beta(T_m - T_a) \tag{222}$$

where $h_{is}(= h_w + h_i)$ is the thickness of the solid ice.

In the above analysis the melting water is assumed to be draining through the cover. Wake and Rumer (1979) examined the magnitude of the error introduced by the assumption of a well-drained ice surface compared to an undrained ice surface. Their analysis indicated that water accumulated over melting ice has no significant effect on the rate of melting.

Thermal decay of ice can take place at the bottom of the cover when $T_w > T_m$. If the rate of melting of solid ice is given by

$$\rho_i L \frac{dh_{is}}{dt} = -h_{wi}(T_w - T_m) \tag{223}$$

where h_{wi} is given by eq 196. If frazil ice is present, decay takes place at the frazil/water interface at a rate given by

$$\rho_i L(1 - e_f) \frac{dh_f}{dt} = -h_{wi}(T_w - T_m). \tag{224}$$

Effect of frazil ice accumulation

The presence of a frazil ice layer on the underside of the ice cover can accelerate the growth of ice cover thickness because the frazil ice layer insulates the ice cover from the warm water below and because only the pore water in the frazil layer needs to be solidified for the downward growth of the ice cover. If a frazil ice layer is present below the solid ice cover, solid ice growth will take place into the frazil ice layer when $T_s < T_m$. The rate of growth is given by

$$e_f \frac{dh_{is}}{dt} = \frac{-\phi_R + \alpha + \beta(T_m - T_a)}{\rho_i L \beta\left(\frac{1}{\beta} + \frac{h_s}{k_s} + \frac{h_w}{k_w} + \frac{h_i}{k_i}\right)}. \tag{225}$$

where h_{is} is the position of the interface with respect to solid ice. Equation 225 is the same as eq 205 or 207 when there is no decay at the bottom, except that $\rho_i L(dh_i/dt)$ is replaced by $e_f \rho_i L(dh_{is}/dt)$ in the equation. Equation 225 is valid only when the solid ice does not grow beyond the bottom of the frazil accumulation. This condition is satisfied when the rate of frazil ice deposition dh_{fd}/dt is more than the rate of solidification in the interstices of the frazil layer, i.e. $dh_{fd}/dt > dh_{is}/dt$. The corresponding rate of change of frazil ice thickness in the absence of thermal erosion is

$$\frac{dh_f}{dt} = \frac{dh_{fd}}{dt}. \tag{226}$$

If the rate of frazil deposition is slow such that $dh_{fd}/dt < dh_{is}/dt$, then it is necessary to treat the growth in the frazil layer and the additional growth separately using a procedure similar to that described earlier.

Layered ice cover formation

Layered ice covers may form when repeated heavy snowfalls occur between cold weather spells. Snow slush formed as the result of ice cover submergence can form white ice as a result of cooling. However, a layer of unfrozen slush may remain entrapped if a new slush layer is formed on top of an existing slush layer. This process can lead to a layered formation in the cover. The modeling of this type of ice cover will be discussed in this section.

Submergence of the snow layer

A layer of snow can accumulate on top of the solid ice cover as a result of wind-blown snow or direct snowfall. When the snow accumulation is heavy, the bottom surface of the snow layer will sink below the water surface to form snow slush. The condition for submergence of the snow cover is

$$h_{sub} > h_w + h_i + h_f. \tag{227}$$

Balancing buoyancy forces with weight, and assuming no submergence of snow, the depth of submergence is given by

$$h_{sub} = \frac{1}{\rho_w}\left[(1 - e_s)\rho_i h_s + \rho_i h_i + (1 - e_w)\rho_i h_w + (1 - e_f)\rho_i h_f + e_f \rho_w h_f\right] \tag{228}$$

where e_s, e_w and e_f are the porosities of snow, white ice and frazil ice, respectively, and ρ_i and ρ_w are the densities of ice and water, respectively. Substituting h_{sub} of eq 228 into eq 227, the condition of submergence can be expressed in terms of the snow layer thickness:

$$h_s > \frac{\Delta\rho\left[h_i + h_w + (1 - e_f)h_f\right] + e_w h_w \rho_i}{(1 - e_s)\rho_i} \tag{229}$$

where $\Delta\rho = \rho_w - \rho_i$.

When the snow layer is thick enough to satisfy the condition given by eq 229, snow slush will form. As soon as the bottom of the snow layer submerges, a capillary fringe will form, and water rises to a height CR above the hydrostatic level. The thickness of the slush layer, after considering the effect of the capillary fringe above the phreatic surface, can be calculated assuming free-floating conditions. The thickness of the slush layer formed due to submergence is

$$h_{sw} > \frac{CR\rho_w + (1 - e_s)h_s\rho_i - h_w e_w \rho_i - \Delta\rho\left[h_i + h_w + (1 - e_f)h_f\right]}{\rho_w - \rho_{sw} + (1 - e_s)\rho_i} \tag{230}$$

where h_{sw} = thickness of the snow slush layer including the capillary fringe
ρ_{sw} = density of slush = $(1 - e_s)\rho_i + Se_s\rho_w$
CR = capillary rise
h_s = thickness of snow layer before including the snow slush
S = water saturation of the slush, which is the fraction of voids filled with water.

Equation 230 is valid for $h_{sw} \le h_s$. The thickness of dry snow left is $h_s - h_{sw}$. If $h_{sw} > h_s$, no dry snow can exist, and $h_{sw} = h_s$.

Formation of white ice

A consequence of the presence of the slush layer formed by the submergence of the snow cover is the formation of white ice. As a result of surface heat loss, white ice will grow downward from the top surface of the slush layer, starting from zero thickness. The portion of the cover below the top surface of the slush layer will remain isothermal at 0°C. The surface temperature of the cover can be determined using eq 206 by setting $h_w = h_i = 0$. If dry snow is present on top of the slush,

$$T_s = \frac{\left[\frac{h_{sd}}{k_s}\left(T_a + \frac{\phi_R - \alpha}{\beta}\right) + \frac{T_m}{\beta}\right]}{\frac{h_{sd}}{k_s} + \frac{h_w}{k_w} + \frac{1}{\beta}} \tag{231}$$

where h_{sd} is the thickness of the dry snow layer left over slush. If $T_s < T_m$, the rate of growth of white ice can be calculated using the equation

$$\rho_i L e_s S \frac{dh_w}{dt} = -\phi_R + \alpha + \beta(T_s - T_a) \tag{232}$$

which is valid for $(dh_w/dt) > 0$ or $-\phi_R + \alpha + \beta(T_s - T_a) > 0$, as mentioned before. If there is no dry snow left on the ice cover after the capillary rise, white ice will grow downwards starting from the top surface in the slush layer. The growth rate can be determined by eq 232, with T_s given by

$$T_s = \frac{\left[\frac{h_w}{k_s}\left(T_a + \frac{\phi_R - \alpha}{\beta}\right) + \frac{T_m}{\beta}\right]}{\frac{h_w}{k_w} + \frac{1}{\beta}}. \tag{233}$$

When computing the ice thickness starting from zero, the error term involved with dh_w/dt is large for small values of h_w, as described earlier. The error can be reduced by using an analytical solution similar to eq 212.

In the case of multiple slush layers, if the top slush layer is completely frozen to form white ice, the next layer below will freeze from top to bottom, and the process will continue. The rate of growth of white ice can be determined using eq 205 and 206. Black ice growth starts only after all the snow slush is frozen.

MODEL APPLICATION AND CONCLUSION

Application of the model

The mathematical model RICE for simulating river ice and flow conditions is constructed based on the analytical and numerical formulation developed in the previous sections. A slightly simplified version of RICE has been used in the model RICEOH. This model is applicable to a dendritic river system and has been applied successfully to the Ohio River system (Shen et al. 1988a). In this section the model will be applied to the upper St. Lawrence River.

The upper St. Lawrence River (Fig. 22) flows from Lake Ontario at Kingston, Ontario, to the Moses–Saunders Power Dam at Massena, New York, with a total length of 160 km. Figure 23 is a diagram of the river discretization. This discretization considers the need for the hydraulic computation, with additional nodal cross sections that are needed to reflect controls for ice conditions.

The model parameters must be calibrated when applying the model to a river. The bed roughness coefficients were calibrated first for the open water condition. The bed roughness and heat exchange coefficients are the only parameters that can be calibrated independently from ice conditions. All the remaining parameters described below are related to changes in the ice condition. Since the ice condition is affected by many variables, all these parameters should be calibrated simultaneously. Unfortunately the common calibration method described earlier cannot be used because partial derivatives of the model output with respect to some model parameters (model sensitivities) are not continuous in some cases. An iterative calibration procedure is required in such cases. The following calibration sequence is adopted to obtain values for model parameters.

Parameters related to the ice cover area and thickness are first calibrated to match the field observation. Localized non-uniformities in channel geometry have to be taken into account during this stage of calibration. Parameters calibrated at this stage are the ice cover porosity, cohesion and critical Froude numbers. In the second stage the ice cover roughness coefficients are calibrated using observed water levels. Buoyant velocity is calibrated finally to obtain the correct rate of progression and thickness of frazil deposition. Adjustments on previously calibrated parameters are needed at each stage of the calibration until the simulated ice and hydraulic conditions match field observations.

Simulation runs were carried out for 120 days. The selected starting date was 1 January 1980 to allow open water conditions to prevail for a few weeks before an ice cover formed. One day was used as the time step in the simulation. This is partly because most of the available observed data were for one-day or longer intervals. Diurnal variations of the ice conditions are not simulated.

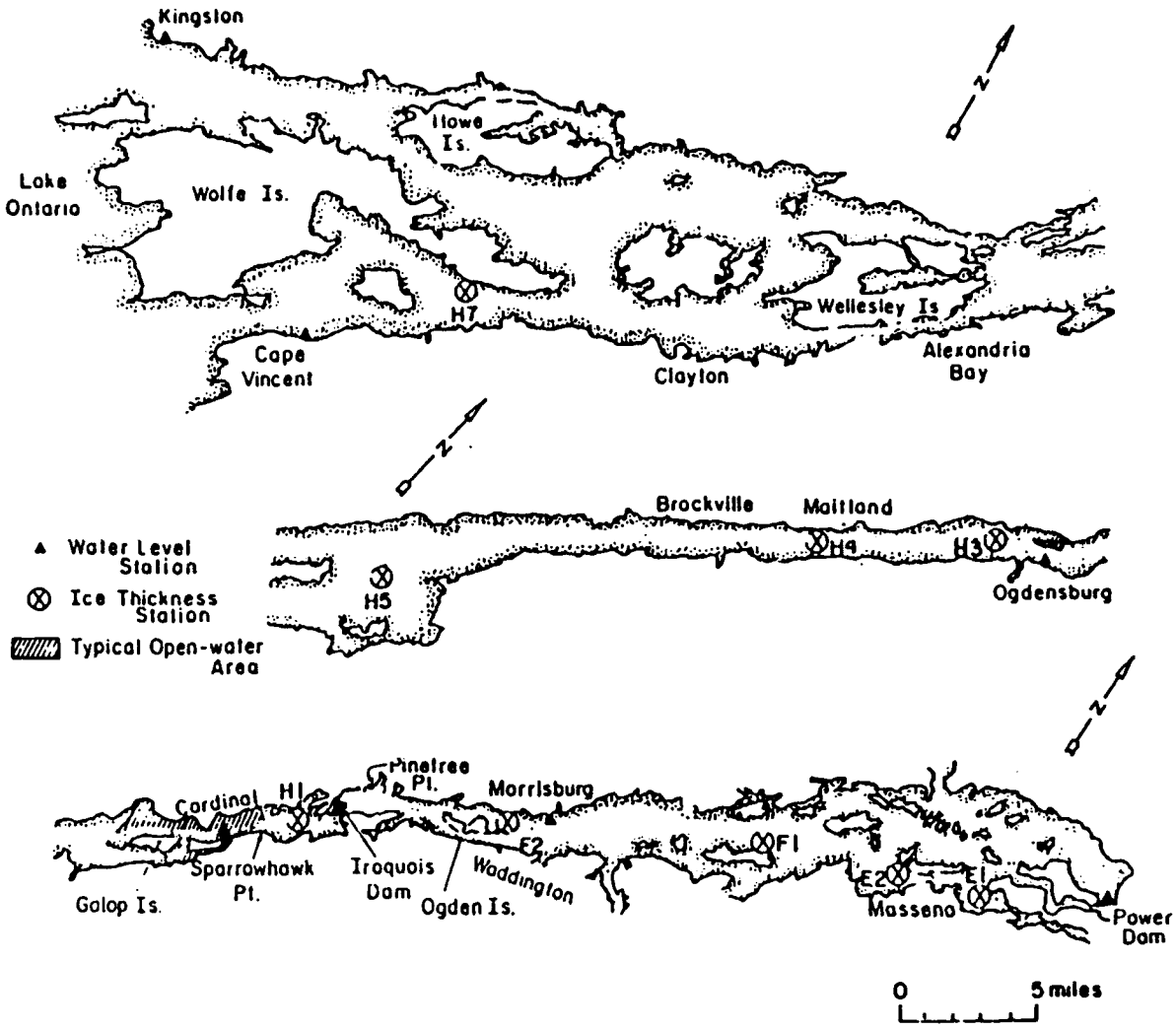

Figure 22. Upper St. Lawrence River.

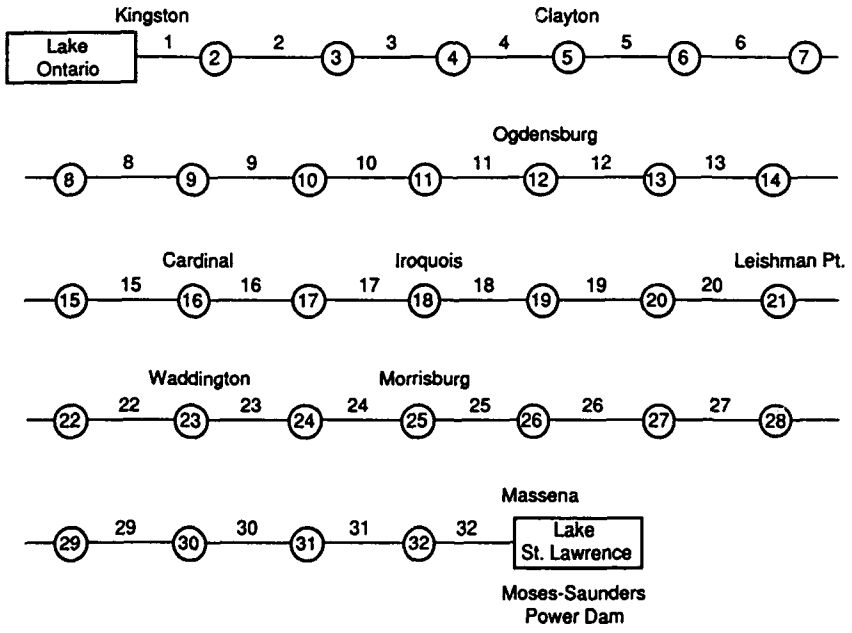

Figure 23. Schematization of the upper St. Lawrence River.

Results and discussion

The results of the simulation for the upper St. Lawrence River are presented in this section. Longitudinal cross sections of the ice cover, time-dependent variations of important ice and flow variables, and statistical indicators are included in the results. Appendix A gives an explanation of the parameters used in the statistical error analysis.

Figures 24 and 25 show variations of the air temperature at Massena and the flow rate at the Moses–Saunders Power Dam. Incorporation of detailed weather data into the heat exchange process is possible using an appropriate heat transfer model (Lal and Shen 1990a). Diurnal variations of ice conditions can also be predicted in the same manner.

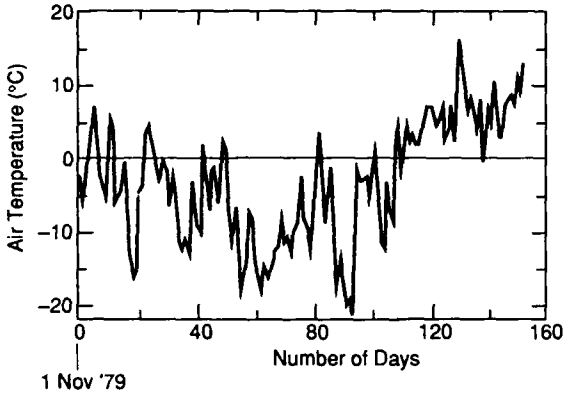

Figure 24. Variation of air temperature with time at Massena.

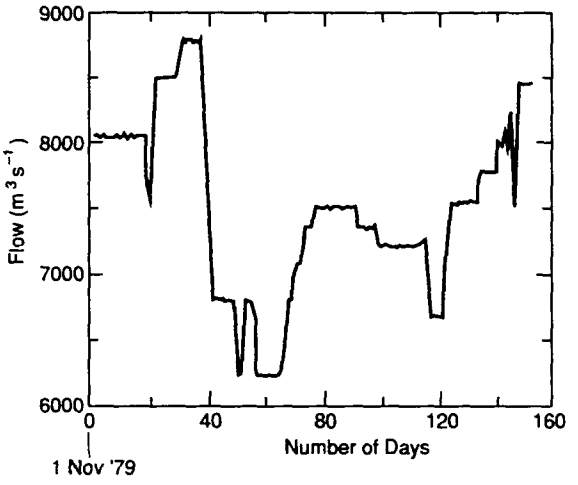

Figure 25. Variation of flow with time at the Moses–Saunders Power Dam.

Cross-section-averaged flow velocity and Froude number along the river change constantly with time. The simulated velocity and Froude number along the river on 30 January 1980 are shown in Figures 26 and 27. These figures indicate regions of possible occurrence of skim ice formation, shoving and control sections for leading edge progression.

Figure 28 shows the progression of the leading edge with time. Observed positions of the leading edge marked in the figure were obtained from aerial photographs. Different markers are used to indicate different leading edges. The figure shows that the simulation agrees reasonably well with the observed data over most parts of the river, except in high-velocity regions. In the upstream region the ice condition is highly nonuniform, with skim ice, juxtaposition and jam formation often coexisting in a river reach. In this region most of the river

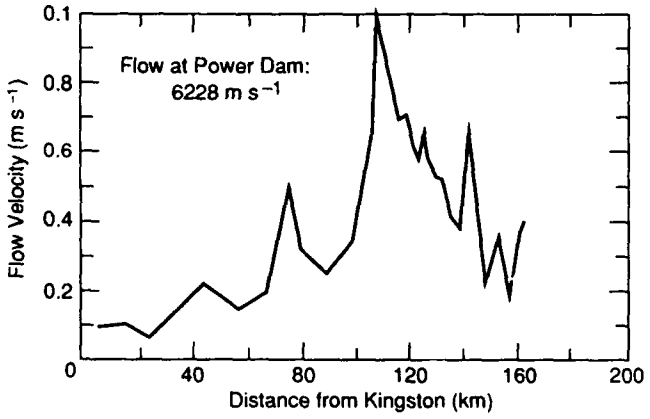

Figure 26. Flow velocity along the river on 30 January 1980.

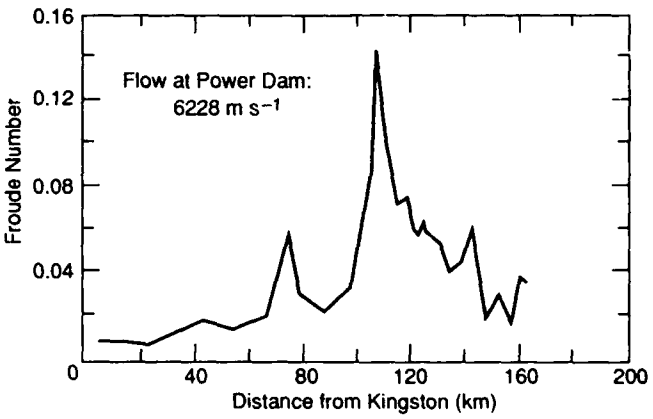

Figure 27. Froude number along the river on 30 January 1980.

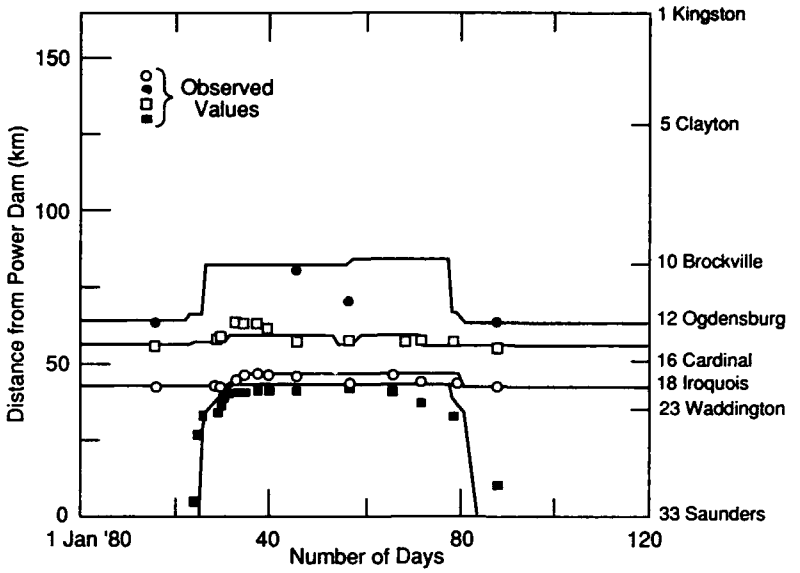

Figure 28. Progression of the leading edges with time. There were four leading edges, with simulated and observed positions for each

surface is covered by thin ice, and the ice condition is very unstable. This makes it difficult to identify the leading edge in the aerial photographs and to compare the observed and simulated results.

A better illustration of ice cover formation with time is shown in Figure 29. In this figure, different shades are used to represent skim ice and accumulated ice. The formation of static ice in the absence of a leading edge is also illustrated. Reaches with static shore ice near banks and accumulated cover in the center of the channel are marked with both shades. Reaches between nodes 6 and 10 had such a formation. Vertical lines indicate observed lengths and locations of ice-covered reaches on specific dates. Figure 30 shows variations of the mode of formation for the ice cover along the river between 25 January and 2 February 1980.

The longitudinal profile and plan area distributions of the ice cover on various dates are shown in Figure 31.

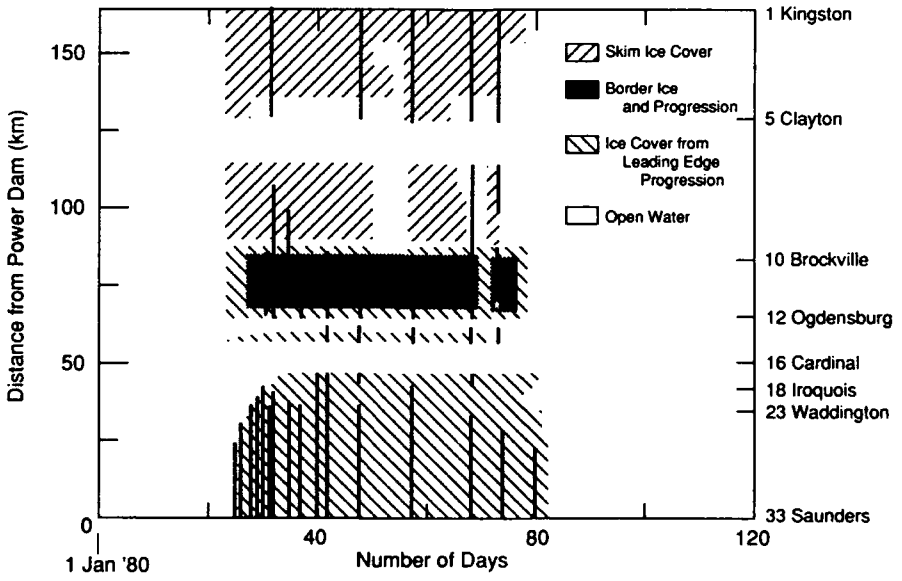

Figure 29. Time-dependent variation of the ice cover distribution along the river.

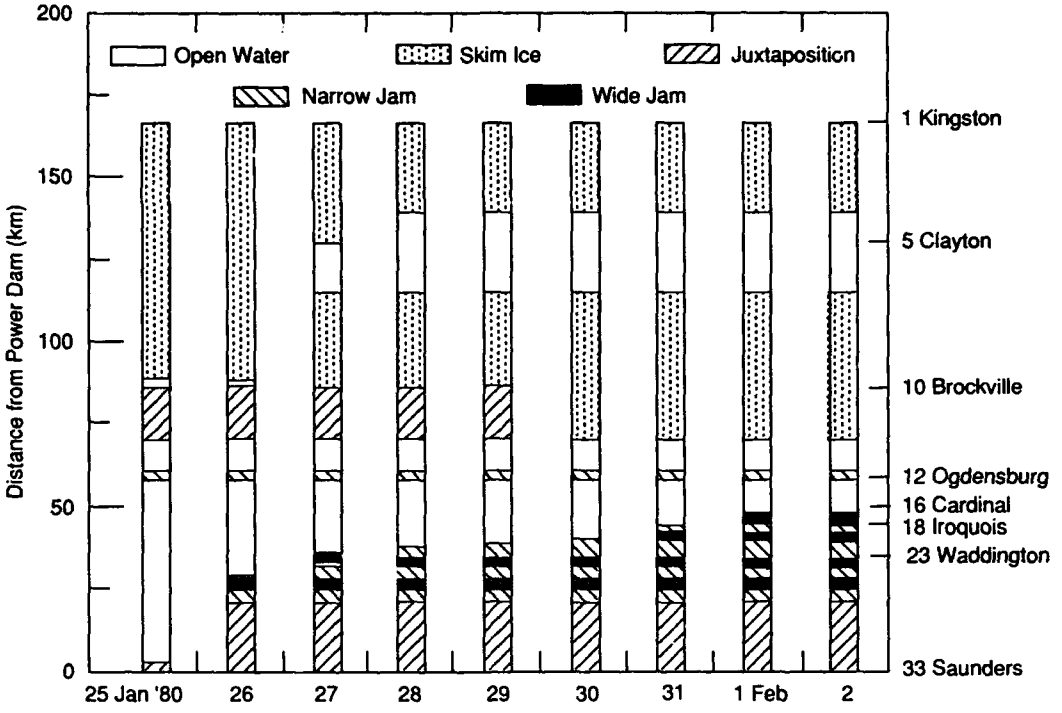

Figure 30. Variation of the ice cover formation modes along the river.

This figure shows the evolution of the ice cover during the period of 22–30 January 1980. Large and small thicknesses in the ice cover correspond to jammed and juxtaposed conditions. Thicker solid ice covers are found in areas with thicker initial covers or frazil deposits. The shape of the average bed profile is shown in Figure 31a.

Figure 32 show variations of solid ice thickness at a number of locations with time. Figure 33 compares the observed and simulated water surface elevations during the entire winter. This shows that the model is capable

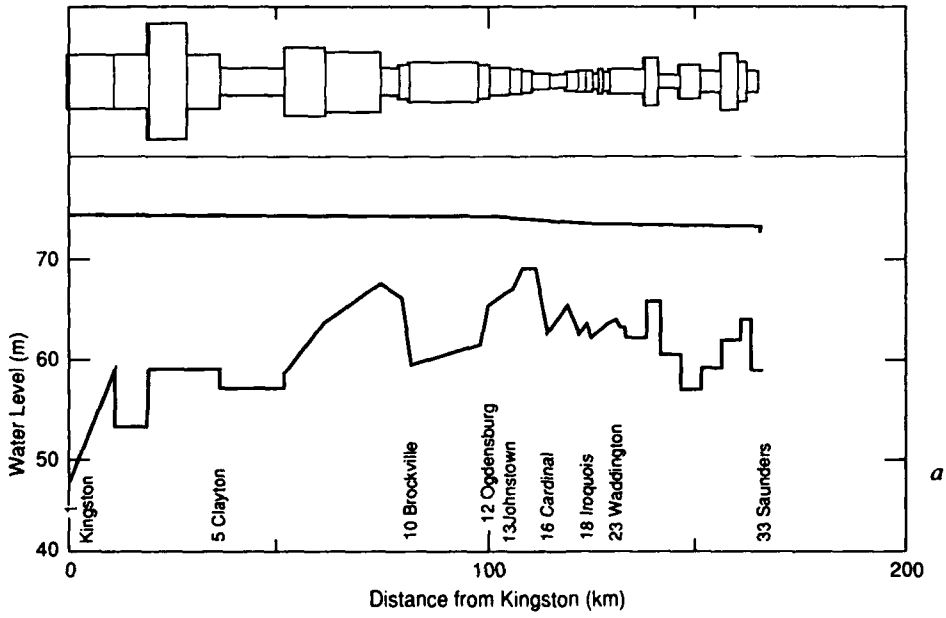

a. 22 January 1980.

Figure 31. Schematized channel surface, channel bottom profile and water surface profile.

b. 24 January 1980.

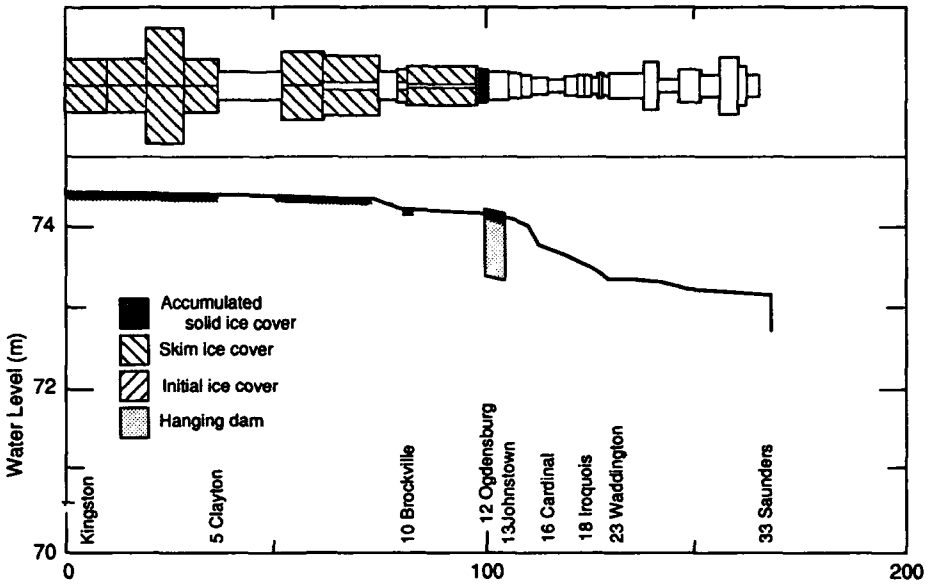

c. 26 January 1980.

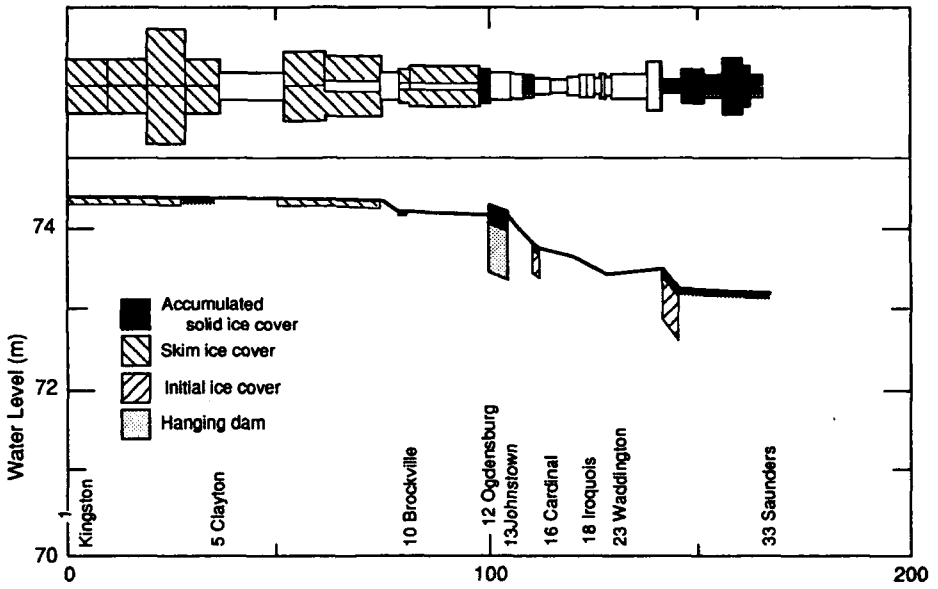

d. 28 January 1980.

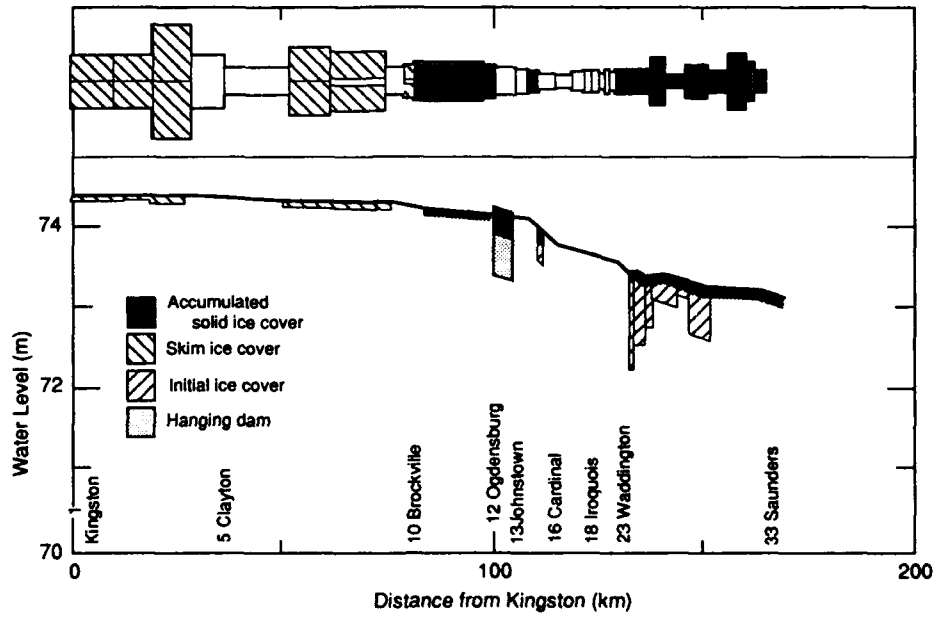

Figure 31 (cont'd).

e. 30 January 1980.

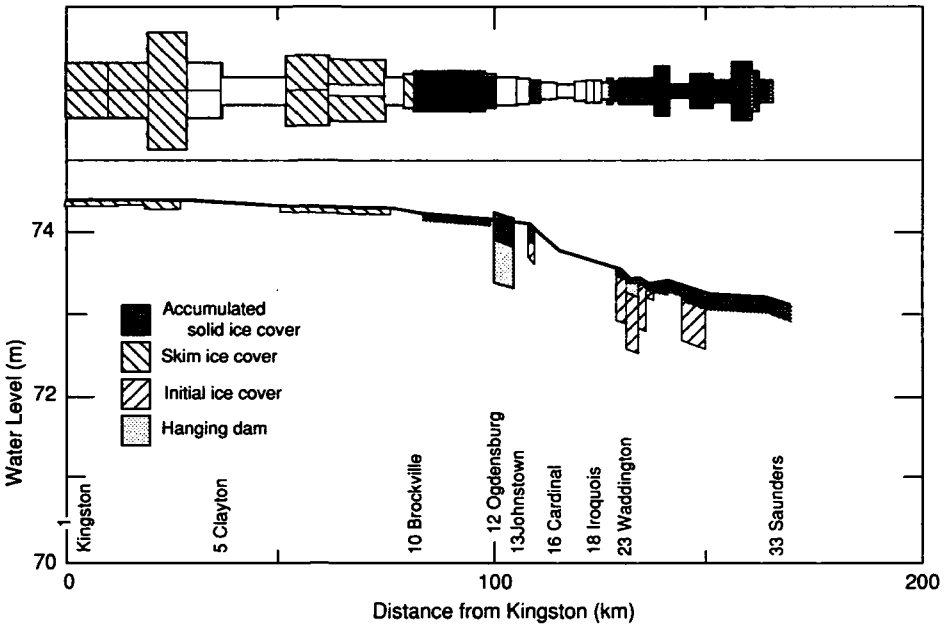

Figure 31 (cont'd). Plan view of schematized channel surface, channel bottom profile and water surface profile.

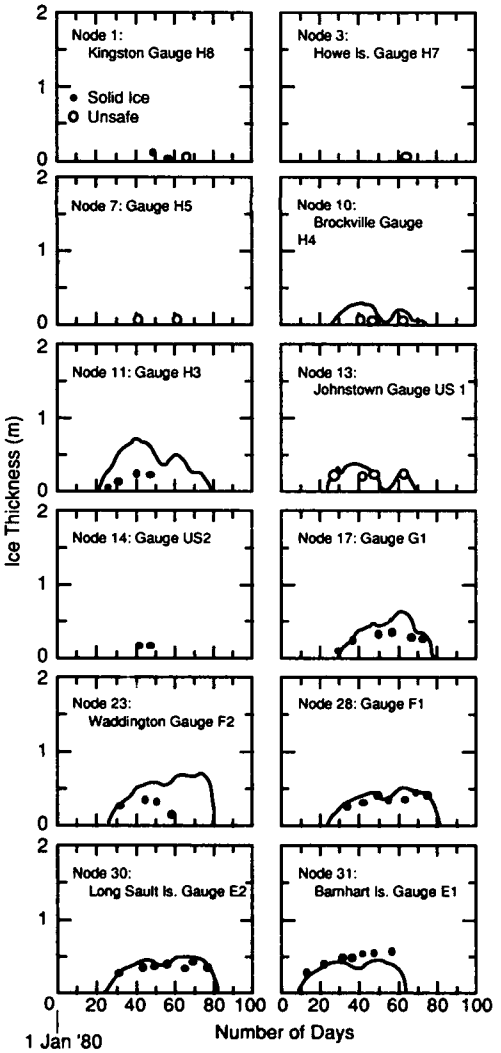

Figure 32. Observed and simulated ice cover thickness.

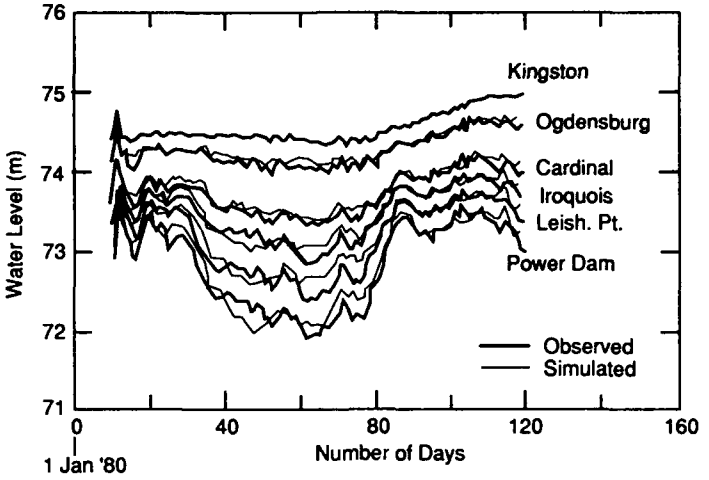

Figure 33. Observed and simulated water levels for the winter of 1980.

of simulating water level variations during both open water and ice-covered conditions. The error in the simulation of water levels is larger during the ice-covered period because of the cumulative effect of errors in the simulated ice cover area, the under-cover thickness and the resistance coefficients. Figure 34 shows the water level differences between gauging stations. Simulated and observed head losses agree well except in the Cardinal–Leishman Point region. Water level differences in this region can be due to inaccuracies in the simulation of the undercover ice accumulation.

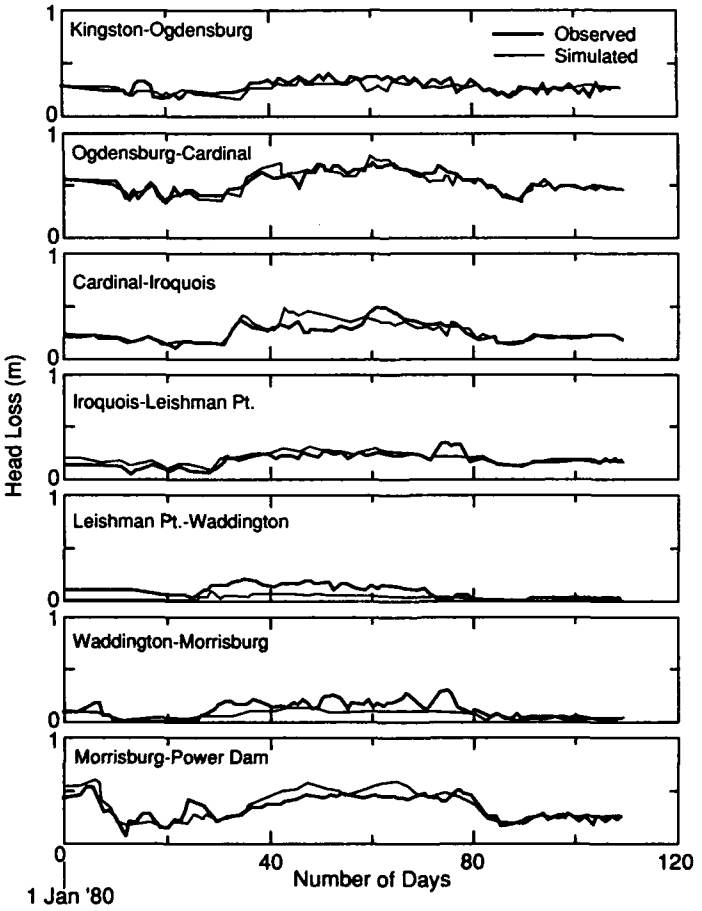

Figure 34. Variations of head losses.

Figure 35 shows the distribution of simulated water temperatures along the river between 17 January and 30 January 1980. Subzero values represent the existence of ice concentration.

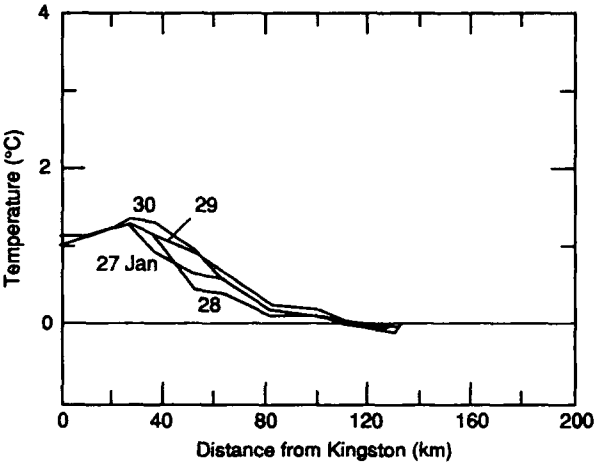

Figure 35. Water temperature profiles along the river from 27 January to 30 January 1980.

Error analysis

Figure 36 shows the relationship between the observed and simulated daily water levels. Graphical comparisons of observed and simulated average daily data provide qualitative information on the accuracy of the simulation. The statistical parameters developed in Appendix A can be used to quantify errors of the simulation. Table 6 gives the definitions of these parameters, which are useful in interpreting the results.

Table 7 compares all the statistical indicators at all the water level observation stations. Values of the standard deviation of observed water levels σ_Y show that water levels fluctuate more at locations closer to the power dam at the downstream end. This is because of variations in the power demand and the relatively stable level at the outlet of Lake Ontario. The error terms e_a, e_b, e_p, e_n and e_s are also larger at the downstream end. However, values of the nondimensionalized parameters V and ρ remain essentially constant along the river, showing that the model is capable of simulating water level fluctuations along the entire river effectively.

In Table 7, e_s and e_a values are on the order of 0.1 m, indicating that the error involved in simulating water levels is relatively small. Correlation coefficients between the observed and simulated water levels are on the order of 0.97. Values of the parameter V are on the order of 0.9, indicating that the model is capable of simulating variations of water levels accurately. Values of b and σ_y are approximately equal to 1.0 and σ_y, respectively.

Table 6. Definitions of statistical parameters for the error analysis.

Variable	*Definition*
n	Number of time steps ($i = 1,2, \ldots, n$) or number of observations
Y_i	Observed value at time step i
y_i	Simulated value at time step i
$\bar{Y}$	Average of observed values, $\frac{\Sigma_{i=1}^{n} Y_i}{n}$
σ_Y	Standard deviation of observed values, $\sqrt{\frac{\Sigma_{i=1}^{n}(y_i - \bar{y})^2}{n}}$
$\bar{y}$	Averaged of simulated values, $\Sigma_{i=1}^{n} y_i$
σ_y	Standard deviation of simulated values, $\sqrt{\frac{\Sigma_{i=1}^{n}(Y_i - \bar{Y})^2}{n}}$
Y_{min}	Minimum observed value
Y_{max}	Maximum observed value
y_{min}	Minimum simulated value
y_{max}	Maximumk simulated value
e_b	Bias, $\Sigma_{i=1}^{n} \frac{y_i - Y_i}{n}$
e_a	Average absolute error, $\frac{\Sigma_{i=1}^{n}\lvert y_i - Y_i\rvert}{n}$
e_p	Maximum positive error, $\text{Max}(y_i - Y_i)$ for all i
e_n	Maximum negative error, $\text{Max}(Y_i - y_i)$ for all i
e_s	Standard error estimate, $\sqrt{\frac{\Sigma_{i=1}^{n}(y_i - Y_i)^2}{n}}$
r	Correlation coefficient between Y_i and y_i for all i
V	$1 - \frac{e_s^2}{\sigma_Y}$
a, b	Constants in a $Y_i = a + by_i$ type model for all i

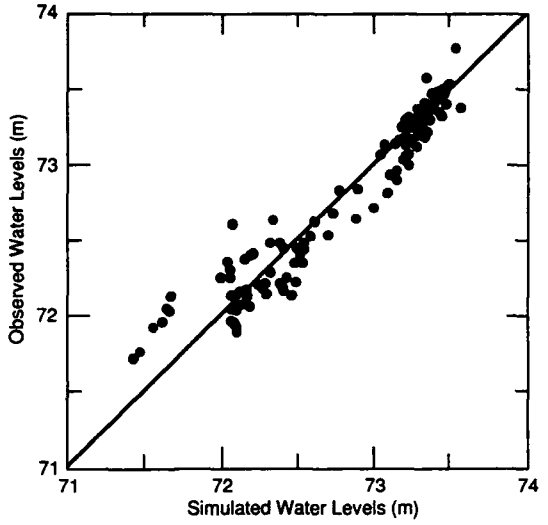

a. Power Dam.

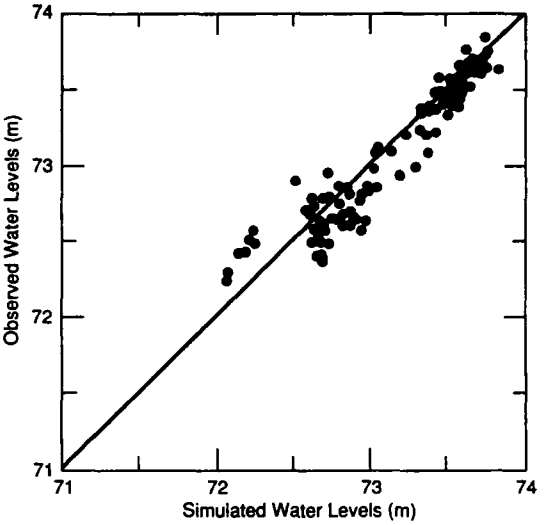

b. Morrisburg.

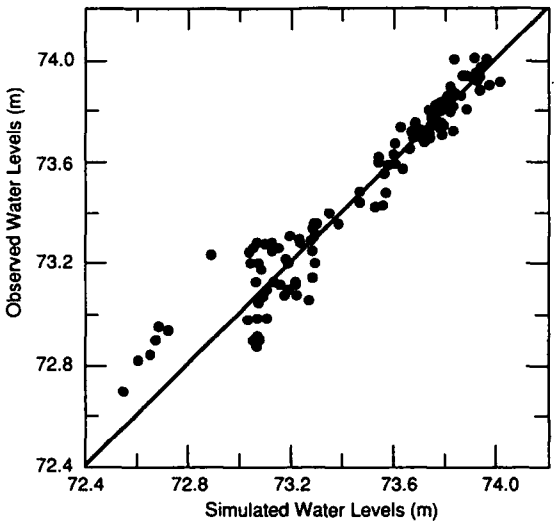

c. Iroquois Dam.

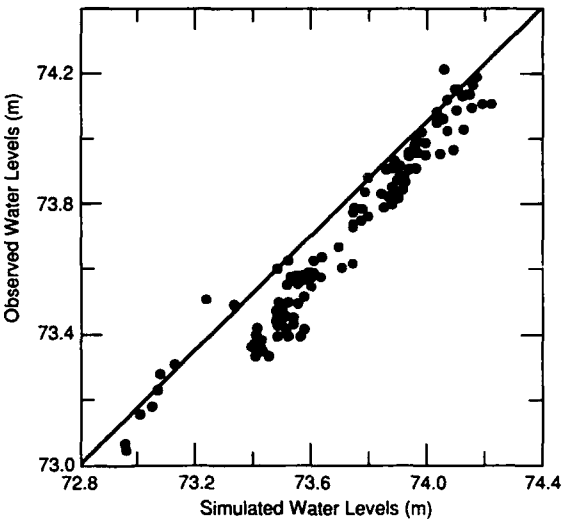

d. Cardinal.

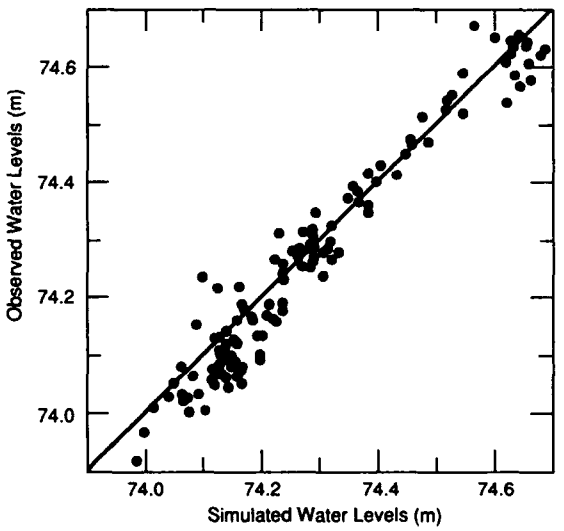

e. Ogdensburg.

Figure 36. Simulated and observed water levels, 1 January to 30 April 1980.

Table 7. Statistical parameters for the water level simulations.

Variable	*Power Dam*	*Morrisburg*	*Iroquois*	*Cardinal*	*Ogdensburg*
n	120	120	120	120	120
$\overline{Y}$ (m)	72.793	73.131	73.453	73.713	74.268
σ_Y (m)	0.5591	0.4649	0.3540	0.2859	0.1977
$\overline{y}$ (m)	72.812	73.147	73.437	73.7114	74.278
σ_y (m)	0.5961	0.4629	0.3762	0.2981	0.1875
Y_{min} (m)	71.726	72.256	72.689	73.042	73.920
Y_{max}(m)	73.798	73.868	73.996	74.219	74.673
y_{min} (m)	71.428	72.046	72.524	72.9503	73.977
y_{max} (m)	73.574	73.808	74.018	74.218	74.685
e_b (m)	0.0107	–0.0016	0.0175	0.0016	–0.0104
e_a (m)	0.1214	0.1091	0.0759	0.0526	0.0368
e_p (m)	0.3094	0.3434	0.2085	0.1606	0.1075
e_n (m)	0.5285	0.4120	0.3474	0.2727	0.1416
e_s (m)	0.1623	0.1425	0.1035	0.0710	0.0463
r	0.9624	0.9531	0.9624	0.9710	0.9736
V	0.9150	0.9053	0.9137	0.9377	0.9446
a	7.0969	3.1215	6.9595	5.0654	–1.9690
b	0.9026	0.9571	0.9054	0.9313	1.0263

Table 8. Statistical parameters for simulated water levels at the power dam during ice-covered and open water conditions.

Variable	*Combined*	*Ice-covered*	*Open water*
n	120	62	36
$\overline{Y}$	72.792	72.470	73.352
σ_Y	0.5591	0.4029	0.1326
$\overline{y}$	72.701	72.5084	73.3504
σ_y	0.6504	0.4336	0.0979
Y_{min}	72.726	71.924	73.015
Y_{max}	73.798	73.368	73.579
y_{min}	71.428	72.000	73.1741
y_{max}	73.576	73.339	73.5741
e_b	0.0913	–0.0383	0.0018
e_a	0.11382	0.125	0.0665
e_p	0.2193	0.3094	0.2171
e_n	0.5252	0.3225	0.2307
e_s	0.1954	0.1499	0.0850
r	0.9701	0.9416	0.7604
V	0.8768	0.8593	0.5776
a	12.1631	9.0234	–2.1746
b	0.8339	0.8750	1.0297

Table 9. Statistical parameters for simulated water temperatures.

Variable	*Clayton*	*Waddington*	*Power Dam*
n	55	55	55
$\overline{Y}$ (°C)	3.1465	2.1908	2.1994
σ_Y (°C)	1.8148	1.9107	1.9879
$\overline{y}$ (°C)	2.9982	2.0108	1.8915
σ_y (°C)	1.5956	1.6550	1.6521
Y_{min} (°C)	0.5000	0.0000	1.1100
Y_{max} (°C)	6.5500	6.0500	0.3278
y_{min} (°C)	0.8614	0.0000	0.0000
y_{max} (°C)	5.8814	5.2456	4.9903
e_b (°C)	0.1484	0.1799	0.3078
e_a (°C)	0.4176	0.5817	0.6113
e_p (°C)	0.8438	1.0181	0.9239
e_n (°C)	1.0723	2.1914	2.6079
e_s (°C)	0.5119	0.7753	0.8792
r	0.9661	0.9187	0.9120
V	0.9189	0.8322	0.3007
a	–0.1478	0.0579	0.1236
b	1.0987	1.0606	1.0974

This indicates that simulated variations are close to the observed variations. Values of $b < 1$ and $\sigma_y < \sigma_Y$ indicate that simulated variations are slightly larger than the observed variations.

Table 8 shows a comparison of water level predictabilities during open water and ice-covered conditions. As expected, this table shows that simulations during ice-covered conditions are not as good as those during open water conditions.

Table 9 summarizes the error indicators for water temperature simulations. Values of e_s and e_a show that the error involved in the simulation is about 0.5°C. Because water temperature stations are often located near the bank and because of the accuracy of the temperature data, this error is acceptable. Values of r and V suggest that the model can simulate variations of water temperature satisfactorily.

The error indicators could not be developed for variables such as ice cover area and thickness because of the limited availability of observed data. Errors in simulations as measured by the error variance e_s^2 can be due to a number of sources. The component due to observational error can only be reduced through accurate instrumentation and better observation station locations. One of the major error sources is the water temperature data. The

effect of stratification in the upstream region, which cannot be modeled accurately due to lack of data, can also have an important effect on the ice condition. A second component of error variance due to bias e_s^2 can usually be eliminated by proper calibration. The part of the error due to the one-dimensional approximation is also unavoidable. A significant part of the error is due to shortcomings in the existing theories on river ice processes. These can be improved only when better theories become available. These shortcomings cover almost all of the river ice processes, including formation of frazil and skim ice, ice jam formation, shore ice accumulation, hanging dam formations or undercover erosion and deposition, and ice cover resistance coefficient.

Summary and conclusion

In this study a one-dimensional model is developed for simulating river ice processes. The model is capable of simulating time-dependent conditions of the river hydraulics, water temperature and ice concentration, formation of an ice cover, undercover accumulation, thermal growth and decay of the ice cover, and mechanical stability of the cover. In the river hydraulics component, the flow condition is determined by an implicit finite-difference solution of one-dimensional unsteady flow equations. In the thermal component, distributions of water temperature and ice concentration are determined by a Lagrangian–Eulerian solution scheme for equations of transport of thermal energy and ice. A two-layer formulation is introduced to model the ice transport. In this formulation the total ice discharge is considered to consist of the surface ice discharge and the discharge of suspended ice distributed over the depth of the flow. The effect of surface ice on ice production as well as formations of skim ice and border ice are included. The dynamic formation and stability of the ice cover is formulated according to existing equilibrium ice jam theories with due consideration to the interaction between the ice cover and the flow. The undercover ice accumulation is formulated according to the critical velocity criterion. The growth and decay of the ice cover is simulated using a finite-difference formulation applicable to composite ice covers consisting of snow, ice and frazil layers. The model has been applied to the upper St. Lawrence River and the Ohio River system with good results. With the generic nature of the model structure, the model can be applied to other rivers. In view of the limited current understanding on river ice processes, further improvements of the model should be made when improved theoretical formulations become available. The model can assist the development of new formulations by analyzing field data in a comprehensive manner. Further improvements on modeling techniques are also possible by including some important two-dimensional aspects of ice processes.

LITERATURE CITED

Ackermann, N.L. and H.T. Shen (1983) Mechanics of surface ice jam formation in rivers. USA Cold Regions Research and Engineering Laboratory, CRREL Report 83-81.

Ackermann, N.L., H.T. Shen and R.W. Ruggles (1981) Transport of ice in rivers. In *Proceedings, IAHR International Symposium on Ice, Quebec City, Canada*, p. 333–346.

Amein, M. and H.L. Chu (1975) Implicit numerical modeling of unsteady flows. *Journal of the Hydraulics Division, ASCE*, **101**(HY6): 717–730.

Ashton, G.D. (1973) Heat transfer to river ice covers. In *Proceedings, 30th Eastern Snow Conference, Amherst, Massachusetts*, p. 125–135.

Ashton, G.D. (1975a) Froude criterion for ice-block stability. *Journal of Glaciology*, **13**(68): 307–313.

Ashton, G.D. (1975b) Movement of ice floes beneath a cover. USA Cold Regions Research and Engineering Laboratory, Technical Note (unpublished).

Ashton, G.D. (1979) Suppression of river ice by thermal effluents. USA Cold Regions Research and Engineering Laboratory, CRREL Report 79-30.

Ashton, G.D. (1982) Theory of thermal control and prevention of ice covers in rivers and lakes. *Advances in Hydroscience*, **13**: 131–185.

Ashton, G.D. (Ed.) (1986) *River and Lake Ice Engineering*. Littleton, Colorado: Water Resources Publications.

Beck, J.V. and K.J. Arnold (1977) *Parameter Estimation in Engineering and Science*. New York: John Wiley and Sons.

Bengtsson, L. (1984) Forecasting snow and black ice growth from temperature and precipitation. In *Proceedings of IAHR Ice Symposium, Hamburg, Germany.*

Bilello, M.A. (1980) Maximum thickness and subsequent decay of lakes, rivers and fast sea ice in Canada and Alaska. USA Cold Regions Research and Engineering Laboratory, CRREL Report 80-6.

Broyden, C.G. (1965) A class of methods for solving nonlinear simultaneous equations. *Mathematics of Computation*, **19**: 577–593.

Burden, R.L. and J.D. Faires (1985) *Numerical Analysis*. Boston: Prindle, Weber and Schmidt Publishers, third edition.

Calkins, D.J. (1984) Numerical simulation of freeze-up on the Ottaquechee River. In *Proceedings of Workshop on the Hydraulics of River Ice, Fredericton, New Brunswick, Canada*, p. 247–277.

Cheng, R.T., V. Casulli and S.N. Milford (1984) Eulerian–Lagrangian solution of the convection–diffusion equa-tion in natural coordinates. *Water Resources Research*, **20**(7): 944–952.

Cunge, J.A., F.M. Holly, Jr. and A. Verwey (1980) *Practical Aspects of Computational River Hydraulics*. Boston: Pitman Publishing Company, p. 92.

Dingman, S.L. and W.F. Weeks, Y.-C. Yen and A. Assur (1969) The effects of thermal pollution on river-ice con-ditions. Part II: Simplified method of calculation. USA Cold Regions Research and Engineering Laboratory, Re-search Report 206.

Filippov, A.M. (1974) Modeling the movement of ice floes drawn in under ice cover. USA Cold Regions Research and Engineering Laboratory, Translation.

Fischer, H.B., J.L. List, R.C.Y. Koh, J. Imberger and N.S. Brooks (1979) *Mixing in Coastal and Inland Waters*. New York: Academic Press, p. 483.

Fread, D.L. (1973) Effects of time step size in implicit dynamic routing. *Water Resources Bulletin*, April, p. 338.

Fread, D.L. (1985) *Hydrological Forecasting* (M.G. Anderson, Ed.). New York: John Wiley and Sons, p. 437–503.

Gabison, R. (1987) A thermodynamic model of the formation, growth, and decay of first-year sea ice. *Journal of Glaciology*, **33**(113).

Greene, G.M. (1981) Simulation of ice cover growth and decay in one-dimensional on the upper St. Lawrence River. National Oceanic and Atmospheric Administration Technical Memo ERL GLERL-36, Great Lakes Environmental Laboratory, Ann Arbor, Michigan, p. 82.

Gunaratnam, D.J. and F.E. Perkins (1970) Numerical solution of unsteady flow in open channels. Department of Civil Engineering, MIT, Cambridge, Massachusetts, R.M. Parson Laboratory for Water Resources and Hydrodynamics, Technical Report No. 127.

Hausser, R., J.P. Saucet and F.E. Parkinson (1984) Coverage coefficient for calculating ice volume generated. In *Proceedings of Workshop on the Hydraulics of River Ice, Fredericton, New Brunswick, Canada.*

Haynes, F. D. and G.D. Ashton (1979) Turbulent heat transfer in large-aspect channels. USA Cold Regions Research and Engineering Laboratory, CRREL Report 79-13.

Holly, F. M. and A. Preissman (1977) Accurate calculation of transport in two dimensions. *Journal of the Hydraulics Division, ASCE*, **103**(HY11): 1259–1277.

Holly, F. M. and J.M. Usseglio-Polatera (1984) Dispersion summation in two-dimensional tidal flow. *Journal of Hydraulic Engineering, ASCE*, **110**(7).

Houkuna, M. (1988) The Finnish River ice project. In *Proceedings, Fifth Workshop on Hydraulics of River Ice: Ice Jams, Winnepeg, Manitoba, Canada.*

Jobson, H. E. (1987) Estimation of dispersion and first-order rate coefficients by numerical routing. *Water Resources Research*, **23**(1): 169–180.

Karaushev, A.V. (1969) Recnaja gidravlika. Gidrometeoizdat, Leningrad, 1st edition (in Russian).

Kivisild, H.R. (1959) Hydrodynamical analysis of ice floods. In *Proceedings, 8th IAHR Congress, Montreal, Quebec, Canada*, Paper 23F.

Lal, A.M.W. and H.T. Shen (1990a) Linear heat transfer models for heat exchange over water and ice. Department of Civil and Environmental Engineering, Clarkson University, Technical Report.

Lal, A.M.W. and H.T. Shen (1990b) Calibration of parameters. Department of Civil and Environmental Engineering, Clarkson University, Potsdam, Technical Report.

Leppäräntä, M. (1983) A growth model for black ice—Snow ice and snow thickness in the subarctic basins. *Nordic Hydrology*, **14**: 59–70.

Mahmood, K. and V. Yevjevich (1975) *Unsteady Flow in Open Channels*. Fort Collins, Colorado: Water Resources Publications.

Marsh, P. and T.D. Prowse (1987) Water temperature and heat flux at the base of river ice covers. *Cold Regions Science and Technology*, **14**: 33–50.

Matousek, V. (1984a) Regularity of the freezing-up of the water surface and heat exchange between water body and water surface. *Proceedings of IAHR Ice Symposium, Hamburg, Germany*, p. 187–200.

Matousek, V. (1984b) Types of ice run and conditions for their formation. *Proceedings of IAHR Ice Symposium, Hamburg, Germany*, p. 315–327.

Maykut, G.A. (1978) Energy exchange over young sea ice in the central Arctic. *Journal of Geophysical Research*, **83**(C7): 3646–3658.

Maykut, G.A. and N. Untersteiner (1971) Some results from a time-dependent thermodynamic model in sea ice. *Journal of Geophysical Research*, **76**(6): 1550–1575.

McCuen, R.H. (1973) The role of sensitivity analysis in hydrologic modeling. *Journal of Hydrology*, **18**: 37–53.

Michel, B. (1971) Winter regime of rivers and lakes. USA Cold Regions Research and Engineering Laboratory, Cold Regions Science and Engineering Monograph III-Bla.

Michel, B. (1986) Course on river ice engineering. Lecture Notes from *Proceedings of Workshop on River Ice Engineering, Montreal, Quebec, Canada.*

Michel, B. and M. Drouin (1975) Equilibrium of an underhanging dam at the La Grande River. Report, Université d'Laval, GCS-75-03-01.

Michel, B and M. Drouin (1982) Backwater curves under ice cover of the LaGrande River. *Canadian Journal of Civil Engineering*, **8**(1): 351–363.

Michel, B., N. Marcotte, F. Fonseca and G. Rivard (1980) Formation of border ice in the St. Anne River. In *Proceedings of the Workshop on Hydraulics of Ice-Covered Rivers, Edmonton, Alberta, Canada*, p. 38–61.

Miller, J.D. (1980) A simple model for seasonal sea ice growth. ASME Winter Annual Meeting, Chicago, Paper no. 80-WA/HT-20, p. 8.

Nezhikhovskiy, R.A. (1964) Coefficient of roughness of bottom surface of slush ice cover. *Soviet Hydrology: Selected Papers*, no. 2, p. 127–148.

Pariset, R. and H. Hausser (1961) Formation and evolution of ice covers on rivers. ASME-EIC Hydraulic Conference Paper No. 61-EIC-6. *Transactions, Engineering Institute of Canada*, **5**(1): 41–49.

Pariset, E., R. Hausse and A. Gagnon (1966) Formation of ice covers and ice jams in rivers. *Journal of the Hydraulics Division, ASCE*, **72**(November): 1–24.

Perrels, P.A.J. and M. Karlse (1981) Salt intrusion in estuaries—Transport models for inland and coastal waters. In *Proceedings of the Symposium on Predictive Ability* (H.B. Fischer, Ed.). New York: Academic Press.

Petryk, S. and R. Boisvert (1978) Simulations of ice conditions in channels. In *Proceedings of the Speciality Conference on Computer Applications in Hydrotechnical and Municipal Engineering, Toronto, Ontario, Canada*, p. 239–259.

Petryk, S., U. Panu, V.C. Cartha and F. Clement (1981a) Numerical modeling and predictability of ice regime in rivers. *Proceedings of IAHR International Symposium on Ice, Quebec*, p. 426–436.

Petryk, S., U. Panu and F. Clement (1981b) Recent improvements in numerical modeling of river ice. *Proceedings of IAHR International Symposium on Ice, Quebec.*

Potok, A.J. (1978) Upper St.Lawrence River hydraulic transient model. Great Lakes Environmental Research Laboratory, Ann Arbor, Michigan, NOAA TM ERL GLERL-24, p 96.

Potok, A.J. and F.H. Quinn (1979) A hydraulic transient model of the Upper St.Lawrence River for water resources studies. *Water Resources Bulletin*, **15**(6).

Ramseier, R.O. (1970) Formation of primary ice layers. In *Proceedings of IAHR Ice Symposium, Reykjavik, Iceland.*

Rodi, W. (1980) Turbulence models and their applications in hydraulics. A state-of-the-art review. Delft, The Netherlands: IAHR Section on Fundamentals of Division II, Experimental and Mathematical Fluid Dynamics, p. 48.

Shen, H.T. (1985) Hydraulics of river ice. Department of Civil and Environmental Engineering, Clarkson University, Report 85-1, p. 80.

Shen, H.T., G. Bjedov, S.F. Daly and A.M.W. Lal (1988a) A numerical model for Ohio River ice conditions. Department of Civil and Environmental Engineering, Clarkson University, Report 88-4.

Shen, H.T., H.H. Shen and S.M. Tsai (1988b) Dynamic transport of river ice. In *Proceedings, IAHR Ice Symposium, Sapporo, Japan*, vol. III.

Shen, H.T. and L.-A. Chiang (1984) Simulation of growth and decay of river ice cover. *Journal of the Hydraulics Division, ASCE*, **110**(7): 958-971.

Shen, H.T. and T.O. Harden (1978) The effect of ice cover on vertical transfer in stream channels. *Water Resources Bulletin, American Water Resources Association*, **14**(6).

Shen, H.T. and A.M.W. Lal (1986) Growth and decay of river ice covers. In *Proceedings of Cold Regions Hydrology Symposium, American Water Resources Association.*

Shen, H.T. and A.M.W. Lal (1990) Linearized heat transfer models. Department of Civil and Environmental Engineering, Clarkson University, Technical Report.

Shen, H.T. and R.W. Ruggles (1982) Analysis of river ice cover roughness. In *Proceedings, Applying Research to Hydraulic Practice, ASCE, Jackson, Mississippi.*

Shen, H.T., R.W. Ruggles and G.B. Batson (1984) Field investigation of St. Lawrence River hanging ice dams, winter of 1983–1984. U.S. Department of of Transportation, Washington, D.C., Report No. DTSL55-84-C0085A.

Shen, H.T. and W.A. Van DeValk (1984a) Field investigation of St. Lawrence River hanging ice dams. In *Proceedings of IAHR Ice Symposium, Hamburg, Germany*, p. 241–249.

Shen, H.T., W.A. Van DeValk, G.B. Batson and I.L. Maytin (1983) Field investigation of hanging dams in the St. Lawrence River, winter of 1981–1982. U.S. Department of Transportation, Washington D.C., Report DTSL55-82-C-C0918A.

Shen, H.T. and P.D. Yapa (1984) Computer simulation of ice cover formation in the Upper St. Lawrence River. In *Proceedings of the 3rd Workshop on Hydraulics of River Ice, Fredericton, New Brunswick, Canada*, p. 227–246.

Shen, H.T. and P.D. Yapa (1985) A unified degree-day method for ice cover thickness simulation. *Canadian Journal of Civil Engineers*, vol. 12.

Shen, H.T. and P.D. Yapa (1986) Flow resistance of river ice covers. *Journal of the Hydraulics Division, ASCE*, **112**(2).

Simonsen C.P.S. and R.W. Carson (1977) Ice processes during the construction of Lamestone Generation Station. In *Proceedings of the Third National Hydrotechnical Conference, Quebec City*, p. 19.

Stefan, J. (1891) Theory of ice formation, specially in the Arctic Ocean. *Wien Sitzunsber. Akad. Wiss.*, Series A, 42, Part 2, p. 965–983.

Sun, Z.-C. and H.T. Shen (1988) Field investigation of frazil ice jams in Yellow River. In *Proceedings of Fifth Workshop on Hydraulics of River Ice: Ice Jams, Winnipeg, Manitoba, Canada.*

Sydor, M. (1978) Ice growth in Duluth–Superior Harbor. *Journal of Geophysical Research*, **83**(C8): 4074–4078.

Tatinclaux, J.-C.M. and M. Gogus (1981) Stability of floes below a floating ice cover. In *Proceedings of IAHR International Symposium on Ice, Quebec*, p. 298-311.

Tennessee Valley Authority (1972) Heat and mass transfer between a water surface and the atmosphere. Water Resources Laboratory, Norris, Tennessee, Report No. 14, Report No. 0-6803.

Tesaker, E. (1975) Accumulation of frazil ice in an intake reservoir. In *Proceedings of IAHR Symposium on Ice Problems, Hanover, New Hampshire.*

Uzuner, M.S. and J.F. Kennedy (1976) Theoretical model of river ice jams. *Journal of the Hydraulics Division, ASCE*, **102**(HY9): 1365–1383.

Viesman, W., J.W. Knapp, G.L. Lewis and T.E. Harbaugh (1972) *Introduction to Hydrology*. New York: Harper and Row Publishers, Second Edition.

Wake, A. and R.R. Rumer, Jr. (1979) Modeling ice regime in Lake Erie. *Journal of the Hydraulics Division, ASCE*, **105**(HY7): 827–844.

Yapa, P.D. (1983) Unsteady flow simulation of rivers with an ice cover. Ph. D. Dissertation, Department of Civil and Environmental Engineering, Clarkson College of Technology, Potsdam.

Yapa, P.D. and H.T. Shen (1986) Unsteady flow simulation for an ice-covered river. *Journal of the Hydraulics Division, ASCE,* **112**(11).

Zacharov, R.O., M.M. Bejlinson and I.N. Satalina (1972), Features of ice conditions in rivers and reservoirs of central Asia. In *Proceedings of IAHR Symposium: Ice and its Action on Hydraulic Structures, Leningrad,* p. 224–228.

APPENDIX A: ERROR ANALYSIS

The validity of a simulation model can be determined by comparing the simulated results with observed data. The most common method of comparison is by graphically comparing observed and simulated results. Graphical comparison gives a qualitative estimate of the accuracy of the model. Quantitative evaluation of a simulation model can be obtained using error estimates. Some of the indicators are similar to those used in the analysis of variance.

Consider a sequence of observations where Y_i and corresponding simulated values y_i where $i = 1,2,...,n$ are the observation numbers. The error e_i of any observation i is

$$e_i = y_i - Y_i \qquad \text{for } i = 1,2,...n \tag{A1}$$

where n is the number of observations. The error e_i can be positive or negative. During an entire simulation, e_i can fluctuate around a nonzero value. This value differs from the actual average value by an amount called the bias:

$$\text{bias} = e_b = \frac{\Sigma_{i=1}^{n} e_i}{n} = \frac{\Sigma_{i=1}^{n}(y_i - Y_i)}{n}. \tag{A2}$$

Bias can be reduced to zero by calibration. In the case of the bed roughness calibration in the present study, the objective was to obtain zero bias for all observation stations. Zero bias does not guarantee error-free simulation. The error in a simulation can also be computed as an average absolute error:

$$\text{average absolute error} = e_a = \frac{\Sigma_{i=1}^{n}|y_i - Y_i|}{n}. \tag{A3}$$

A better indicator of error, which can also be used in variance analysis, is the standard error estimate:

$$\text{standard error estimate} = e_s = \left[\frac{\Sigma_{i=1}^{n}(y_i - Y_i)^2}{n}\right]^{1/2}. \tag{A4}$$

Both e_a and e_s are always nonzero, even in the case of $e_b = 0$, unless observations at all time steps exactly match with simulated values. During the calibration of parameters, minimization of e_a and e_s can be used as the objective functions for optimization. Minimization of the absolute value of maximum positive error e_p or negative error e_n is also a commonly used objective function. The phase lag between observed and simulated results can also be used as an error indicator.

The error term, which is measured by e_s or e_a can be due to a number of causes such as: a) physical phenomena that were not formulated correctly; b) errors introduced in the numerical procedure; c) measurement errors in the observations and d) incomplete calibration. A complete error analysis has to be able to separate contributions to the error variance e_s^2 from these effects. The current analysis only computes e_s^2.

The standard error estimate e_s alone is not capable of measuring the capability of the model to simulate variations. The model should be capable of simulating a known variation of the output variable as closely as possible to its observation. A simple correlation estimation and an analysis of variance is useful in developing an indicator capable of measuring this property in a model. The correlation coefficient between observed and simulated values is defined as

$$r^2 = \frac{\left[\Sigma_{i=1}^{n}(y_i - \bar{y})(Y_i - \bar{Y})\right]^2}{\Sigma_{i=1}^{n}(y_i - \bar{y})^2 \, \Sigma_{i=1}^{n}(Y_i - \bar{Y})^2} \tag{A5}$$

where

$$\bar{Y} = \sum_{i=1}^{n} Y_i \tag{A6}$$

where

$$\overline{Y} = \sum_{i=1}^{n} Y_i \tag{A6}$$

and

$$\overline{y} = \sum_{i=1}^{n} y_i. \tag{A7}$$

The coefficient of correlation r ranges between 0 and 1. A perfect model will have $r = 1$. Values of r closer to 1 indicate better simulations. A value of $r < 0.6$ indicates either that the simulation model is unsuccessful or that the data set used is not capable of supporting the hypothesis that the model is capable of simulating the variation in the observations.

In addition to determining various error terms, an analysis of the behavior of the simulated result in relation to observed results is useful. The best method to determine this behavior in a statistical sense is to obtain a relationship between simulated and observed results. The simplest relationship possible is a linear one:

$$Y_i = a + by_i \qquad \text{for } i = 1,2,...n. \tag{A8}$$

The value of r obtained from eq A5 can also be obtained by simple linear regression of Y_i and y_i. Values of a and b can be used to check the effectiveness of the model. For the perfect model, $a = 0$ and $b = 1$. Any deviation from these values indicates an error in the simulation. The coefficient b gives a statistical estimate for the amplification by the simulation model. Amplification = $\partial y_i/\partial Y_i = 1/b$. When $1/b > 1$, a magnification of the variation by the simulation model is indicated, while $|a| > 0$ indicated the presence of a bias. Amplification of the standard deviation s_y/s_Y can be related to the average amplification $1/b$, using the following equation:

$$\frac{1}{b} = \frac{1}{r}\frac{s_y}{s_Y} = \frac{1}{r}\sqrt{\frac{\Sigma_{i=1}^{n}(y_i - \overline{y})^2}{\Sigma_{i=1}^{n}(Y_i - \overline{Y})^2}}. \tag{A9}$$

The above analysis can be extended and used to explain the overall behavior of simulated results using four statistical parameters. Parameters a, b, k and e_w can be used as statistical estimators of bias, amplification, lag and standard error, respectively. Figure A1 shows the effect of these parameters graphically. Using these parameters, the observed results can be related to simulated results using

$$Y_i = a + by_{i+k}\, w_i e_w \tag{A10}$$

where k = lag
e_w = standard deviation of remaining error
w_i = white noise.

By fitting this model, any error term that cannot be explained using a gross amplification or a bias is assumed as a random error. Lag k for the best fit of eq A10 is the lag for maximum cross correlation between y_i and Y_i:

$$r_k = \sqrt{\frac{\left[\Sigma_{i=1}^{n}(Y_i - \overline{Y})(y_{i+k} - \overline{y})\right]^2}{\Sigma_{i=1}^{n}(y_i - \overline{y})^2\, \Sigma_{i=1}^{n}(Y_i - \overline{Y})^2}}. \tag{A11}$$

Parameters a and b can be determined by linear regression. Both $a \neq 0$ and $b \neq 1$ indicate mostly improper calibration or weaknesses of the model. Their values can suggest the type of parameters to be improved. The parameter e_w is the remaining standard error to be explained by improving the model.

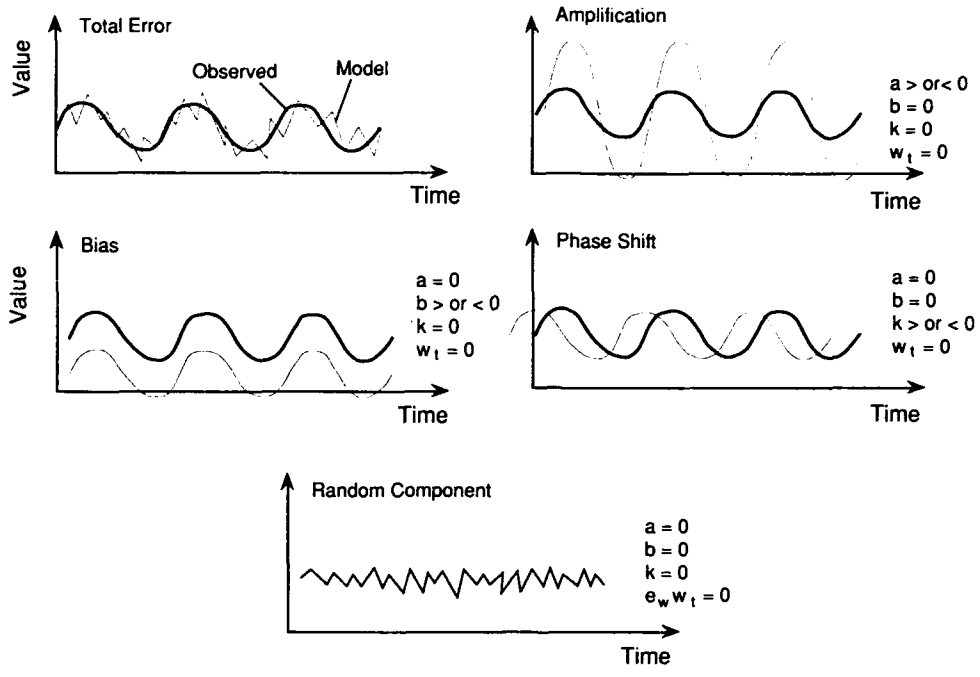

Figure A1. Components of the simulation error.

The effectiveness of the model can also be determined using methods similar to those used in the analysis of variance. Considering that the purpose of the model is to explain the total variation of the observations, components of the variation can be expressed using the following terms:

$$\text{Total sum of squares} = \text{SST} = \sum_{i=1}^{n} (Y_i - \bar{Y})^2 = n\sigma_Y^2 \tag{A12}$$

and

$$\text{SSE} = \text{error sum of squares} = \sum_{i=1}^{n} (Y_i - y_i)^2 = ne_s^2. \tag{A13}$$

If the model is calibrated to make the bias $e_b = 0$, then $\bar{y} = \bar{Y}$, and the percentage variation explained for $b = 1$ is

$$V = \frac{\text{SST} - \text{SSE}}{\text{SST}}$$

$$= \frac{\text{variation explained by the model}}{\text{total variation}} \tag{A14}$$

where V is the percentage variation explained (r^2). Although the bias has not been eliminated in the current model and $a \neq 0$ and $b \neq 1$, the same indicator can be used to explain the effectiveness of the model:

$$V = \frac{\text{SST} - \text{SSE}}{\text{SST}} = 1 - \frac{\Sigma_{i=1}^{n}(y_i - Y_i)^2}{\Sigma_{i=1}^{n}(Y_i - \bar{Y}_i)^2} = 1 - \frac{e_s^2}{\sigma_Y^2} \tag{A15}$$

where σ_Y is the variance of Y_i, $i = 1,2,...n$. V is defined as in eq A15 because it is similar to the definition of percentage variation explained in the linear regression analysis.

The part of SSE due to parameter estimation errors can be easily separated if the parameter sensitivities are known. Let the simulated result of k^{th} system variable as a function of the parameters $\theta_1,\theta_2,\ldots\theta_m$ be $y_k(\theta_1,\theta_2,\ldots\theta_m) = 0$. A small change in the variables can be related to the changes in parameters as

$$\Delta y_k = \frac{\partial y_k}{\partial \theta_1}\Delta\theta_1 + \frac{\partial y_k}{\partial \theta_2}\Delta\theta_2 + \ldots + \frac{\partial y_k}{\partial \theta_m}\Delta\theta_m \qquad \text{(A16)}$$

where $\frac{\partial y_k}{\partial \theta_1}$, $\frac{\partial y_k}{\partial \theta_2}$ are the sensitivities of the variable to the parameters. Equation A16 can be used to write an expression for the variance of y_k, assuming that the above partial differentials or sensitivities are finite and have constant values for a given set of parameters:

$$\sigma^2_{y_k} = \left(\frac{\partial y_k}{\partial \theta_1}\right)^2 \sigma^2_{\theta_1} + \left(\frac{\partial y_k}{\partial \theta_2}\right)^2 \sigma^2_{\theta_2} + \ldots + \left(\frac{\partial y_k}{\partial \theta_m}\right)^2 \sigma^2_{\theta_m}. \qquad \text{(A17)}$$

If the standard error variances of the parameters and the sensitivities are known, the error variance of the simulated result due to parameter errors can be determined using eq A17. This is the part of the total error variance e_s^2 explained by parameter errors. The remaining error variance is due to errors in the observations and the general model structure itself.

REPORT DOCUMENTATION PAGE

Form Approved
OMB No. 0704-0188

1. AGENCY USE ONLY (Leave blank)	2. REPORT DATE	3. REPORT TYPE AND DATES COVERED
	May 1993	

4. TITLE AND SUBTITLE

A Mathematical Model for River Ice Processes

5. FUNDING NUMBERS

DACA 89-84-K-0008

6. AUTHORS

A.M. Wasantha Lal and Hung Tao Shen

7. PERFORMING ORGANIZATION NAME(S) AND ADDRESS(ES)

Clarkson University
Potsdam, New York

8. PERFORMING ORGANIZATION REPORT NUMBER

CRREL Report 93-4

9. SPONSORING/MONITORING AGENCY NAME(S) AND ADDRESS(ES)

U.S. Army Cold Regions Research and Engineering Laboratory
72 Lyme Road
Hanover, New Hampshire 03755-1290

10. SPONSORING/MONITORING AGENCY REPORT NUMBER

11. SUPPLEMENTARY NOTES

12a. DISTRIBUTION/AVAILABILITY STATEMENT

Approved for public release; distribution is unlimited.

Available from NTIS, Springfield, Virginia 22161.

12b. DISTRIBUTION CODE

13. ABSTRACT (*Maximum 200 words*)

River ice processes are complex phenomena that are affected by many factors, including meteorological conditions, thermal inputs, hydraulic conditions and channel geometry. In this study a one-dimensional model called RICE is developed for simulating ice processes in rivers. In the river hydraulics component, the flow condition is determined by an implicit finite-difference solution of one-dimensional unsteady flow equations. In the thermal component, distributions of water temperature and ice concentration are determined by a Lagrangian–Eulerian solution scheme for equations of transport of thermal energy and ice. A two-layer formulation is introduced to model the ice transport. In this formulation the total ice discharge is considered to consist of the surface ice discharge and the discharge of suspended ice distributed over the depth of the flow. The effect of surface ice on ice production, as well as the formation of skim ice and border ice, is included. The dynamic formation and stability of the ice cover is formulated according to existing equilibrium ice jam theories with due consideration to the interaction between the ice cover and the flow. The undercover ice accumulation is formulated according to the critical velocity criterion. The growth and decay of the ice cover is simulated using a finite-difference formulation applicable to composite ice covers consisting of snow, ice and frazil layers. The model has been applied to the St. Lawrence River and the Ohio River system, with simulated results comparing favorably with field observations. Future improvements on the mathematical model as well as theoretical formulations on various ice processes are discussed.

14. SUBJECT TERMS

Ice
Mathematical models
Ohio River
River ice
St. Lawrence River

15. NUMBER OF PAGES

85

16. PRICE CODE

17. SECURITY CLASSIFICATION OF REPORT	18. SECURITY CLASSIFICATION OF THIS PAGE	19. SECURITY CLASSIFICATION OF ABSTRACT	20. LIMITATION OF ABSTRACT
UNCLASSIFIED	UNCLASSIFIED	UNCLASSIFIED	